An investigation on the development of liquid water content in different snow types during slushflow-inducing weather conditions

Thor Parmentier

Master’s thesis in Earth Science

Department of Earth Science

University of Bergen

June 2024

Abstract

Slushflows, defined as rapid mass-movements of water-saturated snow, occur when high liquid water content (LWC) causes bonds to melt and the snowpack to lose cohesion, triggering flow. Characterized by their shallow release angles and the potential for extensive runouts, slushflows typically occur during rain-on-snow events or due to significant melting. The presence of an impermeable layer beneath or within the snowpack is normally required for water to accumulate.

An important consideration for the improvement of slushflow prediction is understanding the role snow type has on the development of LWC in the snowpack. To assess this, LWC was measured in snow profiles before and during weather events conducive to slushflow occurrence, using an SLF Snow Sensor. In addition, the SLF sensor was evaluated as a tool to measure LWC and compared with the traditional hand wetness test.

Results indicate that the formation of preferential flow is important for water transport in snow. While precipitation particles and decomposing, fragmented particles may facilitate preferential flow, ripe melt forms tend to promote matrix flow. Thick ice layers can impede vertical water movement and redirect it laterally. Volume and rate of water supply may be as important as grain form in determining the mode of flow.

Comparisons between LWC estimated using the hand wetness test and values from the SLF Snow Sensor align with existing literature, attesting to the efficacy of the hand wetness test as a qualitative method for assessing LWC, especially for internal comparison. When precise values are required, the hand wetness test is insufficient, and use of the SLF Snow Sensor is more suitable. The requirement for an external density measurement to calculate LWC significantly increases the workload.

Acknowledgements

First, I extend my gratitude to my supervisors, Mathilde Sørensen from the University of Bergen (UiB) and Monica Sund from the Norwegian Water Resources and Energy Directorate (NVE). They helped hone the research questions and supplied high-quality feedback throughout the project. Each video meeting with them served as a motivating boost. A special note needs to be made here for Monica's inspiring tales full of amusement and wisdom, and her bubbling passion for snow and slushflows.

I would also like to acknowledge UiB and NVE for providing equipment and financial support for the fieldwork.

Heartfelt thanks go to my friends and family for their support and encouragement. I would like to thank Tonje for making great figures and for good discussions, sometimes even about our theses. Special mention needs to be made of the other members of the study group Rock-Solid Research, Ola and Lennarth. Good discussions, a feeling of camaraderie and being in this together, and an ever-expanding collection of thesis-related memes has been the staple of our biweekly meetings. Does biweekly mean twice a week or every two weeks? Who knows? Not us.

My deepest gratitude goes to Emma, whose unwavering and ever-present love, support, and humor has been indispensable. She acted as a steadfast field assistant, braving truly terrible weather to help that fool who wanted to go dig in the sopping-wet snow, despite torrential downpours, howling winds, and buckling tent poles.

Table of contents

List of figures

List of tables

1. Introduction

1.1. Motivation

Snow is the weakest natural material, usually being above 95% of its melting temperature in Kelvin (McClung & Schaerer, 2022). Differences in temperature, vapor pressure, water content, and meteorological conditions cause snowpack layers to have great variability and potential for instability. If the volumetric liquid water content (LWC) of a snowpack reaches a necessary threshold (ca. 15%), rapid mass-movements of water-saturated snow, known as slushflows, can occur (Hestnes, 1998). Slushflows differ from other snow avalanches by their relatively low release angles (< 30°), and their exceptionally long runout distances (Gude & Scherer, 1998; Hestnes et al., 2012). Slushflows are a natural hazard that may become more prevalent due to climate change (Relf et al., 2015). The damage potential of slushflows is high, costing Norway about the same as all other types of snow avalanche, measured in economic loss (Hestnes et al., 1994). They can also pose a hazard to people, as seen in Japan in 1945, when 88 people were killed by a single slushflow event (Kobayashi et al., 1994).

The Norwegian Water Resources and Energy Directorate (NVE) are responsible for providing a regional early warning of slushflow hazard in Norway (Sund et al., 2024). Knowledge about the snowpack is important for estimating slushflow hazard (Hestnes & Bakkehøi, 2004). Previous studies have investigated the snowpack conditions necessary for slushflow release. An impermeable layer, such as frozen or saturated ground, is usually required to cause water to accumulate (Onesti & Hestnes, 1989). While fine-grained snow and ice crusts promote stability (Hestnes, 1998), more porous snow types, such as precipitation particles and depth hoar, are more susceptible to slushflow release (Sund et al., 2020, 2024). Certain snow types require a higher water supply to initiate slushflows (Skuset, 2018; Skuset & Sund, 2019), but if the water supply is sufficiently high, snow type becomes less important (Hestnes, 1998).

According to Sund et al. (2024), more information on how specific snow types affect water transport is required to further develop the slushflow early warning. This study aims to investigate that by employing a field-based approach, using a dielectric SLF Snow Sensor to measure LWC in snow profiles before and during weather conditions that can form slushflows.

1.2. Research objectives

The primary research objective of this study is to investigate how liquid water develops in different snow types during weather situations where slushflows can occur. To do this, two research questions are stated here:

RQ1: How do differences in snow type influence the development of liquid water through the snowpack during weather conditions favorable for slushflow formation?

RQ2: What other factors influence the spatial and temporal distribution of liquid water in snow during conditions conducive to slushflow initiation?

The secondary objective of this study is to evaluate the SLF Snow Sensor as a tool for measuring LWC in the field. The following research questions are meant to address this:

RQ3: What are the advantages and limitations of using the SLF Snow Sensor for LWC measurements in the field?

RQ4: How do LWC measurements obtained from the SLF Snow Sensor compare to those derived from the hand wetness test?

2. Background

2.1. Snowpack properties

2.1.1. Grain form

Snow can have a variable microstructure, and no single parameter describes a sample of snow accurately (Armstrong & Brun, 2008). Grain form is assessed and categorized qualitatively, following the standard described by Fierz et al. (2009). In this section, a brief overview of the main grain forms is supplied. For more in-depth descriptions, see, e.g., Fierz et al. (2009) or McClung and Schaerer (2022). In this study, the terms "grain form", and "snow type" are used interchangeably. In addition, the terms snow "grain", "particle" and "crystal" are used as synonyms.

Precipitation particles (PP, +) are formed in the atmosphere and fall to the ground, accumulating as a soft, low-density snow layer. They can come in a variety of shapes, including complex dendrites, plates, needles, to the more rounded graupel, depending mainly on degree of supersaturation and temperature. Since supersaturation is much higher in the atmosphere than in the snowpack, PP undergo rapid metamorphism once they reach the ground (Fierz et al., 2009; Louchet, 2021).

Decomposing and fragmented particles (DF, ⁄) are snow crystals that have started to break down, either mechanically due to wind or by metamorphism. While retaining many of the characteristics of PP, they often appear as broken pieces with rounded edges (Fierz et al., 2009).

Rounded grains (RG, ●) are the product of metamorphism at low vapor pressure gradients (see Section 2.2.1), or mechanically due to wind. They take the form of small, round grains, and often make hard wind slabs (Fierz et al., 2009).

Faceted crystals (FC, □) are formed by metamorphism at high vapor pressure gradients (see Section 2.2.1). Diffusion of water vapor from one grain to the next cause straight edges and facets to form, causing FC to appear as angular crystals. FC bind poorly, have low cohesion, and can form persistent weak layers in the snowpack that keep snow avalanche hazard high over time (Fierz et al., 2009).

Depth hoar (DH, ∧) are the end product of faceting (see Section 2.2.1). They are quite angular and form large, hollow, sometimes striated, cup-like crystals with a large surface area. They often form at the bottom of continental snowpacks and like FC can form persistent weak layers (Fierz et al., 2009).

Melt forms (MF, ○) are the result of wet snow metamorphism (see Section 2.2.2), when liquid water is present in the snowpack, or from melting followed by refreezing. They can appear as clusters of round grains bonded to each other, sometimes with films of liquid water between the ice crystals. If the water freezes, the clusters can turn into a solid polycrystal. At high enough water contents, the bonds melt and large, spherical ice crystals separated by liquid water remain. An important subcategory of MF is melt-freeze crusts (MFcr, ◎), which form when a layer of snow melts, then refreezes into a semi-continuous hard layer of polycrystals, increasing in strength for each melt-freeze cycle (Fierz et al., 2009). Snow grains are classified as MF based on morphology. If a sample of dry snow of different grain form is suddenly exposed to water, it is not classified as MF until it has the rounded grain shape (McClung & Schaerer, 2022).

Ice formations (IF, ■) occur when liquid water infiltrates the snowpack and refreezes at layer boundaries or the base of the snowpack. They are more solid and less permeable than MFcr, though the exact transition between the categories is difficult to pinpoint (Fierz et al., 2009). In this study, IF will generally be referred to as "ice layers", as the focus is on the horizontally extending variant.

2.1.2. Porosity and density

Porosity is a measure of how much "empty" space, or pore space, a medium contains (Louchet, 2021). Snow is the most porous natural material (McClung & Schaerer, 2022). A snowpack is built up from many individual snow crystals, made of ice, forming a skeletal framework with pore spaces of varying size and shape in between. In snow, the pore spaces are usually not truly empty, rather being filled with air or water. Porosity, ϕ, is thus defined as pore volume divided by sample volume (Colbeck, 1978; Kinar & Pomeroy, 2015a):

$$\phi = \frac{(V_a + V_w)}{V_t} \qquad (1)$$

where: ϕ = Porosity of the snowpack [dimensionless]

V_a = Air volume [m^3]

V_w = Water volume [m^3]

V_t = Total sample volume [m^3]

Porosity is given as a number between 0 and 1, where 0 is no pore space and 1 is only pore space, or as a percentage. It does not depend on what the medium is, only how much open space it contains. Density, while similar to porosity in many ways, *does* depend on what the medium is. Density, ρ, is conventionally

defined as mass per unit of volume (kg m^{-3}). Snowpack density, ρ_s, including the effect of liquid water content, can more specifically be defined like this (Madore et al., 2022):

$$\rho_s = \rho_i\theta_i + \rho_w\theta_w + \rho_a\theta_a \quad (2)$$

where: ρ_s = Density of the snowpack [kg m^{-3}]

ρ_i = Density of ice [kg m^{-3}]

θ_i = Volumetric ice content [%]

ρ_w = Density of water [kg m^{-3}]

θ_w = Volumetric water content [%]

ρ_a = Density of air [kg m^{-3}]

θ_a = Volumetric air content [%]

Density is a fundamental property of snow that influences a variety of snow processes and properties (Hao et al., 2021), and is described by Martin and Schneebeli (2023) as the most important property for the structural characterization of snow. In snow avalanche science, snow density determines whether an avalanche will release as a coherent slab or as powdery loose snow. Snow density is linked to bond density (number of bonds per unit of volume) (Techel et al., 2011), which, together with bond strength and grain shape, is a component of cohesion (McClung & Schaerer, 2022). Cohesion, in turn, is a component of snowpack shear strength. Density is also directly correlated with shear strength in avalanche-failure layer studies, and differences between layer densities can indicate instability (McClung & Schaerer, 2022).

When there is no liquid water in the snowpack ($S_w = 0$), the term to the right in Eq. (2) is dominated by ρ_a, which is nearly three orders of magnitude smaller than ρ_i. The density of air depends on pressure, temperature, and humidity, and can be calculated using the ideal gas law (Ahrens & Henson, 2023). For dry air at standard atmospheric pressure (101 325 Pa) and 0 °C it is 1.29 kg m^3, which is the value used in this study. The density of ice depends on pressure and temperature, and for pure ice at standard atmospheric pressure is 916,7 kg m^{-3} at 0 °C and 918,2 kg m^{-3} at -10 °C (Harvey, 2023). To simplify, 917 kg m^{-3} is used in this study. Dry snow density and porosity are, therefore, practically interchangeable (Madore et al., 2022). Porous snow has a low density and dense snow has a low porosity. Dry snow density varies between 30 and 550 kg m^{-3} ($\phi = 0.97$ to 0.40). Fresh new snow is usually between 50 and 100 kg m^{-3}, with values as low as 30 kg m^{-3} and as high as 300 kg m^{-3} reported. New snow tends to be denser in maritime climates than continental ones (McClung & Schaerer, 2022). Snow that has experienced strong wind can have densities up to 400 to 500 kg m^{-3} (Armstrong & Brun, 2008). The upper

density limit for dry seasonal snow is around 550 kg m^{-3} (McClung & Schaerer, 2022). Perennial snow, or firn, is more dense, increasing in density until it reaches around 800–850 kg m^{-3} and is defined as glacier ice (DeWalle & Rango, 2008). Ice crusts in snow can have densities in the range of 700–800 kg m^{3} (Armstrong & Brun, 2008).

When the liquid water content of the snowpack is not zero, however, snowpack density can be higher than the values stated above. Density increases with increasing water content, as the air in the pore spaces is replaced with the much denser water. Snow with a high porosity has a higher capacity of water storage, meaning fresh new snow could theoretically achieve the highest density, if all the pore spaces were fully saturated and the snow matrix remained unchanged.

Snow tends to get denser with time and depth (DeWalle & Rango, 2008). As snow grains undergo metamorphism, they tend to become more spherical. They can therefore be packed more tightly, leaving less pore space between the grains, which increases the density of the snowpack (Barry & Gan, 2022; DeWalle & Rango, 2008; McClung & Schaerer, 2022). Settlement is a second process that leads to densification. As snow becomes buried, the weight of the overlying snowpack causes grains to reorganize into a more compact form (DeWalle & Rango, 2008; McClung & Schaerer, 2022). This generally leads to snowpacks becoming denser with depth, though there are exceptions. Grain types such as faceted crystals, surface hoar, and depth hoar are more resistant to settlement, likely due to their anisotropic nature, which can lower structural integrity (McClung & Schaerer, 2022). Resistance to densification, and thereby resistance to strengthening, is a part of why they have earned the name “persistent weak layer”.

2.1.3. Liquid water content

Liquid water content (LWC), sometimes called free water content, is a measure of how much of a snow sample consists of water in liquid form (DeWalle & Rango, 2008). It is usually given as a fraction of mass or a fraction of volume (Fierz et al., 2009). In this study LWC is expressed as a percentage of volume and symbolized as θ_w or simply θ. LWC in snow comes primarily from rain, snowmelt, or a combination (Fierz et al., 2009). Liquid water can be found moving through a snowpack, either percolating downwards due to gravity, or moving parallel with the snow layers if downward movement is blocked by, e.g., impermeable layers of ice or capillary barriers (DeWalle & Rango, 2008). These processes are described in greater detail in Section 2.3. Some liquid water remains, even in a freely draining snow sample, due to capillary forces larger than gravitational ones, which is known as the irreducible water content, θ_{ir} (Kinar & Pomeroy, 2015a). θ_{ir} has been measured to be around 3% (Colbeck, 1986; Yamaguchi et al., 2010), or,

according to Fierz et al. (2009), 3 – 6%, depending on snow type. At the other end of the scale, when the whole snowpack has warmed to 0 °C, and is so full of liquid water that any additional snowmelt leads to runoff, the snowpack is "ripe" (Kinar & Pomeroy, 2015a).

LWC in snow can be categorized in multiple ways. The most common is the hand wetness test shown in Table 1, classifying snow as dry, moist, wet, very wet, or slush (Fierz et al., 2009). The hand wetness test is the method avalanche workers and snow observers all over the world use to classify wet snow in the field.

Table 1. Classification of wet snow based on liquid water content, including description of the hand wetness test. LWC values are approximate. Adapted from Fierz et al. (2009).

Term	Code	Description	θ
Dry	D	Usually, T_s is below 0 °C, but dry snow can occur at any temperature up to 0 °C. Disaggregated snow grains have little tendency to adhere to adhere to each other when pressed together, as in making a snowball.	0%
Moist	M	$T_s = 0$ °C. The water is not visible even at 10× magnification. When lightly crushed, the snow has a tendency to stick together.	0–3%
Wet	W	$T_s = 0$ °C. The water can be recognized at 10× magnification by its meniscus between adjacent snow grains, but water cannot be pressed out by moderately squeezing the snow in the hands (pendular regime).	3–8%
Very wet	V	$T_s = 0$ °C. The water can be pressed out by moderately squeezing the snow in the hands, but an appreciable amount of air is confined within the pores (funicular regime).	8–15%
Slush	S	$T_s = 0$ °C. The snow is soaked with water and contains a volume fraction of air from 20 to 40% (funicular regime).	> 15%

Another distinction that must be made is between the pendular and funicular regimes (Denoth, 1980; Fierz et al., 2009). In the pendular regime LWC is low, the air in the pores is continuous, and the liquid water is discontinuous. In the funicular regime, the opposite is the case. LWC is high, the air in the pores is discontinuous, and the liquid water is continuous (Denoth, 1980; Fierz et al., 2009). This distinction has important implications for wet snow metamorphism (see Section 2.2.2.). The LWC threshold between the regimes is around $\theta = 8\%$. Denoth (1980) found through dielectric measurements and drainage

experiments that the transition between pendular and funicular regimes happens between 11% and 15% pore saturation. Note that this is different from θ, which depends on porosity (ϕ). Snow with a higher ϕ needs a higher θ for transition. The upper limit of the pendular regime is around 14% pore saturation, according to Brun (1989).

LWC in snow can also be looked at in terms of percolation systems (Louchet, 2021). Louchet (2021) presents three systems with increasing LWC. The first is when the snow is packed so tight that water cannot infiltrate. This virtually only happens when ice layers are present, as natural snow is not dense enough to prevent percolation. In the second system, the snow grains form a continuous framework, but water can filter through the framework. The third system has so much liquid water that the snow grains no longer form a continuous chain and are separated by water. The snow is then defined as slush.

One can measure LWC directly using chemical dilution (Pirazzini et al., 2018), freezing or melting calorimetry (Kinar & Pomeroy, 2015a), or centrifugal separation (Mavrovic et al., 2020). These methods are often time-consuming, destructive, and difficult to perform in the field, so more efficient, indirect methods are used instead (Kinar & Pomeroy, 2015a; Mavrovic et al., 2020). Indirect methods have the advantage of being less destructive to the snow sample, and include methods such as upwards facing GPRs (Donahue & Hammonds, 2022), hyperspectral imaging (Donahue et al., 2022; Donahue & Hammonds, 2022), acoustic methods (Kinar & Pomeroy, 2015b), or using GPS (Koch et al., 2014, 2019). One of the main methods LWC is measured is through dielectric properties. The dielectric permittivity of snow, ϵ, is dominated by the permittivity of water ($\epsilon \approx 86$) compared to the values for air ($\epsilon \approx 1$) and ice ($\epsilon \approx 3.15$) (Techel & Pielmeier, 2011). Examples of instruments using dielectric methods are the Denoth meter (Denoth, 1994), the Finnish Snow Fork (Techel & Pielmeier, 2011), the Open-Ended Coaxial Probe (Mavrovic et al., 2020), a new handheld capacitive sensor (Wolfspeger et al., 2023), and the SLF Snow Sensor used in this study (FPGA Company, 2018).

2.1.4. Permeability and hydraulic conductivity

Hydraulic conductivity, K, and permeability, k, are related, but distinct, terms that pertain to how easily a fluid can flow through a porous material (Clerx et al., 2022). Permeability is an inherent property of the material and does not depend on the fluid. It is primarily determined by porosity, but grain size, grain form and pore connectivity play a role as well (Brun, 1989; Clerx et al., 2022). One can have a highly porous material that leads water poorly if the pores are unconnected (Louchet, 2021; Pietzsch, 2009). The

permeability of snow tends to be between $6 \times 10^{-10} m^2$ and $524 \times 10^{-10} m^2$ (Katsushima et al., 2013), and can be calculated using equation (3) (Webb et al., 2018).

$$k = (3.0 \pm 0.3) r_{es}^2 \times e^{(-0.0130 \pm 0.0003)\rho_s} \quad (3)$$

where: k = Permeability [m^2]

r_{es} = Equivalent sphere radius [mm]

ρ_s = Density of the snowpack [kg m^{-3}]

Hydraulic conductivity, on the other hand, takes into account the properties of the fluid and can be calculated using equation (4) (Clerx et al., 2022).

$$K = k \frac{\rho_l g}{\mu} \quad (4)$$

where: K = Hydraulic conductivity [m s^{-1}]

k = Permeability [m^2]

ρ_l = Density of the fluid [kg m^{-3}]

g = Gravitational acceleration [m s^{-2}]

μ = Dynamic viscosity of the fluid [Pa s]

In snow, the fluid in question is usually water. The hydraulic conductivity of snow cannot be measured precisely in the field, and requires considerable time and effort in a cold laboratory (D'Amboise et al., 2017). Permeability is easier to measure, so that has been used to calculate the saturated hydraulic conductivity, which typically is in the range 10^4 – 10^6 mm h^{-1} (Katsushima et al., 2013). However, most water flow in snow occurs in unsaturated conditions, which is different (Yamaguchi et al., 2010). Yamaguchi et al. (2010) found that unsaturated hydraulic conductivity likely depends on grain size, but they could not quantify it due to needing more information about the tortuosity of snow (the amount a fluid needs to deviate from a straight line to flow through). Following this, Yamaguchi et al. (2012) found that the relationship between density and grain size could be used to model unsaturated hydraulic conductivity in melt forms. Rounded grains did not show the same dependency, meaning grain type needs to be considered as well (Yamaguchi et al., 2012). Hydraulic conductivity in snow increases with degree of wet snow metamorphism, as grains coarsen, pore sizes increase, and efficient meltwater channels are formed (Gude & Scherer, 1998).

2.2. Snow metamorphism

In a seasonal snowpack, heat flow is the dominant mechanism behind metamorphism (McClung & Schaerer, 2022). In dry snow, vapor transport is dominant, but in wet snow, thermal diffusion through liquid water and the effects of melting and refreezing also become important (DeWalle & Rango, 2008). Figure 1 shows the main metamorphic processes snow crystals can undergo, which are described in further detail in this section.

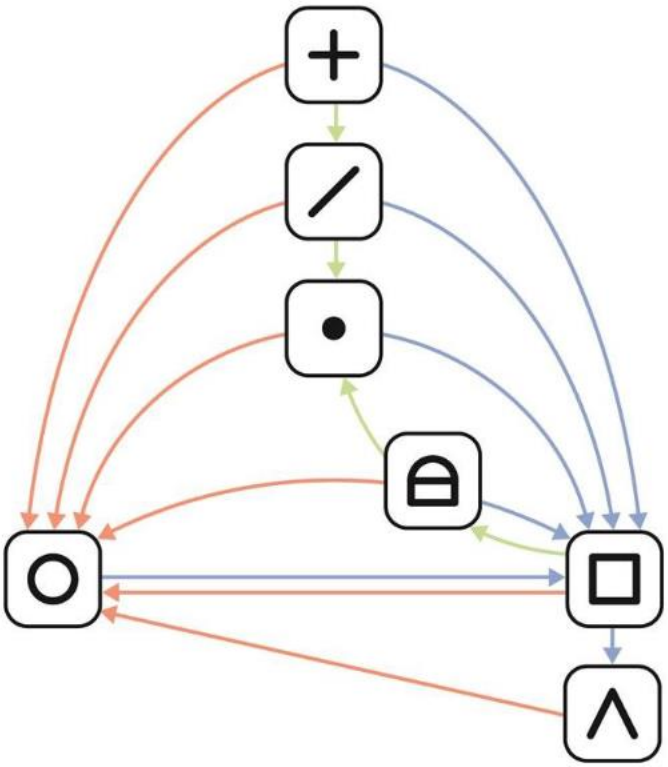

Figure 1. Schematic of snow metamorphism between the main snow types. Green arrows indicate rounding, blue arrows indicate faceting, and orange arrows indicate wet snow metamorphism (NVE, 2020).

2.2.1. Dry snow metamorphism

Dry snow metamorphism depends on temperature gradients, temperature, and pore-space size (McClung & Schaerer, 2022). Of these, temperature gradients, or rather vapor pressure gradients induced by temperature gradients, are the most important factor for grain type (LaChapelle & Armstrong, 1977; McClung & Schaerer, 2022). Dry snow metamorphism can, based on differences in vapor pressure gradients, be split into two processes. In older literature, they have been referred to as “destructive” and

"constructive", or "equi-temperature" and "temperature gradient" metamorphism. However, true equi-temperature conditions virtually never occur (McClung & Schaerer, 2022). The closest is when the entire snowpack is melting, and the temperature is near 0 °C throughout, but there are still minute temperature differences between snow crystals. Therefore, temperature gradients can be said to exist in both modes of metamorphism. The American Avalanche Association (2022) uses the terms "equilibrium growth" and "kinetic growth". In this study, the terms "rounding" and "faceting" are used. The vapor pressure gradient threshold that separates the two processes was found by LaChapelle and Armstrong (1977) to be around 500 Pa m^{-1}. Since temperature is markedly easier to measure than vapor pressure, temperature gradients are typically used by avalanche workers to differentiate between rounding and faceting (American Avalanche Association, 2022; NVE, 2020). 500 Pa m^{-1} equates to a temperature gradient of 10 K m^{-1} at 0 °C.

Rounding occurs when vapor pressure gradients are below the 500 Pa m^{-1} threshold. This process is shown in green arrows in Figure 1. In this mode of metamorphism, the dominant effect of vapor transport is diffusion due to curvature (McClung & Schaerer, 2022). This process is known as the Kelvin effect (Dunlop, 2008), which describes that the vapor pressure over a convex surfaces, such as the tip of a stellar dendrite branch, is higher than that over flat planes at the same temperature. The inverse is the case for concave surfaces. A fresh particle of dendritic new snow (PP) will, upon landing, immediately start rounding, as mass is transported by diffusion from the convex branches to the flat or concave regions near the base between crystal branches or in the bonds between snow grains. A sphere, being the shape with the lowest specific surface area, is the goal of rounding (Armstrong & Brun, 2008). This creates, as the name implies, rounded grains (RG), where sharp edges and branches have been rounded away (Fierz et al., 2009). Rounding causes bond growth and strengthening, a process known as "sintering". Although rounding tends to happen at a much slower pace than faceting (McClung & Schaerer, 2022), the first signs of sintering can become apparent in only a few seconds in the right circumstances (Louchet, 2021).

Faceting occurs when snowpack vapor pressure gradients exceed 500 Pa m^{-1}. Faceting is represented in Figure 1 by blue arrows. In these conditions, the hand-to-hand effect of vapor transport in pore spaces outstrips the Kelvin effect (Pinzer et al., 2012). In short, water molecules sublimate from warmer crystals closer to the bottom of the snowpack, diffuse upward through the pore spaces, and deposit on warmer crystals. The shape of the crystals formed by faceting tend to have straight edges (facets). Faceted crystals and their end product, depth hoar, can vary a lot in shape and size, from small clusters of lightly faceted grains to large cups and chains of well-developed depth hoar (Fierz et al., 2009). Under rapid growth conditions, above the threshold for faceting, mass is preferentially deposited near the snow crystal base

rather than the bonds between crystals (McClung & Schaerer, 2022). As a result, faceted crystals are poorly bonded to each other and exhibit an anisotropic nature, demonstrating strength in compression but weakness in shear. They can hold the weight of an overlying slab without collapsing, but under specific triggering conditions can both fail and propagate that failure over long distances. Faceting is a faster process than rounding and happens more quickly in warmer (still subfreezing) snow. Faceted crystals are more common in continental climates, where the snowpack tends to be thin, allowing for greater temperature gradients to form. Depth hoar can often be found at the base of these snowpacks and can persist throughout the whole season (Barry & Gan, 2022). In continental climates, the snowpack is usually deeper, and the temperature gradients lower, but facets can still be found there under the right conditions.

2.2.2. Wet snow metamorphism

The addition of water in liquid form changes how snow metamorphism works. This process is shown in Figure 1. One major difference from dry snow is that the thermal conductivity of liquid water (0.567 W m^{-1} K^{-1}) is much higher than that of air (0.025 W m^{-1} K^{-1}), meaning energy exchange, and therefore metamorphism, occurs much quicker with increasing LWC (Brun, 1989; DeWalle & Rango, 2008; McClung & Schaerer, 2022). The main driver of metamorphism in wet snow is the effect of curvature, which causes ice surfaces with small radii of curvature to melt at lower temperatures (Figure 2). Other factors that reduce the melting temperature include impurities in the water (Armstrong & Brun, 2008), pressure, and reduced area of contact (McClung & Schaerer, 2022).

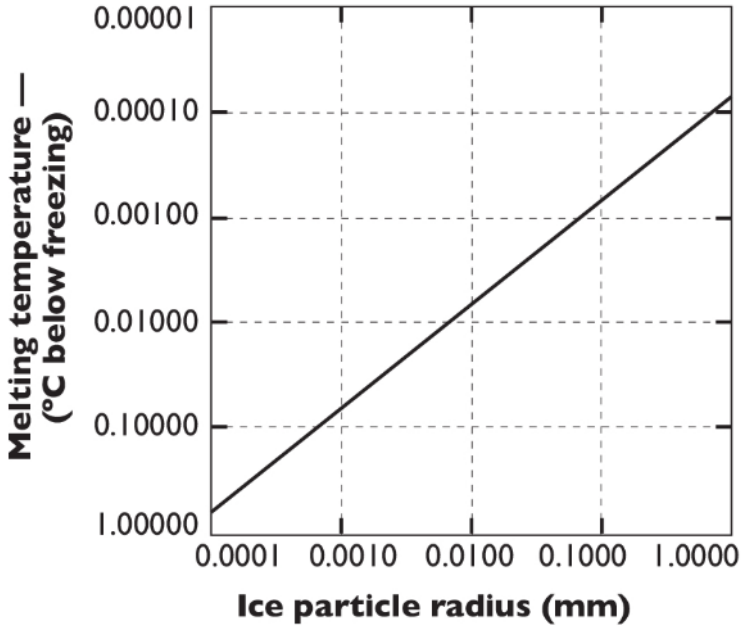

Figure 2. Melting temperature of snow grains by particle radius (McClung & Schaerer, 2022).

This leads to grain growth through a cannibalization process where small snow crystals melt at lower temperatures and are "eaten" by larger crystals (DeWalle & Rango, 2008). The difference in melting temperature is very small (Figure 2), but heat exchange through water is so effective that it is significant (McClung & Schaerer, 2022). This means that as the snowpack is heating, small crystals melt first. The energy for melting comes from the large grains, which cool, then refreeze the liquid water, and thereby grow. The curvature effect also leads to net rounding, as mass is removed from convexities and deposited in concavities. According to McClung and Schaerer (2022), growth rates are high when grains smaller than 1 mm are present, but this slows over time. In theory, metamorphism would stop when all snow grains are spheres of equal size, but such conditions are nearly impossible to achieve in the real world. As LWC in the snowpack increases, these processes accelerate (Armstrong & Brun, 2008).

For snow in the pendular regime ($\theta < 8\%$), heat transfer occurs through vapor diffusion in the pore spaces, as in dry snow (McClung & Schaerer, 2022). At this relatively low LWC, clusters of round MF snow grains readily form to reach force equilibrium (Colbeck, 1979a). The clusters have strong ice bonds and can have a film or vein of liquid water between the crystals (Figure 3a). For a cluster to be in force equilibrium, changes in LWC cause the change of grain radius, water vein radius, and cluster size, thereby resisting large changes in capillary pressure (Colbeck, 1979a). If the water refreezes, the clusters turn into large polycrystals. While the addition of liquid water usually weakens snow due to bond melting, at low values of LWC, capillary forces are high (Figure 3b), causing wet grains to be pulled together in a process known as capillary cohesion (Schlumpf et al., 2024).

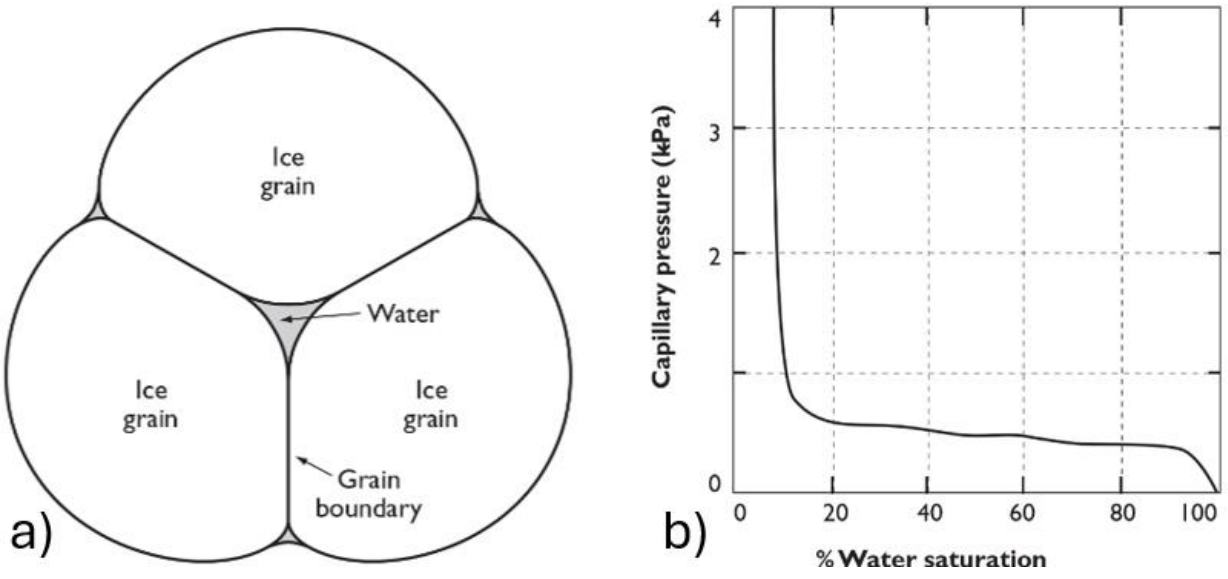

Figure 3. a) Grain cluster in wet snow. b) Capillary pressure as a function of pore saturation in snow. From McClung and Schaerer (2022).

In the funicular regime ($\theta > 8\%$), metamorphism is driven by thermal diffusion through the continuous liquid water (Colbeck, 1986). This is much faster than vapor diffusion in the pores, meaning rounding and grain growth from cannibalization are accelerated (McClung & Schaerer, 2022). According to Colbeck (1986), the mean grain size approaches 1 mm in just a few days. At high enough water content ($\theta > 15\%$), all bonds are melted and spherical grains separated by liquid water are what remain (Colbeck, 1979a). Such slushy snow is virtually cohesionless (McClung & Schaerer, 2022).

During melting, bonds are preferentially melted, which reduces snow strength. If the capillary water refreezes, the snow strength increases substantially (DeWalle & Rango, 2008). Melt-freeze cycles can be caused by diurnal temperature variations. The grain size increases, as small grains and bonds are melted. During the night, the layer can refreeze, creating hard and brittle melt-freeze crusts (McClung & Schaerer, 2022).

2.3. Water movement through the snowpack

The generation of meltwater due to atmospheric interactions usually only occurs near the surface of the snowpack (Gude & Scherer, 1998). Once the irreducible liquid water content is surpassed, water starts percolating downward (Fierz et al., 2009). Percolation in snow can be viewed as multi-phase flow in a porous medium, with liquid water and air being the two phases, and snow being the medium (Clerx et al., 2022). It is difficult to simulate water movement through the snowpack due to large temporal and spatial variability (Madore et al., 2022). Many aspects can be borrowed from soil mechanics, but snow is especially challenging since the matrix is so close to the melting point and changes rapidly (Juras et al., 2017; Katsushima et al., 2013). The velocity of vertically percolating water is controlled by permeability, capillary pressure, hydraulic conductivity, and the flux of added water (Clerx et al., 2022; Madore et al., 2022). In general, snow travels slowly through new snow due to capillary effects, and more quickly as grain sizes increase and pores become more interconnected (Sund et al., 2020).

The following sections describe the processes that determine the paths rain- or meltwater takes within the snowpack. Section 2.3.1 explains how vertically percolating water can be diverted laterally by hydraulic barriers. Sections 2.3.2 and 2.3.3 detail the differences between the two modes of flow within snow: matrix flow and preferential flow.

These processes have traditionally been studied in the field through the use of dye tracers to mark the flow of liquid water (e.g., Avanzi et al., 2016; Clerx et al., 2022; Eiriksson et al., 2013; Marsh & Woo, 1984,

1985; Schneebeli, 1995; Waldner et al., 2004). The use of dye tracers is destructive, meaning only one timestep can be captured. Newer advancements utilizing non-destructive methods, such as MRI (Katsushima et al., 2020), or upward-facing radar, coupled with hyperspectral imaging to visualize the rain- or meltwater paths in 3D (Donahue et al., 2022; Donahue & Hammonds, 2022), allow for more continuous monitoring at higher resolutions.

2.3.1. Hydraulic barriers and lateral flow

Snow has such a high permeability that in a freely draining snowpack, the presence of snow wetter than moist (Table 1) is relatively rare (McClung & Schaerer, 2022). Static pore pressure, a staple of soil mechanics, is normally irrelevant in snow. To reach the LWC values for very wet or slushy snow, a mechanism that prevents percolation and causes pooling is nearly always necessary (McClung & Schaerer, 2022). This also promotes lateral flow (Techel & Pielmeier, 2011). Schlumpf et al. (2024) distinguish between capillary barriers, where high suction in the layer above allows water to accumulate, and permeability barriers, where the permeability of a snow layer is lower than the rate of infiltrating water. Hydraulic barrier is a term that encompasses both (Katsushima et al., 2020).

Permeability barriers are snow layers with a low enough permeability that water cannot easily penetrate through. The classical permeability barrier is the ice layer, but other configurations exist, e.g., thinner melt-freeze crusts or tightly packed windblown grains (Clerx et al., 2022). Permeability barriers prevent water from moving deeper into the snowpack, causing pooling or lateral flow above the layer, depending on the slope. Water can bypass the barrier either by melting through it, which takes a long time, or flowing around it, which typically takes much less time. Marsh and Woo (1985) describe the redistributing effect of ice layers on water flow in snow, as the water is concentrated toward some areas while it is removed from others. Ice layers are not necessarily laterally persistent, meaning they lead water laterally a short distance, then channel it deeper (Eiriksson et al., 2013). The lateral extent of ice layers can range from tens of centimeters for very thin (< 1 mm) layers to 2 – 3 m for slightly thicker layers (Marsh & Woo, 1984). The distance water travels along a hydraulic barrier before reaching the edge or breaking through is the diversion length (Webb et al., 2018). Webb et al. (2018) found diversion lengths between 2.5 m and 9.5 m in south-facing slopes. Although ice layers primarily are thought to impede the vertical movement of water, Furbish (1988) found, through modeling, that ice layers might speed up the vertical flow speed of water through isothermal snow. Matrix flow (see Section 2.3.2), which occurs as unsaturated flow through snow is slow. Ice layers can block the water from going straight down and lead it laterally instead. This can concentrate the water into saturated (or nearly saturated) flow fingers, which is much faster than

unsaturated flow. When the water is diverted to the edge of the ice layer, there can also be so much of it there that the vertical flow is fast. Ice layers can therefore speed up the time it takes for water to reach the ground even though it travels a much longer distance.

Capillary barriers can be found in unsaturated snow where a layer with small grains is on top of a layer with larger grains (Waldner et al., 2004). The smaller pores of the fine-grained upper layer hold the water in due to capillary forces, preventing water from entering the coarse-grained lower layer (Pietzsch, 2009). Densities above and below the capillary barrier can be the same (Pietzsch, 2009; Williams et al., 2010), but greater diversion lengths are observed when the top layer has lower density (Webb et al., 2018). The larger the difference in grain size, the stronger the barrier is (Avanzi et al., 2016). Webb et al. (2018) found that the top layer must have a grain diameter smaller than 0.6 mm for a capillary barrier to form, and that the lateral diversion length increases the smaller the grains in the upper layer are. They found diversion lengths between 1 m and 25 m in a north-facing stratified snowpack. Avanzi et al. (2016) observed much more rapid flow in the lower layer (coarse grains) of their percolation experiments. With a capillary barrier, the water flow rate is affected by ponding in the upper layer, and in the lower layer it is affected by the speed the water can get through the capillary barrier. Both those factors limit the effect of surface infiltration rate to an extent. However, with a large enough influx of water, the capillary barrier can be overcome (Pietzsch, 2009). Capillary barriers do not persist as long as ice layers (Webb et al., 2018). When the fine-grained upper layer is subjected to liquid water, grain growth accelerates (Figure 4). As the grain sizes across the barrier become more similar, the capillary forces equalize, and the barrier disappears. This can occur within days or even hours (Webb et al., 2018). If the snowpack refreezes before the capillary barrier is disrupted, liquid water ponded at the barrier can form ice layers, turning it into a permeability barrier (Juras et al., 2017).

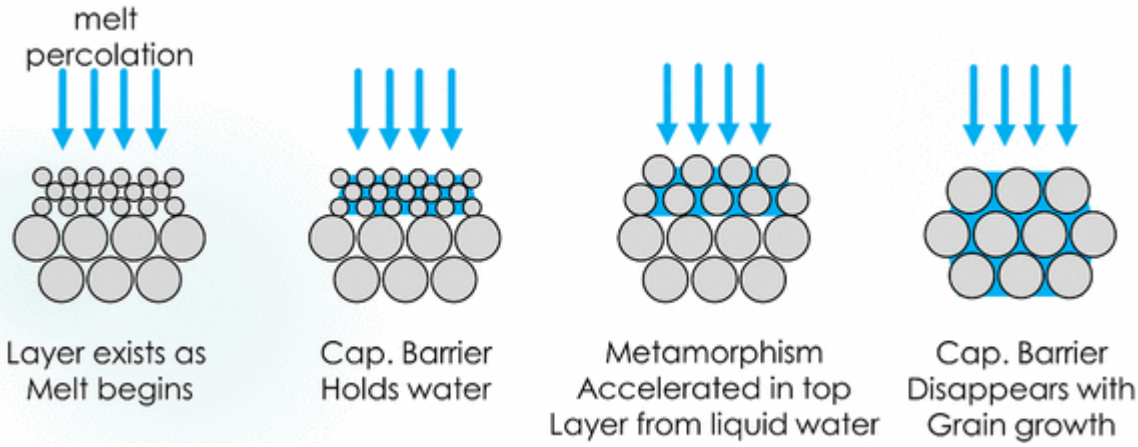

Figure 4. Capillary barrier due to difference in grain size. Webb et al. (2018).

Gravity causes the net movement of water in snow to be downward, but layer-parallel movement can occur above permeability or capillary barriers (Techel & Pielmeier, 2011). Saturated layers in the snow can cause lateral flow, as the direction of highest hydraulic conductivity shifts to be slope-parallel (Marshall & CryoGARS, 2014). Eiriksson et al. (2013) found that water flows laterally downslope along hydraulic barriers, until it reaches a feature that allows it to break through vertically, then it flows laterally along the next barrier, taking a stepped path through the snowpack (Figure 5). The diversion lengths of hydraulic barriers can be in the meter to tens of meters scale, being largest during small melt events in ripening snowpacks (Webb et al., 2018). Eiriksson et al. (2013) also found that stratified, cold, midwinter snowpacks promoted lateral flow within the snow, while ripe springtime snowpacks moved more water along the base of the snowpack. Water can flow along the ground through Hortonian overland flow, where the permeability of the surface soil is so low that the infiltrating water reaching it is diverted laterally instead (Eiriksson et al., 2013). Basal ice layers can amplify this process and cause rapid runoff (Juras et al., 2017). The speed of lateral flow depends on the slope (Gude & Scherer, 1998). The lateral flow velocities Eiriksson et al. (2013) measured ranged from 1 m h^{-1} to 7 m h^{-1}. Both Marshall & CryoGARS (2014) and Eiriksson et al. (2013) emphasize the importance of lateral snow within the snowpack on the catchment scale.

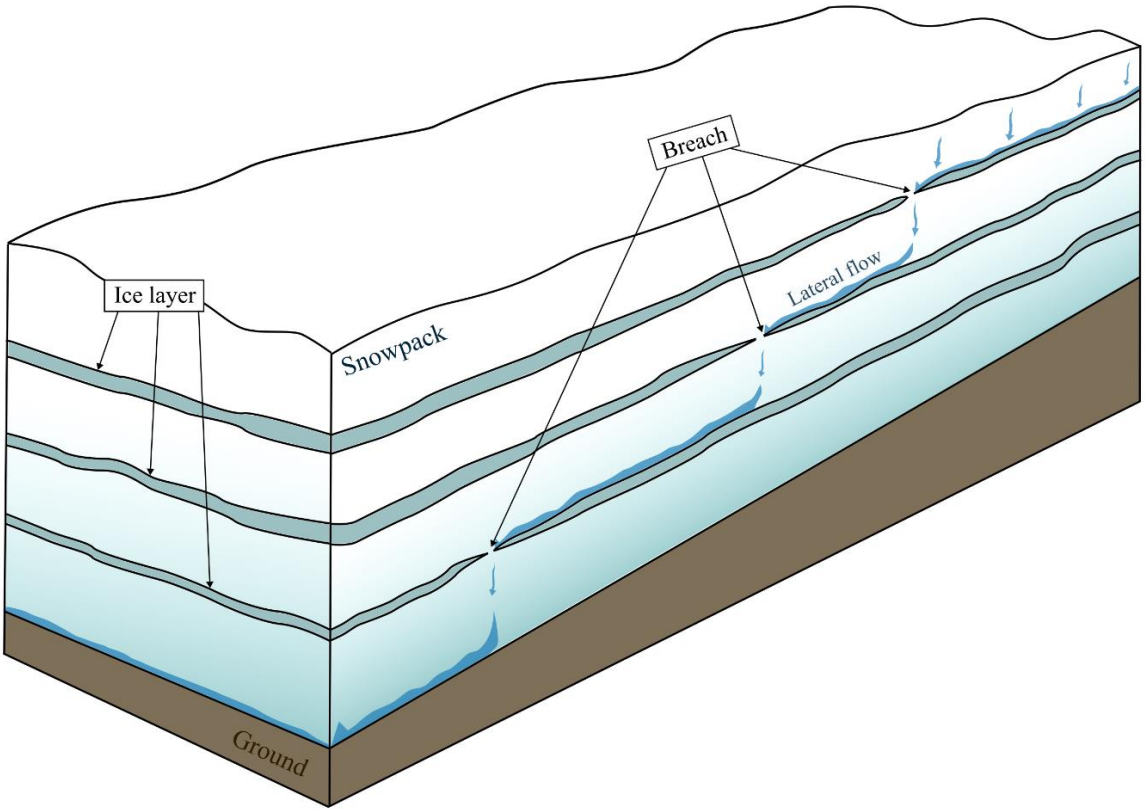

Figure 5. Water being diverted laterally by ice layers and flowing through the snowpack in a step-like pattern. Figure by Tonje Sælensminde.

2.3.2. Matrix flow

Matrix flow, also referred to as uniform or diffusive flow, is one of the ways liquid water can travel through the interconnected pore spaces in a snowpack (Figure 6). It is described as a semi-uniform wetting front, which gradually and evenly wets the entirety of the snowpack, usually starting from the snow surface (Donahue & Hammonds, 2022). Matrix flow can appear either as a background wetting front following preferential flow (Donahue & Hammonds, 2022; Marsh & Woo, 1984, 1985; Techel et al., 2011), or on its own (Brandt et al., 2022; Williams et al., 2010). Homogenous snow promotes matrix flow, and as the snowpack ripens, especially in uniform, springtime snowpacks made of melt forms, matrix flow becomes the dominant flow pattern (Brandt et al., 2022; Williams et al., 2010). While the flow is generally downward due to gravity, capillary forces play a key role, drawing water into small pores first. This means that, despite it being described and modeled as uniform, true homogeneity rarely occurs in nature (Waldner et al., 2004), or even in controlled laboratory settings (Techel et al., 2011). When preferential flow is present (see Section 2.3.3), matrix flow can occur as horizontal spread from the flow fingers into the surrounding, dry snow, rather than as an even wetting front from above (Waldner et al., 2004). Matrix

flow occurs as unsaturated flow, which is much slower than saturated flow. According to Marsh and Woo (1984), the velocity of the wetting front through dry snow is controlled by how quickly liquid water reaches the front, fills available pore spaces and refreezes, releasing latent heat, until the cold content of the snow directly below the wetting front is overcome and the snow reaches 0 °C. When the snowpack is cold, refreezing can slow matrix flow considerably, both vertically and horizontally (Waldner et al., 2004).

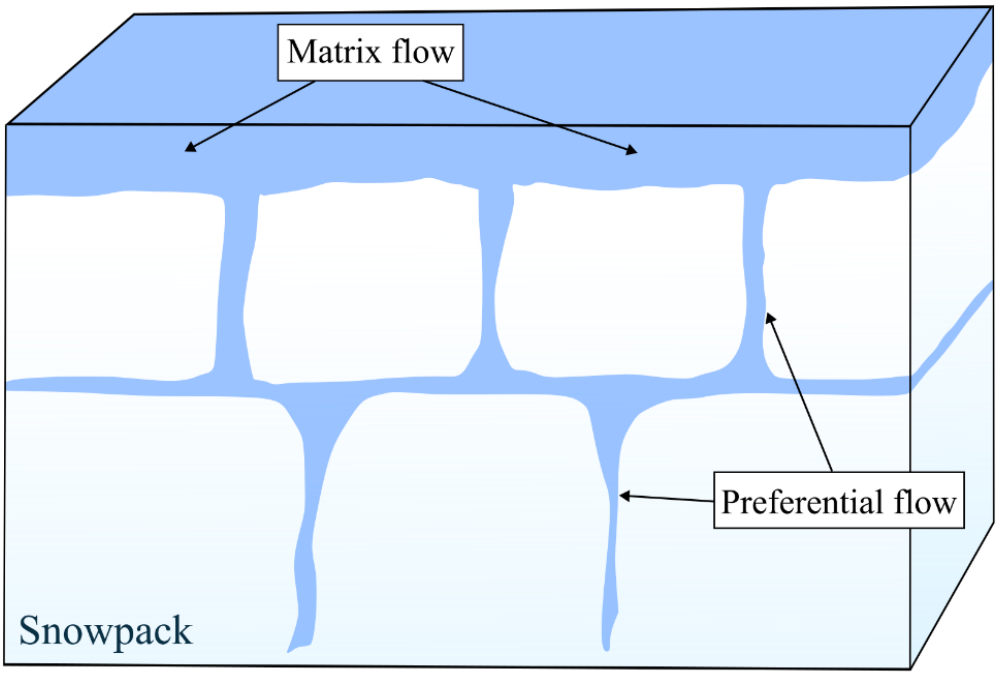

Figure 6. Matrix flow vs preferential flow. Figure by Tonje Sælensminde.

2.3.3. Preferential flow

Preferential flow is the heterogenous counterpart to matrix flow, shown in Figure 6. Liquid water is channeled into preferential flow paths, or flow fingers, which lead it efficiently downward, ahead of a background wetting front (see Section 2.3.2; Marsh & Woo, 1984). Water-entry capillary pressure head, the pressure required for water to infiltrate into dry snow, decreases with increased water supply, increased grain size, and increased pore space (Katsushima et al., 2013). The water supply is higher and the pores are more saturated during preferential flow, making preferential flow much quicker than matrix flow (Clerx et al., 2022; Marsh & Woo, 1984). In a deep snowpack, flow fingers generally reach the ground much earlier than matrix flow. However, in cold, arctic snow, Marsh and Woo (1984) found that

flow fingers and the background wetting front stayed relatively close, due to refreezing of the flow fingers at stratigraphic horizons.

As represented in Figure 6 and Figure 7, preferential flow paths lead water vertically until it reaches a hydraulic barrier, where the flow spreads laterally until it finds its way deeper in a new place (McGurk & Marsh, 1995; Waldner et al., 2004). These layers can be undetectable in a standard snow pit investigation (Williams et al., 2010). Preferential flow paths allow for large amounts of water to be transported vertically though the snowpack (Brandt et al., 2022; Donahue & Hammonds, 2022). Flow fingers make vertical heat transport more efficient as well (Schneebeli, 1995). Stratified, heterogenous snowpacks appear to promote preferential flow, but the exact mechanisms are not perfectly understood yet (Brandt et al., 2022). This makes preferential flow more difficult to model than the more predictable matrix flow (Waldner et al., 2004).

Figure 7. Photo of flow fingers (Marsh & Woo, 1984).

Snowpack structure and meteorological conditions affect the size and distribution of flow fingers (Schneebeli, 1995), though the exact details are not fully understood. Katsushima et al. (2020) found that continued water input increases the number of preferential flow paths, and point to pore size as an important factor for their formation. Juras et al. (2017) state that flow finger area decreases with grain size

and increases with water supply rate. Avanzi et al. (2016), on the other hand, found flow finger area to increase with grain size, but water supply rate showed no clear relation. Preferential flow paths in a warm, melting snowpack were measured by McGurk and Marsh (1995) to occupy between 3% and 8% of a cross-sectional area. In an arctic snowpack Marsh and Woo (1984) found the area to be around 22%. Williams et al. (2010) reported values ranging from 5% to 30%, and up to 95% where water pooled at hydraulic barriers. In firn, flow fingers are wider, giving the name "piping" (Hirashima et al., 2019).

Colbeck (1979b) argues that once flow fingers form, they persist. Since the snow in the flow fingers is wetter than the surrounding snow, metamorphism will occur more quickly there, increasing the hydraulic conductivity and maintaining preferential flow in the same area. Refreezing at the boundaries of the flow fingers could also reinforce this (Waldner et al., 2004). Flow fingers may be more persistent in PP than in RG due the rapid metamorphism dendritic crystals experience when they come into contact with liquid water (Waldner et al., 2004). However, Schneebeli (1995) found that flow fingers in snow subjected to multiple melt-freeze cycles moved laterally due to refreezing of the first flow fingers. Waldner et al. (2004) suggested that preferential flow paths may migrate gradually, as pores become saturated and water needs to find a different way down. Hirashima et al. (2019) found through observations in a cold lab and modeling that flow fingers migrate, steadily wetting more of the snow until a transition to matrix flow is reached. With an increased water flux the transition happened more quickly. Translocation only occurred when they simulated grain growth. Without it, the flow fingers remained stationary. When grain sizes and densities were high, meaning grain growth was low, as in ripe snowpacks, flow fingers moved little. Consequently, Hirashima et al. (2019) suggest that grain growth is the driver behind the transition between preferential flow and matrix flow, as flow fingers migrate over time, gradually making the snowpack more homogenous.

Juras et al. (2017) performed sprinkling experiments on ripe and non-ripe snow. They found that preferential flow paths formed quickly in non-ripe snow, increasing in efficiency as sprinkling went on, while the ripe snow showed signs of matrix flow. Outflow started comparably quickly in both snowpack types, but in non-ripe snow the rainwater arrived much earlier than in the ripe snow. In ripe snow, the added rainwater functioned as a piston on the water already in the snowpack, pushing it out first before rainwater arrived at the outflow. The ripe snowpack had more cumulative runoff than the non-ripe, though both had more runoff than the input, meaning melting occurred. Refreezing was observed in the non-ripe snowpack.

2.4. Slushflows

Slushflows are defined as "rapid mass-movements of water-saturated snow" by Hestnes (1985), a definition that Varsom (2023) still employs. The origin of the term "slushflow" traces back to Washburn and Goldthwait (1958, as cited in Hestnes, 1998), and it was officially adopted during the Circum-Arctic Slushflow Workshop held in Kirovsk, Russia in 1992 (Hestnes, 1998; Hestnes et al., 2012).

Slushflows were thought to predominantly be found in the Arctic, but can also happen in any region with seasonal snow (Onesti & Hestnes, 1989). The main slushflow season in Norway extends from November to May (Hestnes et al., 1994; Sidorova et al., 2001). Areas with maritime climates are prone to slushflows and can experience them throughout the winter due to rain. (Onesti & Hestnes, 1989). The western side of the mountains of coastal Norway are normally on the windward side when cyclonic fronts pass, therefore tending to receive more rain and greater amounts of sensible and latent heat from the atmosphere (Hestnes, 1998). In continental climates, the primary trigger for slushflows is spring melt, with areas exposed to incoming shortwave radiation from the sun being particularly susceptible (Hestnes, 1998; Scherer et al., 1998).

Typically releasing from and following streams and drainage channels, slushflows can also release from open slopes or swamps, resulting in less predictable paths (Hestnes, 1998; Onesti & Hestnes, 1989). The release areas for slushflows are flatter than other snow avalanches, rarely exceeding 30°, with 15° being the more normal, and as flat as 2° reported (Gude & Scherer, 1998; Hestnes, 1998). They also have exceptionally long runouts due to their high water content, often continuing until they reach lakes or fjords (Decaulne & Sæmundsson, 2006; Gude & Scherer, 1998). Slushflows, though usually less viscous than debris flows, can entrain rocks, trees, and other debris, increasing their flow density and thereby increasing their impact force (Kalland, 2022). If the snowline is at a high altitude, a mass-movement may initiate as a slushflow and subsequently transform into a debris flow as it continues down to areas without snow. The deposits from slushflows can often not be told apart from those from debris flows (Hestnes et al., 2012).

2.4.1. Slushflow release mechanisms

The fundamental conditions necessary for slushflow release involve the accumulation of rain- or meltwater, which increases the hydraulic pressure gradient within the snowpack until it surpasses a critical threshold, usually with snowpack LWC exceeding 15%. This is reached when the basal friction and cohesion of the snowpack are reduced to the point where they cannot hold the weight of the snowpack

(Gude & Scherer, 1995, 1998; Hestnes, 1998; Hestnes et al., 1994). Several factors contribute to this process, including the topography, ground conditions, snow depth and structure, and the volume and intensity of the water input. Typically, an impermeable layer is present, preventing liquid water from escaping (Hestnes et al., 1994). While permafrost conditions were previously considered necessary, it is now understood that bare rock, frozen or saturated ground, or in some cases, thick ice layers can fulfill the same purpose (Gude & Scherer, 1998). Snow depths between 25 cm and 150 cm are optimal for slushflow release (Gude & Scherer, 1995; Hestnes et al., 1994).

Slushflows are distinct from other types of snow avalanches in that they do not require an external trigger like a skier or a cornice collapse for their release (Gude & Scherer, 1995). However, there have been instances where slushflows were initiated by snow avalanches or rocks falling into lakes, creating large waves that flood into wet snow and form slushflows (Hestnes et al., 2012). Additionally, cornice collapses and snow avalanches can block streams, leading to water accumulation and slushflow formation (Decaulne & Sæmundsson, 2006). Human activity, particularly construction work that alters natural drainage channels, have also been known to trigger slushflows by causing liquid water to accumulate in new areas (Hestnes, 1998).

2.4.2. Slushflows and snow type

The type of snow present plays a crucial role in the stability of a snowpack when considering slushflow hazard. According to Hestnes (1998), new snow and coarse-grained snow (e.g., DH) are prone to slushflows because of their high porosity. In addition, the presence of DH at the snowpack base increases the likelihood of large slushflows. Large slushflows can also occur during springtime melting, even without DH (Hestnes et al., 1994). Conversely, fine-grained snow (e.g., RG) tends to be more stable due to the higher amount of inter-grain bonds, and the presence of ice layers and MFcr increases stability. Refreezing of the snowpack limits slushflow occurrences by stabilizing the snowpack and by limiting meltwater production during the day (Scherer et al., 1998). Solid ice layers can still provide tensile strength after three days of submersion (Hestnes, 1998; Hestnes et al., 1994). Hestnes et al. (1994) identified three primary snow categories that slushflows form in. The first is cohesionless new snow in the early winter. The second is coarse-grained snow, which may include DH at the base, throughout the winter. The third is stratified snowpacks featuring different snow types and crusts during the spring thaw.

Newer studies find comparable results. Skuset (2018) found snow that has undergone multiple melt-freeze cycles requires more water to release as a slushflow and Sund et al. (2024) state that MF snowpacks need

to be completely soaked for slushflows to release. PP and FC/DH are the grain forms most prone to slushflow release due to their porous nature (Sund et al., 2020, 2024). PP right on impermeable ground is the snow type that requires the least amount of water to release as a slushflow (Skuset & Sund, 2019; Sund et al., 2020). When the water supply volume and rate is high enough, the effect of snow type is less important and slushflows can occur in all grain forms. However, snowpacks consisting of PP or FC/DH are still likely to produce more slushflows than the less susceptible snowpacks (Sund et al., 2020, 2024).

When it comes to snow strength studies, Techel et al. (2011) found that FC and DH weakened at low water contents (LWC < 4%), while PP, DF, and small RG did not weaken at that same LWC. Schlumpf et al. (2024) found that RG and FC start losing shear strength immediately after first wetting. The strength reduction in the FC layers was significantly higher than the RG layers at the same LWC. They also found that DF strengthened when wet and attributed this to the strengthening effect of capillary cohesion outweighing the weakening effect of bond melting, at least for the duration of their experiment (< 2 h). Over a longer time, Schlumpf et al. (2024) suspected the DF layers would round and densify, and act more like their RG samples.

3. Methods

The primary objective of this study was to identify various snow types and measure LWC in the snowpack during weather conditions favorable for slushflow initiation. Measurements were strategically planned to capture the snowpack conditions before it became wet, and then during or following significant rain or melt events in the snow seasons of 2022-2023 and 2023-2024. The secondary objective was to evaluate the SLF Snow Sensor as a tool for measuring LWC in the field. This involved assessing its use based on the data collected for the primary objective. In addition, LWC values from the SLF sensor were compared with those derived from the standard hand wetness test. This comparison aimed to determine the efficacy of the hand test, which is less labor-intensive. Section 3.1 outlines the methods and tools used in the data collection process, while Section 3.2 describes how the obtained data was analyzed.

3.1. Data collection

3.1.1. Sampling strategy

An overview of the field locations is provided in Figure 8. The selection of field sites was governed by several criteria. Firstly, all sites needed to be accessible on short notice. In practice, this meant within 4-5 hours by car and/or less than 3 hours of hiking. The most limiting factor for site selection, both temporally and spatially, was the weather. The weather forecast was continuously monitored, and when reports indicated more than ca. 30 mm of rain in a day or sudden increases in temperature, I would get ready to mobilize. Proximity to weather stations was another consideration, since this would influence the accuracy of the meteorological data used to estimate precipitation and snowmelt (Section 3.1.3).

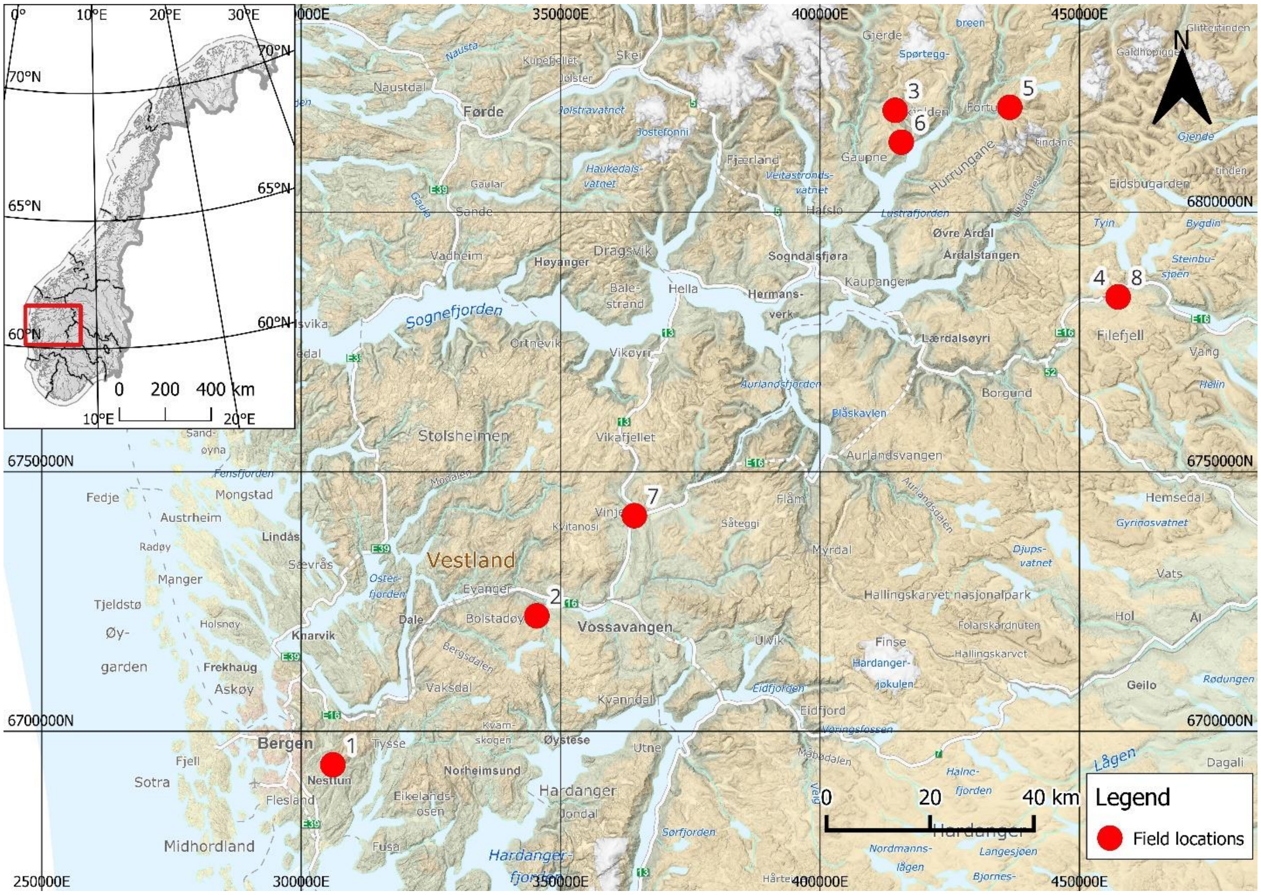

Figure 8. Overview of field locations. Red dots mark field locations. The numbers next to each dot represent experiment numbers.

Snow depth and type were also critical criteria. The ideal snow depth ranged from 50 to 100 cm, allowing for observation of water flow through the whole snowpack. This is also a good range for slushflow release (see Section 2.4.1). To find areas with appropriate snow depths, I used the tool Varsom Xgeo, which shows, among other things, snow depth data on a 1 km by 1 km grid (Varsom, 2024b). Although this resolution is coarse, it was an adequate indicator for areas with the desired snow depth. To find information about snow types, the tool Varsom Regobs was used to monitor snowpack observations (Varsom, 2024a). The observations are point registrations by both professional avalanche workers and nonexperts. Snowpack observations close-by, registered by avalanche professionals, could give the most representative indication of actual field conditions. Such data was not always available precisely in the area of interest. Therefore, snowpack data from Varsom Regobs needed to be considered in combination with applied knowledge of the formation processes of different snow types (see Section 2.2), to establish a qualified assumption of what snow type was most likely present.

When narrowing down potential areas, I looked for terrain conducive to water accumulation. This includes

flat ground, which helps prevent rapid runoff, and impermeable or fully saturated ground, e.g., swamps, lakes, and frozen ground, to deter water from infiltrating into the soil. A factor that could not be compromised was choosing safe terrain. Since much of the fieldwork was conducted during periods of high snow avalanche danger, slushflow hazard, and intense downpour, it was imperative to select a field site and tent spot away from any potential runout zones.

Balancing these criteria often required compromises, as not all conditions could be met at the same time. The need for specific snow depths and liquid precipitation confined the search to certain altitude belts. Too low, there would be no snow on the ground. Too high, precipitation would fall as snow, not rain. Consequently, proximity to weather stations was often deprioritized. Having access to a cabin or house was beneficial as it allowed me to go inside and dry my equipment. However, this option was not always available, so using a tent allowed for a greater degree of flexibility in site selection. Tent-based fieldwork demands more planning and safety considerations, especially in the weather conditions central to this study. Despite these challenges, effective field measurements were performed by selecting multiple potential locations and deciding which to go to prior to departure, based on the latest weather report and snowpack observations.

An overview of the field experiments is shown in Table 2. The main experiments were 2, 4, 5, 6, and 7, because they included two measurement series, allowing for analysis on LWC change with time. Of these, experiments 4 and 5 were taken during warm days with strong melting, and 2, 6, and 7 were done in rainy conditions. Experiments 1, 3, and 8 only contained a single measurement series. The data from these experiments could therefore not be part of a temporal analysis, but they were still used for the secondary objective, comparison with the hand wetness test. During experiment 7, two sub-experiments were conducted to measure the LWC in a flow finger (experiment 7.1), and to compare the use of dry vs wet snow density as input to the SLF sensor (experiment 7.2).

Table 2. Metadata for field experiments.

Experiment	Number of measurement series	Primary snow types	Source of water flux	Time between measurement series	Distance to weather station	Impermeable layer	Comment
1	1	MF, RG			5 km	Field without impermeable layer	Test of SLF sensor
2	2	IF	Rain	18.5 h	4 km	Swamp	
3	1	PP, MF			11 km	Field without impermeable layer	No second measurement due to snow instead of rain
4	2	MFcr, MF, RG, DH	Melt	6 h	3 km	Swamp	
5	2	MF	Melt	7 h	5 km	Swamp + lake	
6	2	PP, RGxf	Rain	21 h	11 km	Frozen gravel road	
7	2	DF, FC	Rain	17 h	400 m	Frozen gravel road/basal ice	
7.1	1	DF, FC	Rain		400 m	Frozen gravel road/basal ice	Flow finger measurement
7.2	1	DF, FC	Rain		400 m	Frozen gravel road/basal ice	Dry snow density as input
8	1	DF, RG, MF, FC, DH			3 km	Swamp	Comparison between SLF sensor and hand wetness test.

3.1.2. Measurement procedure

The start of each experiment consisted of noting down general information about the field location, such as GPS coordinates, date, and time. Secondly, meteorological data was recorded, including air temperature, wind speed, wind direction, cloud cover, and relative humidity. Air temperatures were measured at chest height (ca. 1,5 m) above the snow surface with a Cooper Atkins-DFP450W digital stem thermometer, which was validated in an ice bath prior to the fieldwork. Relative humidity was measured using a Skymaster SM-28 Handheld Weather Meter.

Following this, a traditional snow pit investigation was performed, including measuring snow temperature, layering, hardness, grain shape, and grain size, as described briefly in NVE's field handbook for snow observations (NVE, 2022), and more rigorously in Snow, Weather, and Avalanche Guidelines (SWAG) (American Avalanche Association, 2022), based on the standard methods from Fierz et al. (2009). An important part of the snow pit investigation was the hand wetness test, described in Table 1. The snow profiles were excavated to 2 – 3 m width and always went to the ground, since the snow-ground interface was of particular interest.

After completing the standard snow pit investigation, LWC measurements were conducted using an SLF Snow Sensor. It uses a capacitive sensor to measure the dielectric permittivity of a 45 × 95 × 17 mm sample of snow (FPGA Company, 2018). It can measure density, directly, in dry snow. When liquid water is present, a separate measurement of dry snow density is required to calculate LWC using empirical calibration equations (see Section 3.2.1). The equations are based on reference measurements of dry snow density and LWC measured by dilution methods. The SLF sensor can measure LWC in the range 0 – 20 vol. % at an accuracy of ± 0.5 vol. % (FPGA Company, 2018).

Due to the lateral variability in snowpack structures and flow patterns, Techel and Pielmeier (2011) recommend measuring LWC profiles several times with more than half a meter of horizontal distance. Figure 9 shows an example of the standardized measurement setup employed in this study. It consisted of three profiles in parallel, as a compromise between efficiency and the desire to acquire as much data as possible. The LWC columns were spaced > 50 cm apart, usually between 60 – 80 cm. For the SLF sensor to calculate LWC, snow density is required. A 250 cm^3 snow density wedge sampler was used to extract samples of snow, which were subsequently weighed with a spring scale to calculate density. Two samples were extracted from each measurement depth, usually from the two snow columns between the LWC profiles (Figure 9). If the snow got disturbed or a sample in any other way was compromised, I would take new density samples from the pit sidewalls at the relevant depth. The mean density value was used as

input for the SLF sensor. The LWC measurements need to be done on a flat surface (FPGA Company, 2018), so I used a shovel to carefully, but efficiently, dig out the snow in the LWC profile to a flat surface at the required depth. The SLF sensor was placed (not pressed) horizontally on the newly exposed snow surface, and two measurements were taken in each shovel-sized snow column, slightly spread apart. This resulted in six LWC measurements per depth.

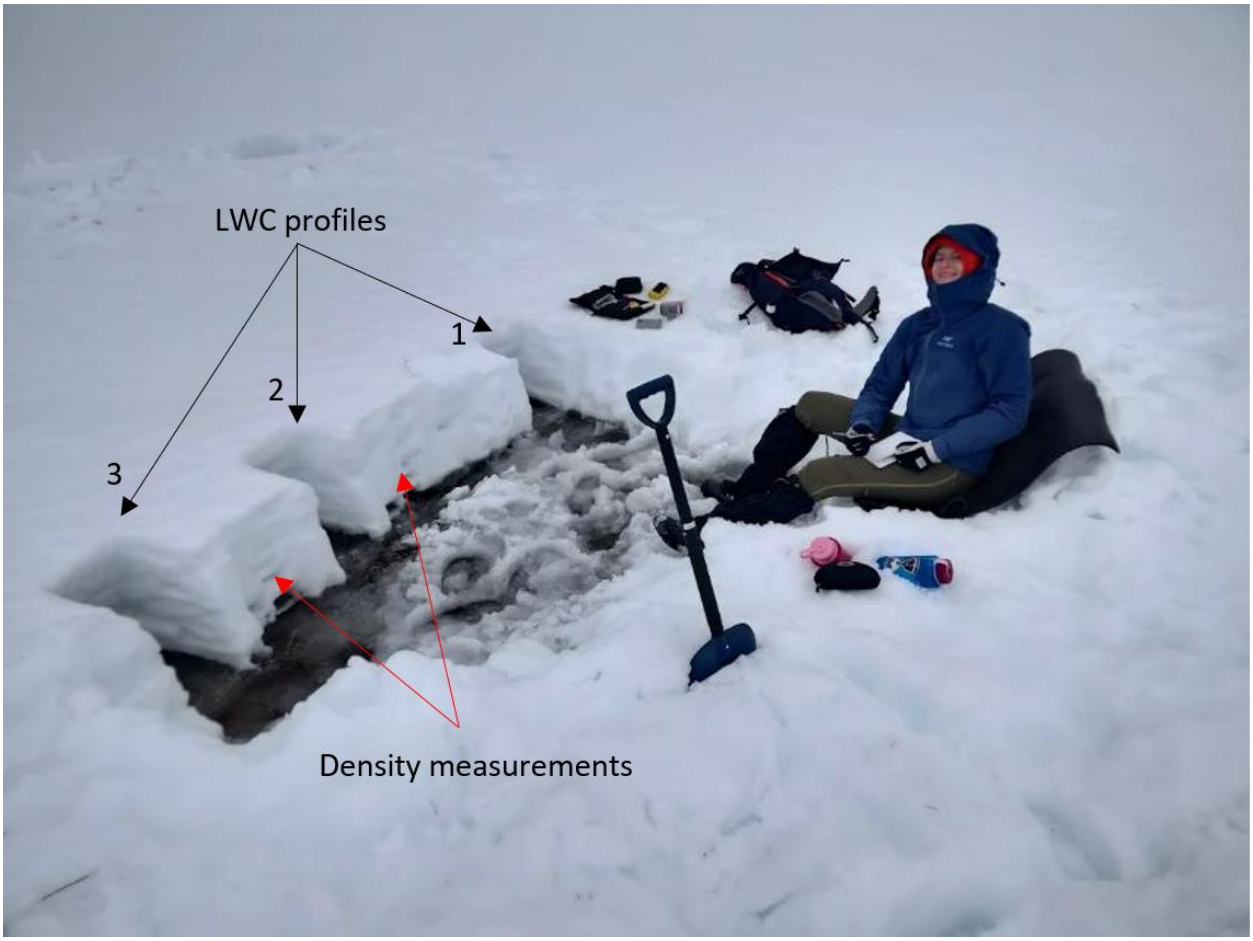

Figure 9. Field measurements being performed in experiment 5.

Since snow is such a good insulator, air temperatures and internal snowpack temperatures can be quite different. Once a previously buried snow surface is exposed to the air, the differences in temperature cause the snow to change rapidly. As multiple of the snowpacks I studied were isotherm, any additional heat would lead to melting, affecting the LWC measurements. Potential sources for added water between the moment of exposure and measurement include rain, shortwave radiation from the sun, and longwave radiation from the surroundings or bodies. Shea and Jamieson (2011) found that body heat from an

operator could penetrate more than 12 cm into the snowpack in 30 minutes. To minimize the exposure time of each measuring surface, I left the snow undisturbed as long as possible as a buffer and measured quickly after exposure. The LWC measurements were taken in this order:

1. Extract first density sample, weigh, and calculate density.
2. Extract second density sample, weigh, calculate density, and calculate mean density for that depth.
3. Put calculated mean density into the SLF sensor.
4. Excavate LWC profile 1 to required depth and perform two LWC measurements immediately.
5. Excavate LWC profile 2 to required depth and perform two LWC measurements immediately.
6. Excavate LWC profile 3 to required depth and perform two LWC measurements immediately.
7. Repeat steps 1 – 6 for each depth.

When I came back to the snow pit to do the follow-up LWC measurement series, I removed around 70 – 100 cm of snow, measured horizontally into the pit wall, to access snow that had not been thermally affected by previous work in the pit. An assumption I make is that snowpack properties remain the same over short lateral distances. I argue that is a reasonable assumption to make for snow layering, hardness, grain form, and grain size, since the weather conditions that cause this do not vary significantly over such short distances in the flat, open terrain I measured in. Percolation patterns and flow fingers, however, *do* vary over these distances, potentially leading to discrepancies between measurement series. The density and LWC measurements are inherently a destructive method, making it impossible to measure the exact same snow hours later. Having three LWC profiles compensates for some of this lateral variability and allows me to compare general trends in snow wetness regardless.

Another limitation during the measurements performed in the rain was wetting of the LWC sensor. According to the instruction manual (FPGA Company, 2018), water droplets should be removed from the sensor when conducting measurements. This was not always possible, due to the wet nature of the fieldwork. To limit this error, the SLF sensor was always kept sensor-side down. Additionally, when winds were calm enough, an umbrella was set up to keep the equipment drier.

Experiment 8 had to be cut slightly short due to equipment malfunction. Blowing snow froze onto the spring scale used to weigh snow samples, causing the mechanism to get stuck. Attempts to melt the refrozen snow in the field were only partially successful, as new snowdrift quickly froze the mechanism again.

3.1.3. Estimating rain and snowmelt

The amount of added water due to rain was estimated using the tool Varsom Xgeo for all experiments. The tool provides precipitation data interpolated from the surrounding weather stations (Varsom, 2024b). During experiment 6, a cylindrical garden rain gauge was also used to measure precipitation.

Snowmelt was also estimated using Varsom Xgeo, in a similar fashion. It uses an energy balance model and gets wind, cloud cover, radiation, and relative humidity data from a weather forecast model (MEPS-pp) (Varsom, n.d.). In addition, during experiments 4 and 5, snowmelt was estimated using the graphs in Figure 10, based on the energy balance model by Skaugen and Saloranta (2015). The correct graph was chosen by date, latitude, cloud cover, and relative humidity, and the input for each graph is wind speed and temperature. Experiments 4 and 5 were conducted in a single day, meaning data on air temperature, wind speed, and relative humidity was gathered regularly. This allowed for a coarse estimate of snowmelt to be made using Figure 10. A daily value for snowmelt was estimated by using the mean temperature and wind speed as input. Following this, a minimum value for snowmelt was calculated by multiplying the daily value with the duration between measurement series and dividing by 24 h. This assumes constant melting through day and night, which is incorrect, as the melting likely occurred during the day. A final, more realistic value was calculated based on how much of the day air temperatures remained above 0 °C. This is still a very rough estimate, and the absolute values must be interpreted with caution.

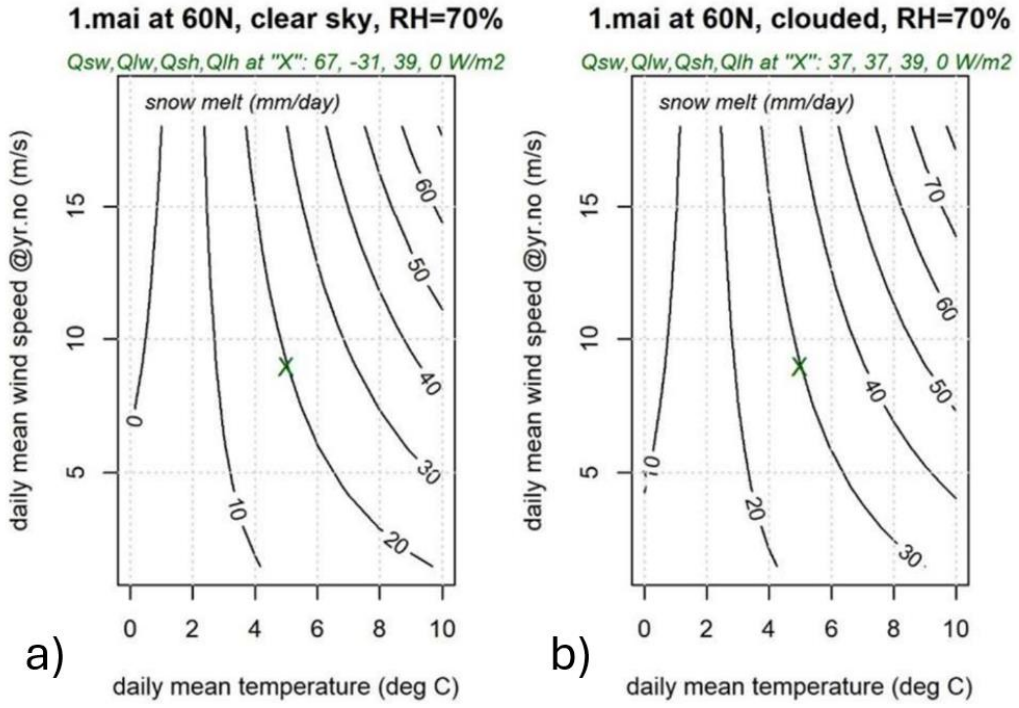

Figure 10. Snowmelt estimation graphs for a) experiment 4 and b) experiment 5 (Skaugen & Saloranta, 2015).

3.2. Data analysis

3.2.1. Processing

All LWC data from the SLF sensor and snowpack data from the field notes, such as snow type and hand wetness, were collected and organized in Excel, and from there, DataFrames in Python. Excel, Geogebra, and Python were used during data exploration, but all analyses and final plots were made with Python. Data points that may look like outliers were not removed, due to the unknown effect of lateral variability in snow. An "outlier" could in fact represent snowpack conditions accurately, and not be the result of measurement error.

A central processing step was performing a correction to the LWC values. Dry snow density is required as input for the SLF sensor to calculate LWC (FPGA Company, 2018). The instruction manual suggests measuring density before the snow gets wet, but this was not always possible, and wet snow density had to be used. Another option is to use the empirical calibration equations (5) and (6), supplied in the manual, to iteratively approach true density and LWC (FPGA Company, 2018).

$$\rho = -59.9383\epsilon_{dry} + 586.514\epsilon_{dry} \quad (5)$$

where: ρ = Density [kg m^{-3}]

$\epsilon_{dry} = \epsilon_{snow} - \epsilon_{air}$ [F m^{-1}]

$$\theta = 0.2715\Delta\epsilon^3 - 2.6877\Delta\epsilon^2 + 10.337\Delta\epsilon \quad (6)$$

where: θ = Volumetric liquid water content [%]

$\Delta\epsilon = \epsilon_{wet} - \epsilon_{dry}$ [F m^{-1}]

This was done as following:

1. Solve for the lower value of ϵ_{dry} in equation (5) using measured ρ.
2. Solve for $\Delta\epsilon$ in equation (6) using measured θ.
3. Calculate ϵ_{wet} by $\epsilon_{wet} = \Delta\epsilon + \epsilon_{dry}$.
4. Calculate an updated ρ by subtracting mass of water from measured ρ.
5. Solve for new value of ϵ_{dry} using updated density.
6. Calculate new value of $\Delta\epsilon$ using $\Delta\epsilon = \epsilon_{wet} - \epsilon_{dry}$.

7. Calculate updated θ using equation (6) and $\Delta\epsilon$ from step 6.
8. Repeat steps 4 to 7 until the updated ρ and θ values approach a number. In this study, 10^4 iterations were used.

The maximum range of the SLF sensor is 20% (FPGA Company, 2018), and raw LWC values for slushy snow went into the hundreds, so to make data management easier, all values above 20% were set to 20%. In experiments 5, 6, and 7, some measurements were taken in standing water at the base of the snowpack. These values were all set to 15% for plot clarity (Section 4.1). During the fieldwork, half-classes of hand wetness (e.g., D – M or M – W) was used in a few cases. During processing, the wettest class was chosen (e.g., M – W are treated as W), to reduce the number of categories.

3.2.2. Statistical methods

Due to the skewed distribution of the LWC data, the median was used as the measure of central tendency. Hypothesis testing using permutation was utilized to test whether median LWC at each depth differed significantly between measurement series. This non-parametric test was chosen because it makes fewer assumptions about the distribution of the underlying data. Specifically, it does not require the data to come from a normal distribution and does not assume equal sample size or variance between groups.

For each depth, the difference in median LWC between the first and second timestamp was calculated. The data from both timestamps were pooled, then randomly resampled without replacement into two variables, each containing six data points, like the original data. A new median was calculated for this permutation. This process was repeated 10^6 times to create a distribution of differences in median. The p-value was found by calculating the fraction of permutations where the difference in medians was greater than the observed difference. To check for significant differences in either direction, this test was two-tailed. A potential weakness to this method is the small sample size of only six data points. The limited number of unique permutations might affect the power of the test, though the extent is not known.

The same test was also used to determine if median LWC differed significantly between snow samples of varying hand wetness class. In this case, the potential limitations due to sample size do not apply.

4. Results

Results from the main experiments of this study (2, 4, 5, 6, and 7) are presented in Section 4.1. While most experiments were conducted in snowpacks consisting of more than one snow type, they are presented under the title of the main snow type of interest for that experiment. Results from the comparison between the hand wetness test and the SLF sensor, using data from all experiments, are presented in Section 4.2.Additional snowpack data for all experiments can be found in Appendix A: Snow profiles.

4.1. LWC profiles in slushflow-inducing weather

4.1.1. Ice layer results

Experiment 2 was conducted at Træn, Voss during a rainstorm in late January 2023. The snowpack consisted of a surface layer of DF from the previous snowfall over primarily MF, separated by a thick ice layer of around 4 – 5 cm at 10 cm depth (Appendix A2). Figure 11 shows the LWC profiles taken before (T1, blue) and during (T2, red) the storm. The T1 (Træn 1) measurement series was taken 21:30 28.01.23, around 30 min after it started raining. The uppermost snow layer was thin, but still hard MFcr. Although the snow above the ice layer was near 0 °C (Appendix A2), the first measurement at 5 cm was nearly completely dry ($\theta_m = 0.1\%$). However, the snow directly above the ice layer (10 cm depth) was already moist ($\theta_m = 1.9\%$). The temperature of the snow was slightly subfreezing below the thick ice layer, indicating a dry snowpack, with the coldest temperature being -1.0 °C at 25 cm depth. The dryness was confirmed by the LWC measurement, which showed 0% LWC from 20 to 70 cm. The T2 measurement series was taken 16:00 29.01.23, after 18.5 hours had elapsed. Estimated values for rain from Varsom Xgeo were 53 mm between 18:00 28.01. and 18:00 29.01., meaning slightly less than 53 mm arrived between T1 and T2. The snow above the ice layer showed a significant increase in LWC, from 0.1% to 8.5%. Under the ice layer, however, the snow remained dry. The snowpack was not noticeably thinner at the T2 measurement series.

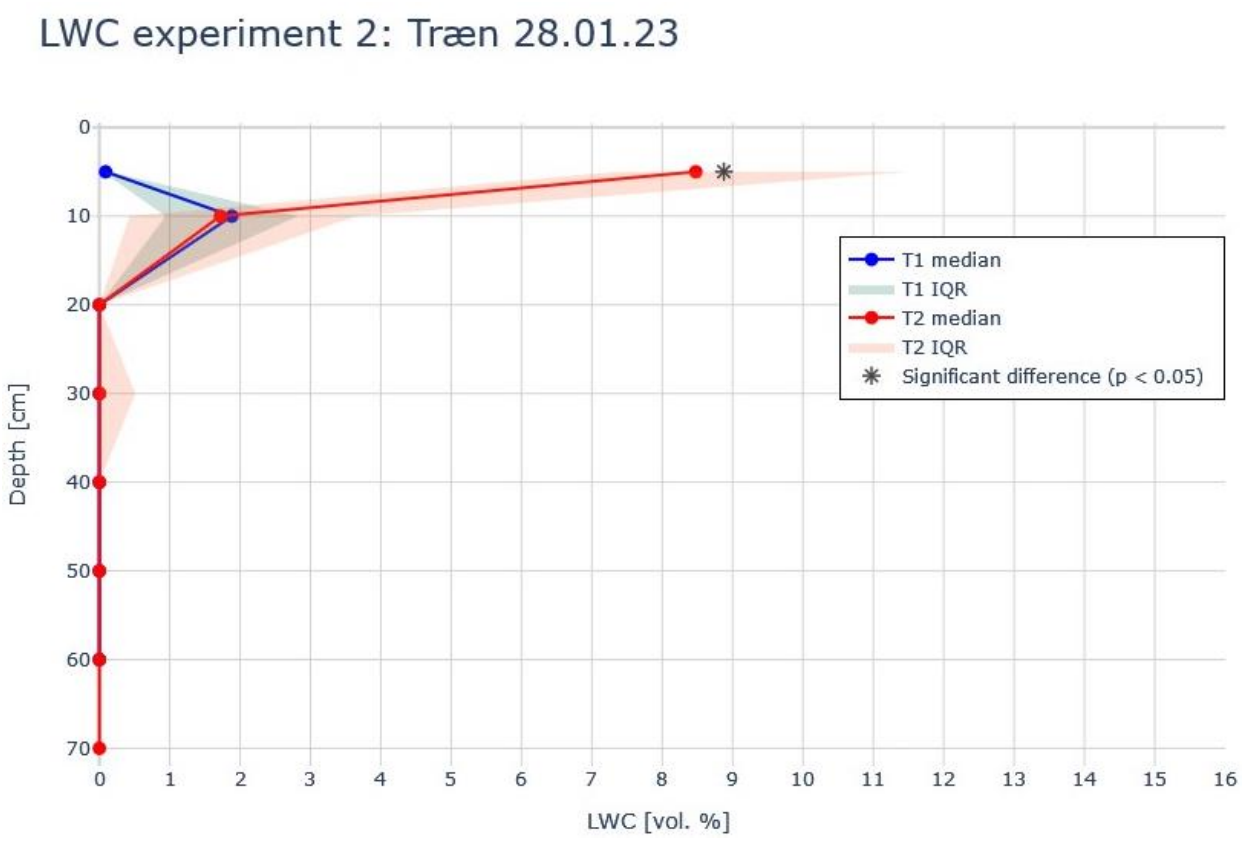

Figure 11. Comparison of LWC profiles in experiment 2, where the snowpack contained a 4-5 cm thick IF at 10 cm depth, between DF above and MF below. The first measurement (T1, blue) was taken at 21:30, and the second measurement (T2, red) was taken at 16:00 the following day. Dots represent median LWC at their respective measurement depths, solid lines indicate linearly interpolated median LWC, and shaded areas denote the interquartile range. Asterisks (*) mark depths where the difference in median LWC between T 1 and 2 is statistically significant ($p < 0.05$). The estimated precipitation and snowmelt between the measurements was at the most 53 mm.

4.1.2. Melt form results

Experiment 5 was done on a partly cloudy day near Bingen hans Sjur in Luster. The snowpack was isothermal throughout, and MF grains comprised the entirety of its depth (Appendix A.5). The field site was set between a lake and a marsh, due to the impermeable nature of the ground conditions. Figure 12 shows both LWC profiles taken 14.05.23, the first at 10:00 (BHS1, blue), and the second at 17:00 (BHS2, red). For BHS1, the water table could be found between 40 and 45 cm, as the leap in LWC at the bottom of the profile indicates. 7 hours after the first measurement series, the water table had risen 5 cm, not allowing for LWC measurements to be taken at 45 cm depth for BHS2. There was an estimated snowmelt of 26 mm, with a minimum value of 9 mm, and 32 mm melt for the whole day. Snowmelt retrieved from Varsom Xgeo was 29 mm for the whole day. Snowpack depth changed less than 1 cm between BHS1 and BHS2. Median LWC increased at every depth except at 10 cm, but only four of the depths were

statistically significantly wetter (Figure 12). The variability was relatively similar for all depths, the IQR typically spanning 3% – 4% LWC.

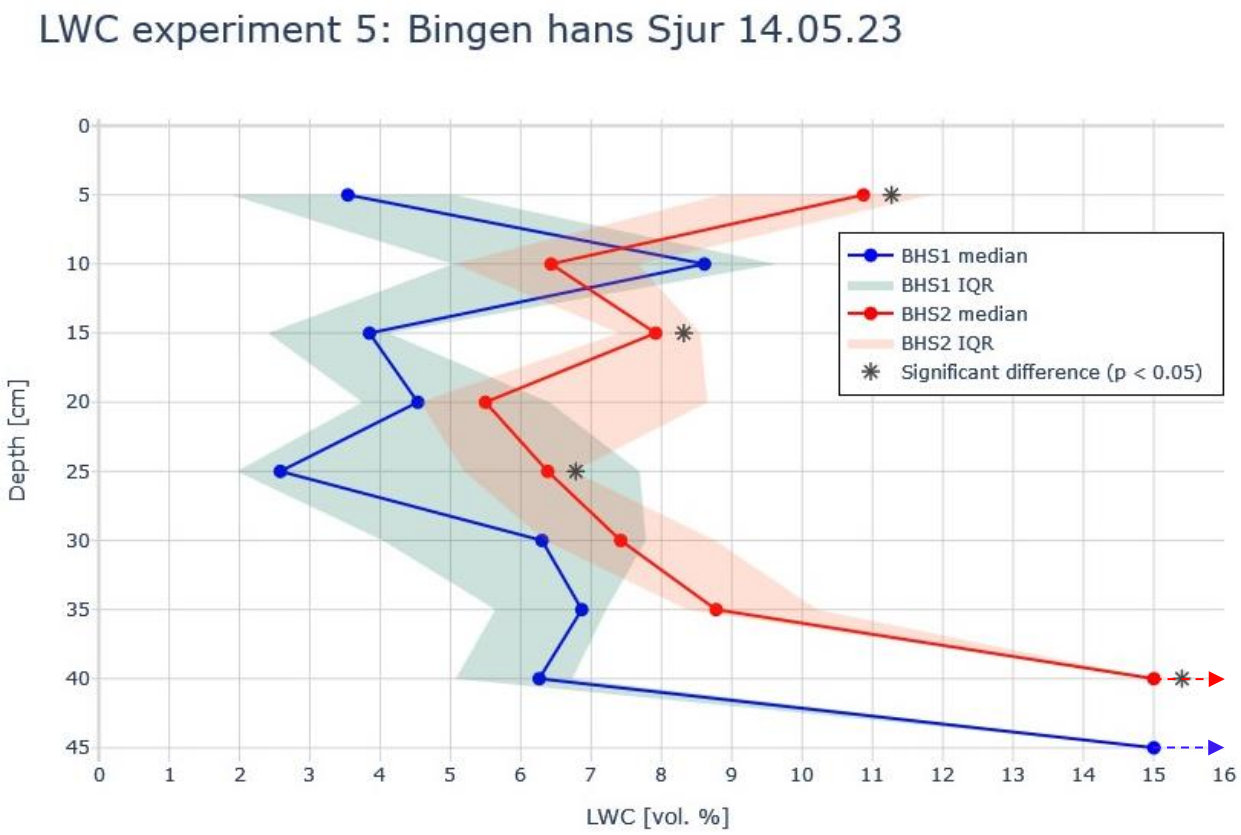

Figure 12. Comparison of LWC profiles in experiment 5, where the snowpack consisted of MF. The first measurement (BHS1, blue) was taken at 10:00, and the second measurement (BHS2, red) was taken at 17:00. Dots represent median LWC at their respective measurement depths, solid lines indicate linearly interpolated median LWC, and shaded areas denote the interquartile range. Asterisks (*) mark depths where the difference in median LWC between BHS 1 and 2 is statistically significant (p < 0.05). LWC values above 15% are shown as 15%. The estimated snowmelt between the measurements was 26 mm.

4.1.3. Depth hoar results

Experiment 4 was conducted on a sunny day at Filefjell. The snowpack was stratified, with layers of RG, MF, intermittent crusts and ice layers, and a 25 cm thick basal layer of DH (Appendix A.4). The field site was chosen due to the underlying swamp, but excavation revealed heather, not saturated marshlands, meaning the impermeability was questionable. Figure 13 shows the two LWC profiles taken 21.04.23, the first at 11:00 (FF1, blue), and the second at 17:00 (FF2, red). The estimated snowmelt over this 6-hour timespan was 9 mm, with a minimum value of 3 mm, and 13 mm for the whole day. Snowmelt retrieved from Varsom Xgeo was 11 mm for the whole day. The snowpack did not get noticeably thinner at the FF2 measurement series. The results show that in general, the snowpack started drier at the surface and wetter

at the bottom, then shifted to wetter at the surface and drier at the bottom. Though not all the differences between FF1 and FF2 are statistically significant, the ones that are show this pattern. The profiles show large variation in LWC, particularly in the upper half, with the FF2 IQR spanning from 1.4% to 10.8% LWC at 30 cm depth. The temperature was 0 °C everywhere but the top 10 cm, which froze during the night and was warming at 09:40, when the first temperature profile was taken. As the day went on, the near-surface temperatures rose to 0 °C and the upper snow layers got softer as they melted. Liquid water could be seen pooling at stratigraphic boundaries in the top 40 cm of the snowpack, the clearest examples being at 30 cm depth and 40 cm depth. The DH crystals at the base of the snowpack were recognizable as DH for both FF1 and FF2 but showed signs of partial melting.

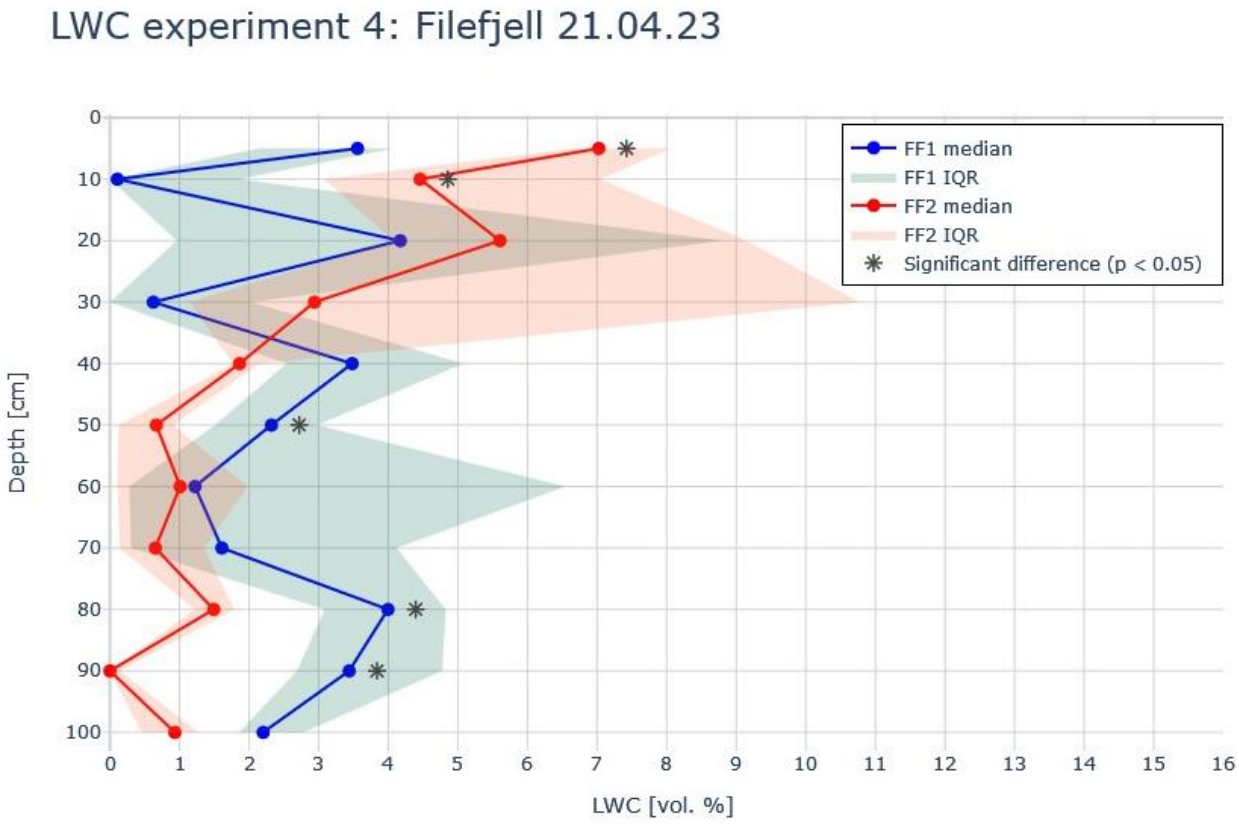

Figure 13. Comparison of LWC profiles in experiment 4, where the snowpack consisted of MF, RG, intermittent MFcr, and a thick basal layer of DH. The first measurement (FF1, blue) was taken at 11:00, and the second measurement (FF2, red) was taken at 17:00. Dots represent median LWC at their respective measurement depths, solid lines indicate linearly interpolated median LWC, and shaded areas denote the interquartile range. Asterisks (*) mark depths where the difference in median LWC between FF 1 and 2 is statistically significant ($p < 0.05$). The estimated snowmelt between the measurements was 9 mm.

4.1.4. Precipitation particles/decomposing and fragmented particles results

Experiment 6 was done at Røssesete, Luster, during a storm in mid December, 2023. The snowpack had a layer of fresh PP on top of RGxf, with a layer of DH at the base (Appendix A.6.). The field location was set on a gravel parking lot, with the frozen ground acting as an impermeable layer. The temperature at the bottom of the snowpack was -0.9 °C. Figure 14 shows the LWC profiles taken before (RS1, blue) and during (RS2, red) the storm. The RS1 measurement was taken 18:00 15.12.23. The whole snowpack was colder than 0 °C (minimum temp = -2.5 °C) and the LWC measurements also show a completely dry snowpack. The RS2 measurement was taken 15:00 16.12.23, 21 hours later. According to Varsom Xgeo, the estimated rain and snowmelt, between 18:00 15.12. and 18:00 16.12., was 39 mm and 3 mm, respectively. For this experiment, I also used a garden rain gauge to measure precipitation. It was set up at 18:00 15.12. before any rain arrived. At 12:00 the next day it was overflowing, meaning more than 50 mm of rain. At 15:00, when I started measuring RS2, the rain gauge showed another 12 mm. The snowpack got ca. 10 cm thinner between RS1 and RS2. Most of the difference in depth came from the surface layer of PP, which changed from 19 cm to 10 cm. The median volumetric LWC, θ_m, for RS2 shows very wet snow ($\theta_m = 12.8\%$) in the top 5 cm of the snowpack, then much drier snow ($\theta_m = 1.0\%$) at 10 cm. RS2 gets gradually drier from 10 cm to 30 cm, but the difference between RS1 and RS2 is not significant there. The bottom of the snowpack, previously containing DH, was completely saturated, the frozen gravel acting as a plug, not allowing water to infiltrate into the ground.

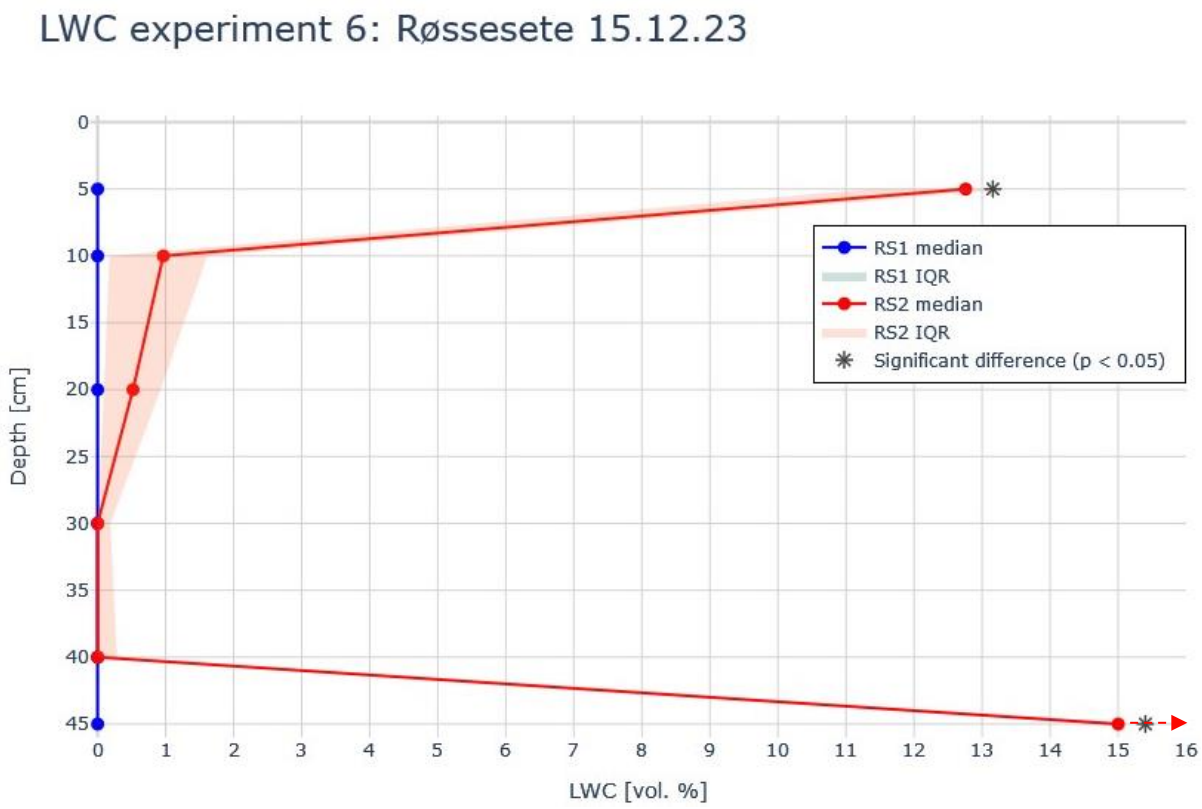

Figure 14. Comparison of LWC profiles in experiment 6, where the snowpack consisted of PP over RGxf. The first measurement (RS1, blue) was taken at 18:00, and the second measurement (RS2, red) was taken at 15:00 the following day. Dots represent median LWC at their respective measurement depths, solid lines indicate linearly interpolated median LWC, and shaded areas denote the interquartile range. Asterisks (*) mark depths where the difference in median LWC between RS 1 and 2 is statistically significant ($p < 0.05$). LWC values above 15% are shown as 15%. The estimated precipitation and snowmelt between the measurements was around 40 mm, according to Varsom Xgeo, and at least 62 mm measured with a rain gauge.

Experiment 7 was conducted at Vinje, Voss during a storm in late January 2024. The snowpack contained a surface layer of refrozen MF, a layer of DF, then a thick layer of FC, and a solid basal layer of ice (Appendix A.7.). The field site was the gravel floor of a quarry, with the frozen and ice-covered ground acting as the impermeable layer. Figure 15 shows the LWC profiles taken at the start of the storm (V1, blue) and during the storm (V2, red). The V1 measurement was taken 23:00 21.01.24. It had already started raining, so at 5 cm depth the temperature was 0 °C and the snow was wet ($\theta_m = 6.1\%$). The remainder of the snowpack was relatively cold (min temp = -3 °C) and dry ($\theta_m = 0\%$). The V2 measurement was taken 16:00 22.01.24, 17 hours later. Estimated precipitation and snowmelt 18:00 22.01. and 18:00 22.01. was 26 mm and 3 mm, respectively. The snowpack became ca. 5 cm shorter between V1 and V2, primarily due to change of thickness in the upper layers. A temperature profile taken at 15:30 showed 0 °C throughout the snowpack. There were statistically significant increases of LWC at the

surface, at the base of the snowpack, and at 40 cm depth, The rest of the snow was measured to be dry, despite the isothermal conditions.

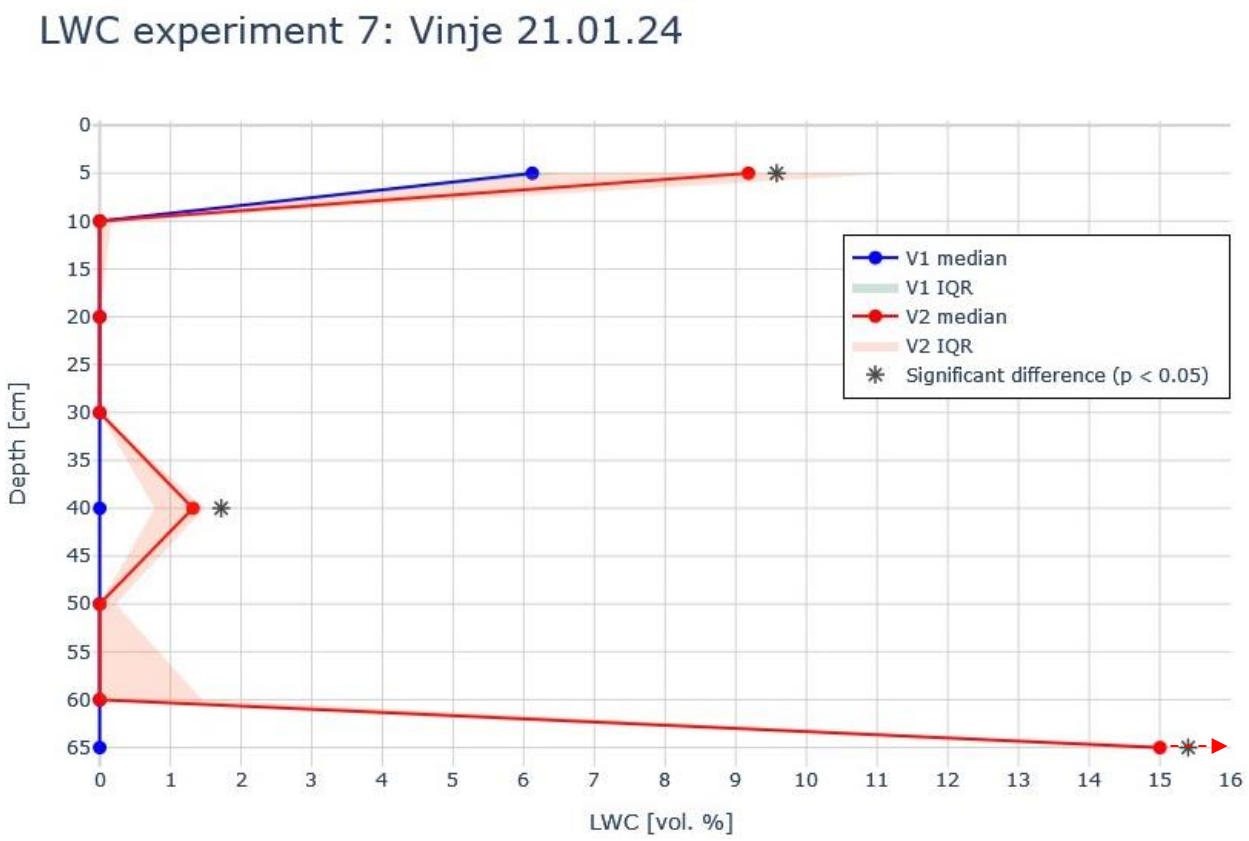

Figure 15. Comparison of LWC profiles in experiment 7, where the snowpack consisted of DF over FC. The first measurement (V1, blue) was taken at 23:00, and the second measurement (V2, red) was taken at 16:00 the following day. Dots represent median LWC at their respective measurement depths, solid lines indicate linearly interpolated median LWC, and shaded areas denote the interquartile range. Asterisks (*) mark depths where the difference in median LWC between V 1 and 2 is statistically significant ($p < 0.05$). LWC values above 15% are shown as 15%. The estimated precipitation and snowmelt between the measurements was nearly 30 mm.

4.1.5. Flow finger observation

The snow measured in experiment 7 (Figure 15) with the SLF sensor was very dry given the amount of rain during the night and having an isothermal temperature profile. In addition, water was reaching the base of the snowpack, despite the measurements showing a dry snowpack interior. After excavating a substantial area when performing experiment 7, it became clear that a network of dimples in the snow surface indicated the presence of flow fingers (Figure 16). A very rough estimate based on photos taken in the field puts the average minimum horizontal distance between flow finger dimples between 40 cm and 60 cm, and the diameter of the saturated zone to be around 10 cm. The observed and excavated flow fingers were vertical and continuous, with wet snow appearing in a column from snow surface to base.

Wet zones and flow fingers starting below the snow surface due to lateral flow after initial surface infiltration were not directly observed during experiment 7.

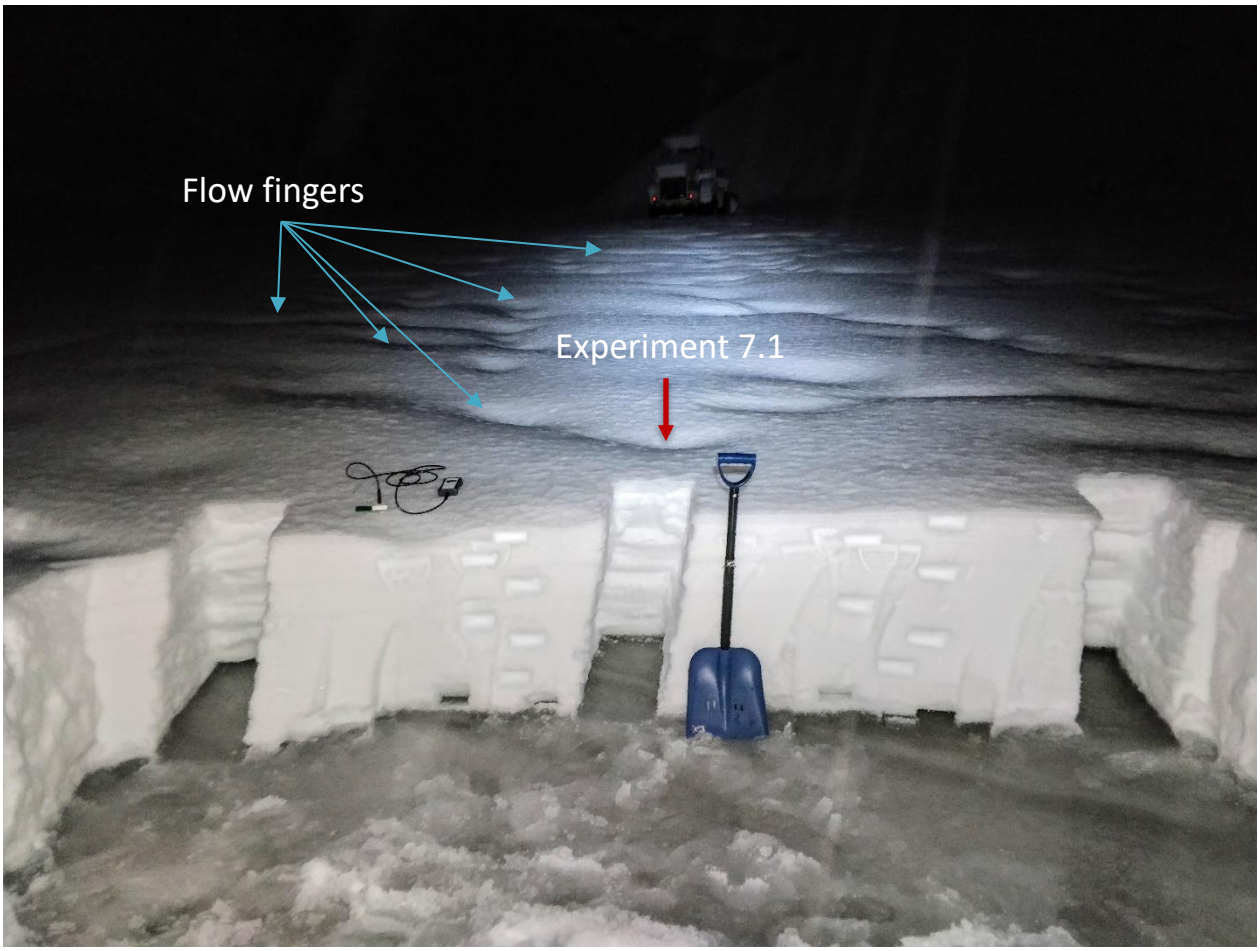

Figure 16. Photo of snow profile excavated for experiments 7, 7.1, and 7.2. The photo was taken at 16:53, right after experiment 7 was completed. Flow finger dimples are visible in the background. The marked flow finger dimple was excavated in experiment 7.1.

LWC values from the excavated preferential flow path marked as “experiment 7.1” in Figure 16 can be seen in Figure 17. V2 (green) is the LWC profile taken in experiment 7 at 16:00 using the standard method. VFF (purple) shows the LWC profile from the flow finger, measured directly afterwards, at 17:00. VFF shows significantly higher median LWC values than V2, between 9% and 14% for everything over the water table at 65 cm depth.

Figure 17. Comparison of LWC profiles in experiment 7.1, showing the difference in LWC between a flow finger and the surrounding snowpack. The surrounding snow (V2, green) was measured at 16:00, and the flow finger (VFF, purple) was measured at 17:00. The surrounding snowpack consisted of DF over FC, while the snow in the flow finger had already turned into MF. Dots represent median LWC at their respective measurement depths, solid lines indicate linearly interpolated median LWC, and shaded areas denote the interquartile range. Asterisks (*) mark depths where the difference in median LWC between V2 and VFF is statistically significant ($p < 0.05$). LWC values above 15% are shown as 15%.

4.1.6. Capillary barrier observation

A second observation made during experiment 7 was that certain wet layers that were clearly visible with the naked eye were not registered using the rigid preset measurement depths. Figure 18 shows two wet layers that were not detected using the SLF sensor. The lower wet layer appeared right above the boundary between DF and FC. The upper wet layer appeared within what I had identified as one homogenous layer of DF. Both these layers can also be seen spanning the width of the profile in Figure 16, attesting to a lateral extent of at least 3 – 4 m.

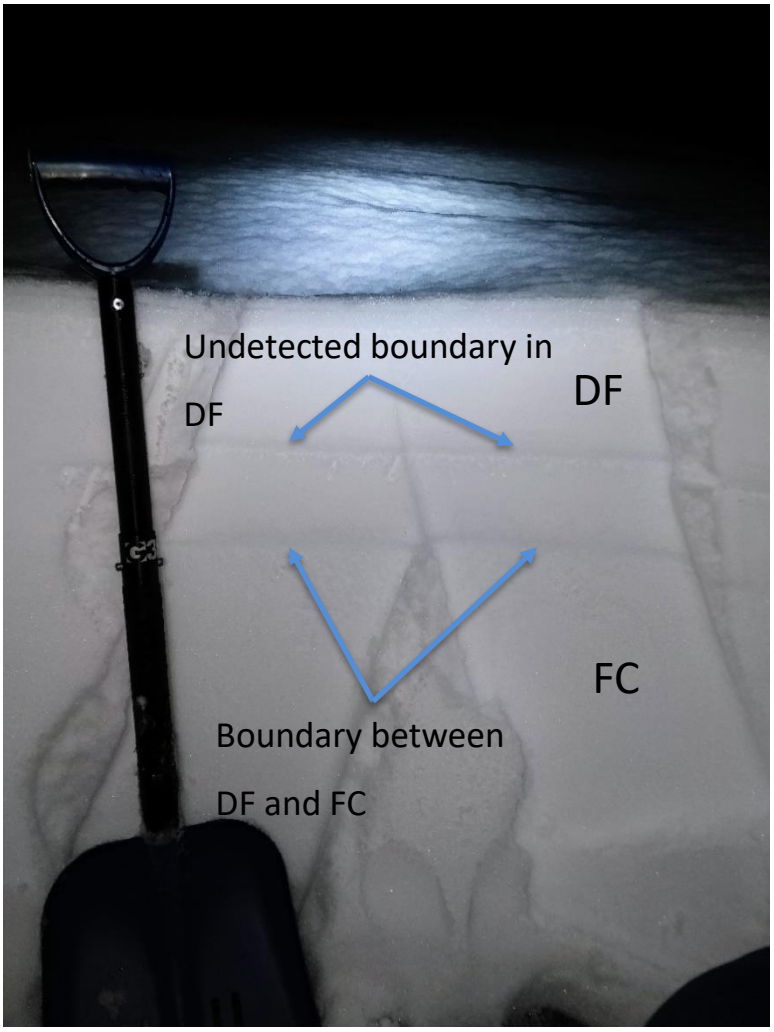

Figure 18. Photo of wet layers surrounded by dry snow during experiment 7. One of the wet layers appeared at the boundary between DF and FC. The upper wet layer appeared within the apparently homogenous DF layer.

4.1.7. Dry vs. wet snow density

During experiment 7 I had the option to measure snow density before most of the snow received any liquid water. In experiment 7.2 (Figure 19), I compare LWC profiles taken shortly after one another, V2 (green) using wet snow density as input and shown with corrected values, and VDSD (purple) using dry snow density as input. The results show statistically significant differences at each depth except the surface, 30 cm depth, and the base of the snowpack.

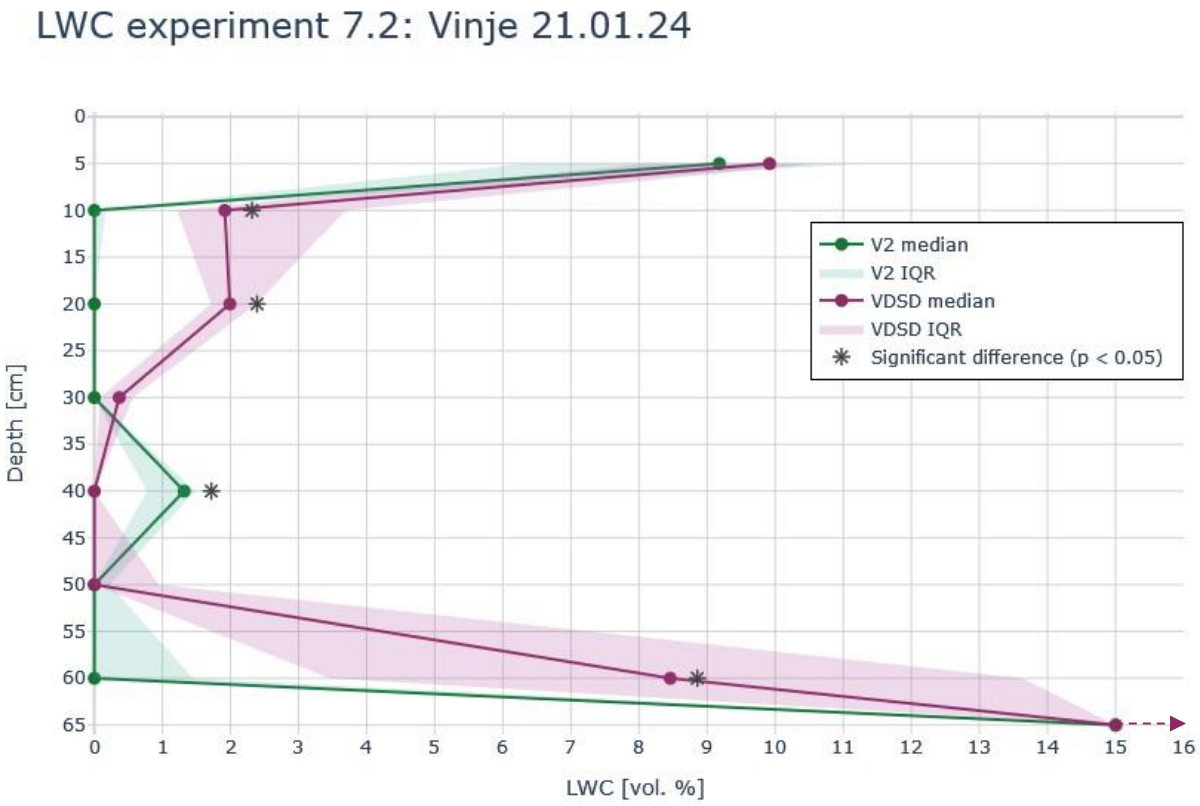

Figure 19. Comparison of LWC profiles in experiment 7.2, showing the difference between using wet or dry snow density as input. The measurement using wet snow density as input (V2, green) was taken at 16:00, and the measurement using dry snow density as input (VDSD, purple) was taken at 15:30. Dots represent median LWC at their respective measurement depths, solid lines indicate linearly interpolated median LWC, and shaded areas denote the interquartile range. Asterisks (*) mark depths where the difference in median LWC between V 2 and VDSD is statistically significant ($p < 0.05$). LWC values above 15% are shown as 15%.

4.2. Hand wetness test vs SLF sensor

Figure 20 shows a comparison between LWC values measured using the SLF sensor and hand wetness levels classified using Table 1. Data from all experiments was included in the analysis. LWC appears to increase exponentially with hand wetness class. The medians for all groups are statistically significantly different from each other.

The results from this study are also compared to the values in *The International Classification for Seasonal Snow on the Ground* by Fierz et al. (2009) and the results from Techel and Pielmeier (2011) who used a Snow Fork and a Denoth meter to investigate the same properties.

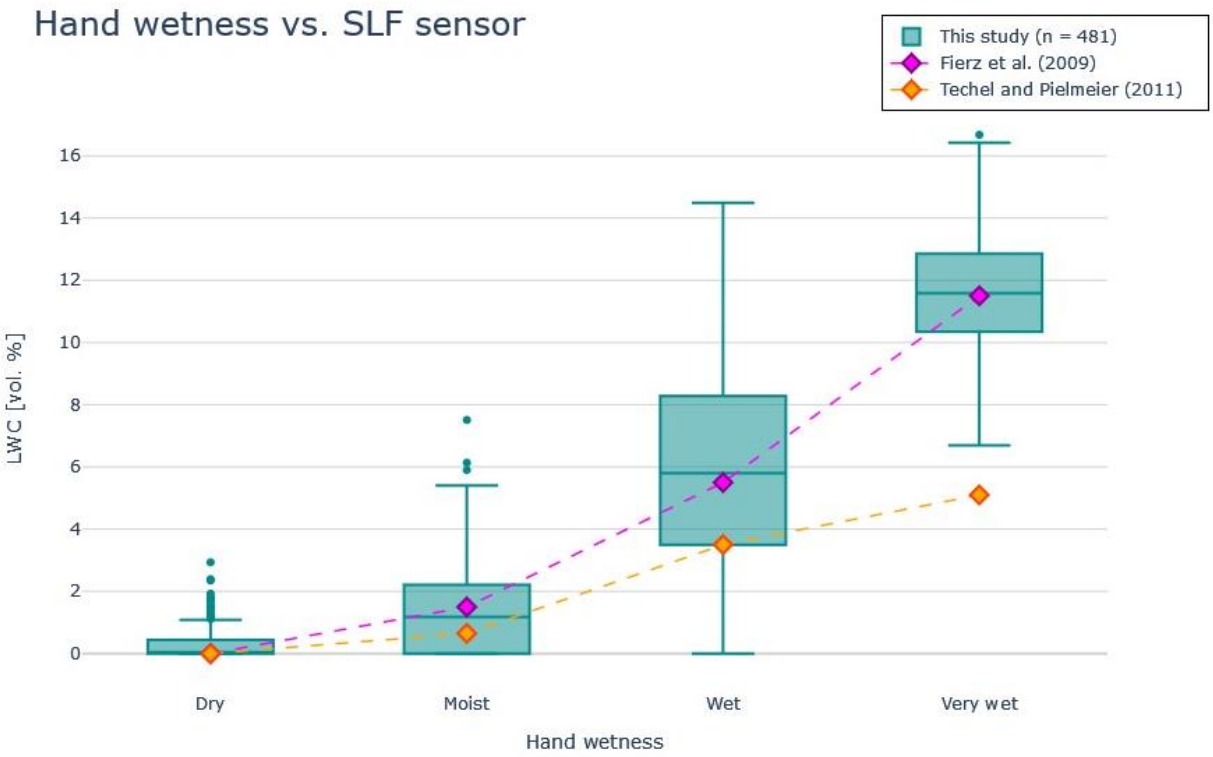

Figure 20. Box plot comparing liquid water content estimated with the hand wetness test with measurements from the SLF sensor. For comparison, the mean values from Fierz et al. (2009) and median values from Techel and Pielmeier (2011) are shown.

5. Discussion

5.1. Interpretation of field results

5.1.1. Ice layer and melt-freeze crust discussion

The most distinct ice layers in all experiments were a 4 – 5 cm thick ice layer at 10 cm depth in experiment 2 (Appendix A.2) and a 5 – 6 cm thick layer of basal ice in experiment 7 (Appendix A.7.). The basal ice in experiment 7 acted as an impermeable layer, causing liquid water to collect at the bottom of the snowpack and form a water table. The pooling water and fully saturated snow can be seen by greatly increased LWC at 65 cm depth in Figure 15 and as free-standing water and slush at the bottom of the snow pit in Figure 16. The ice layer in experiment 2 was also functionally impermeable, as virtually no liquid water was detected under it even after it had rained 50 mm, as shown in Figure 11. The snow directly above the ice layer in experiment 2 was classified as very wet, but there was no standing water, despite the snowpack receiving similar amounts of precipitation as experiment 7 and the ice layer being much higher in the snowpack. This suggests that the incoming rainwater could not pool atop the ice layer but flowed laterally away from the field site, potentially being channeled to a flow finger or topographic depression on the ice layer. There it could have formed a subsurface “lake”, slowly melting through the ice layer before percolating deeper.

These results match well with how permeability barriers are described in the literature (e.g., Clerx et al., 2022; Eiriksson et al., 2013; Schlumpf et al., 2024; Techel & Pielmeier, 2011; Webb et al., 2018), where ice layers, having a much lower permeability than the overlying snow, prevent vertical percolation of water and cause lateral flow instead. The lateral extent of ice layers can vary, from layers only tens of centimeters long (Marsh & Woo, 1984, 1985), to meters or tens of meters (Webb et al., 2018). Since the snow pits excavated during the experiments never covered a horizontal distance more than about five meters, the lateral extent of the ice layers cannot be determined beyond that. The ice layer in experiment 2 was continuous at least on the meter-scale, and due to its thickness, solidity, and uniformity across the snow profile I suspect it stayed continuous into the tens of meters.

Thinner ice layers and melt-freeze crusts (MFcr) were observed in multiple experiments. In experiments 2, 4, and 7 the topmost snow in the first measurement was a thin (< 1 cm) MFcr stemming from the cold air temperatures prior to the melting observed during the experiments (see Appendix A.2, Appendix A.4, and Appendix A.7. for snow profiles). In all those locations the MFcr was completely broken down by water at the time of the second measurement. Experiment 4 showed the clearest example of this, where the top 20 cm of snow were knife hard after nighttime freezing and snow temperatures were below 0 °C when

measuring in the morning. During the day, the top 20 cm softened considerably from melting due to incoming solar radiation as θ_m increased by around 3 – 4% at 5 cm and 10 cm depth (Figure 13). The melting of melt-freeze crusts at the snow surface matches the literature, since the surface receives the brunt of the added energy from precipitation and radiation (Gude & Scherer, 1998).

The snowpack in experiment 4 had multiple thin layers of MFcr, as well as two IF layers (1.5 cm thick at 60 cm depth and 1 cm thick at 77 cm depth) farther from the snow surface (Appendix A.4). Pooling water could be seen at the uppermost of these layers, especially at the 1 cm thick MFcr at 40 cm depth. None of the layers appeared to be fully impermeable, as liquid water could be found both above and below them.

The results as a whole indicate that thin (< 1.5 cm) ice layers and melt-freeze crusts either melt or are not impermeable enough to prevent water from percolating through, while thick (> 4 cm) layers do prevent water from reaching the underlying snow, at least for a time. This effect might, however, be constrained to the snow pit scale of a few meters. At a slightly larger scale, ice layers may concentrate the flow of liquid water into flow fingers (Marsh & Woo, 1984). In some cases, this could speed up the vertical flow and allow water to reach the bottom of the snowpack quicker than if there had been no ice layer (Furbish, 1988), as described in Section 2.3.1.

5.1.2. Melt form discussion

Melt forms were the most common snow type in all experiments, being present in all snowpacks prior to the first LWC measurement (Appendix A: Snow profiles). The only exception is the snow measured in experiment 6. This may partially be a result of the sampling strategy (Section 3.1.1). Although I aimed to investigate a variety of snow types, the requirement for warm weather meant MF was the easiest grain type to find. The two springtime experiments, 4 and 5, had isothermal snowpacks (at least for parts of the day), again making MF a common grain type. Experiment 4 is discussed in greater detail in Sections 5.1.1 and 5.1.3, so experiment 5 will be the focus of this section.

The snowpack in experiment 5 consisted entirely of MF (Appendix A.5), and revealed a general increase in LWC between measurements BHS1 and BHS2 (Figure 12). After 7 hours of melting due to solar radiation, the snowpack also appeared wetter to eye and touch. The largest increases in LWC were at the surface, where the incoming shortwave radiation caused the most melting, and at the base, where the water table rose and wetted more snow. In the rest of the snowpack, the increase in LWC was largely consistent. Pooling of water at the base of the snowpack meant that percolation into the ground was impeded. The

snowpack was isothermal and could no longer contain its liquid water, making it ripe, according to the definition by Kinar and Pomeroy (2015a). Much of the snow was at the boundary between the pendular and funicular regimes, around 8% LWC (Fierz et al., 2009; McClung & Schaerer, 2022). Based on the findings of Denoth (1980), the transition between pendular and funicular is between 11% and 15% pore saturation, which can be recalculated to LWC based on the dry snow density (or porosity). The mean dry density of the snow in BHS2 above the water table was 362 kg m^{-3}, putting the transition between 6.7% and 9.2% LWC.

My findings of homogenous snow coupled with an even increase in LWC is consistent with the literature. Juras et al. (2017) found that ripe snowpacks tend to show signs of matrix flow rather than preferential flow. Brandt et al. (2022) states that homogenous snowpacks promote matrix flow. Multiple sources (e.g., Armstrong & Brun, 2008; Brandt et al., 2022; DeWalle & Rango, 2008; Marsh & Woo, 1984) write that matrix flow is slower than preferential flow when first wetting the snowpack due to unsaturated flow being slower, and refreezing at the wetting front causing delay. The rising water table in experiment 5 means the water flow was relatively quick, but the snowpack was already wet at the BHS1 measurement, meaning there was little refreezing to slow percolation. In addition, hydraulic conductivity increases with degree of wet snow metamorphism (Gude & Scherer, 1998), and the snow in experiment 5 was at a very high degree.

Due to the nature of the field site of experiment 5, lateral meltwater flow may have contributed to the rise in the water table. The snow pit was dug in a topographical depression, at the border between a lake and swampy ground. Meltwater flowing from the edges of the depression could have raised the lake level. This means the 5 cm increase of standing water was not necessarily only due to melting of the snow directly above. Eiriksson et al. (2013) found that lateral flow in a ripe snowpack tends to be along the ground rather than within the snowpack. Their flow velocities of 1 – 7 m h^{-1} mean that in the 7 hours between BHS1 and BHS2, water from 7 – 49 m away may have contributed to the pooled water at the snowpack base.

Another indicator of lateral flow is that the snowpack did not shrink noticeably during the experiment despite warm temperatures and clear melting. This could, however, also be due to measurement error. Since the snowpack was not particularly deep, a minor change in depth may be significant, but difficult to register. The snow-ground boundary may have been incorrectly defined through the water at the base of the snowpack. Another possibility is that due to the destructive methods implemented, lateral variability in snow height could make up for the reduced snow depth due to melting. If, e.g., the snow shrank 2 cm, and

the snow at BHS2 by chance was 2 cm deeper, this would be registered as no change in snow depth.

Many of the snow types measured likely turned into MF over the course of the experiment, but I did not perform a follow-up snow pit investigation to accurately record it. Metamorphism with liquid water present leads to the formation of MF (Figure 1). An example is the basal layer of FC during experiment 6 (Appendix A.6.) which was completely submerged in water and had turned to MF when the second measurements were taken (RS2 in Figure 14).

5.1.3. Depth hoar discussion

The fact that the lower half of the snowpack in experiment 4 was drier during the second measurement series (FF2 in Figure 13), despite the sunny and warm day was noteworthy and warrants further discussion. One explanation could be that although the field site was located on a swamp, the ground was not saturated or impermeable, allowing the liquid water to drain into the soil. This is unlikely, however, as much of the snowpack had LWC values close to the irreducible levels of 3% (Colbeck, 1986; Yamaguchi et al., 2010) or between 3% and 6% (Fierz et al., 2009). This means that the snow could not have drained to become drier, and also means that little water flow occurred in the lower half at all, since the irreducible water content needs to be satisfied before water can begin to percolate.

A second possibility is refreezing of liquid water, which would effectively lower LWC. However, this seems unlikely given the warm conditions during the day. The top 20 cm refroze during the night, but diurnal temperature swings seldom reach deeper than 20 – 30 cm (Birkeland, 1998). Most of the apparent drying occurred near the ground, where the snow is warmest.

The third, and most likely explanation, is the lateral variability of snow. Due to the destructive nature of the procedure, it is not the same sample of snow being measured at both timesteps. The FF2 measurement series were likely taken in drier snow. Another argument in favor of lateral variability is that FF2 was measured six hours after FF1, and the DH layer at the base was still clearly identifiable as DH. The higher the LWC, the faster grains undergo metamorphism (DeWalle & Rango, 2008). A dry sample of DH, due to lateral variability, is therefore more likely to remain as DH, compared to the sample in FF1, which showed clear signs of melting.

In fact, the observations of DH during the melting phase may have been a stroke of luck, since the large specific surface area of DH promotes rapid melting. The crystals were still clearly DH, with their

characteristic cup-like shapes, but some crystals showed rounded edges and slight effects of melting. The snow grains had not yet turned to MF. The DH crystals were recognizable both at FF1 and FF2, indicating that at low levels of LWC, DH can persist for multiple hours, and potentially days, as I do not have information on when they were first wetted or when they at last turned to MF. An example of MF that may previously have been DH can be seen in the fist hard layer of MF near the bottom of the snowpack in Appendix A.2.

5.1.4. Precipitation particles/decomposing and fragmented particles discussion

PP and DF are discussed together, due to their similar characteristics and the similarities between experiment 6 (Figure 14), which had a ~20 cm thick surface layer of PP (Appendix A.6.), and experiment 7 (Figure 15), which had a ~25 cm thick layer of DF nearly at the surface (Appendix A.7.). Both snowpacks started dry and with subzero snowpack temperatures, apart from the surface during experiment 7, which was already wet due to rain. The pattern of LWC was similar during the second series of measurements, with a wet or very wet surface layer, slushy snow and standing water at the base, and a nearly completely dry interior.

Since the base of both snowpacks were saturated at the second timestamp, water clearly found a path through the snow that was not adequately registered by the standard measurement procedure. This is discussed further in Section 5.2.1 on flow fingers. An exception to the dry interior is the moist snow at 40 cm depth for V2 in experiment 7 (Figure 15), which is discussed in Section 5.2.1.

Experiment 6 and 7 showed similar increases in water level of around 5 cm at the base of the snowpack. However, experiment 6 may have received more than twice the amount of rain, and had a thinner snowpack, meaning less distance for rainwater to travel. This indicates that the basal ice layer found in experiment 7 was less permeable than the frozen gravel bed of experiment 6. Experiment 7 was also conducted on frozen gravel, meaning the basal ice could act as an additional water-impeding layer, compared to experiment 6.

The mean dry snow density of RS2 above the water table was 220 kg m^{-3}. This puts the transition between pendular and funicular regimes between 8.4% and 11.4% LWC, according to Denoth (1980). The low density of this snowpack pushes the transition values higher than for the denser MF (Section 5.1.2).

Experiments 6 and 7 were the only ones where the snowpack got noticeably thinner between measurement

series. PP and DF are the newest, least dense and settled snow types, and having them on the surface exposes them to the incoming rain first, shielding the underlying snow, while melting occurred near the surface. The soft and porous texture of PP and DF promotes rapid changes when exposed to liquid water and allows for much more settling than snow types that have been on the ground longer. Large cups of DH may have a similar potential for shrinking, but they tend to be found at the bottom of the snowpack, far from the incoming rain. This means that preferential flow might cause settling in the places flow fingers appear, while the surrounding dry snow maintains structural integrity and delays the snowpack from shrinking.

In experiment 7, a temperature profile taken right before the second LWC series showed 0 °C through the whole snowpack, indicating the presence of liquid water. Due to the seemingly dry interior, the consistent readings at 0 °C were unexpected. The thermometer was tested in the air and on skin to see if instrument error had caused it to stay at 0 °C, but the values seemed reasonable. The temperature profile was taken in freshly uncovered snow, so thermal influence horizontally into the pit wall, e.g., from operator heating (Shea & Jamieson, 2011), is assumed to be negligible. The explanation deemed most likely was that the temperature profile was taken in a preferential flow path, containing wet snow at 0 °C, while the surrounding snow remained dry. It is theoretically possible that the snow may have been at or right below the melting point and no liquid water was present, but it is unlikely. In hindsight, taking multiple temperature profiles would have been desirable.

5.2. Water movement through the snowpack discussion

Two important factors that appear to influence the vertical movement of liquid water through a snowpack are the effects of hydraulic barriers and the difference between the flow modes matrix flow and preferential flow. The effects of permeability barriers in the form of ice layers are discussed in Section 5.1.1, so the following section will focus on capillary barriers.

5.2.1. Capillary barriers discussion

The chief observations of capillary barriers were from experiment 7, where water could be seen pooling in layers in the snowpack (Figure 18). Both layers spanned the width of the profile as can vaguely be seen in Figure 16. None of these layers coincided with measurement depths in Figure 15, which exposes a weakness to the methods of this study. Visibly wet snow was not measured in the main experiments due to rigid adherence to the decided vertical measurement resolution. The upper layer may, however, have been

measured in experiment 7.2, with VDSD in Figure 19 showing $\theta_m \approx 2\%$ at 20 cm depth.

The lower wet layer observed in Figure 18 was found at the boundary between DF (1 mm grain size) above, and FC (2 mm grain size) below. This corroborates the observations of capillary barriers at fine-over-coarse layer boundaries in the literature (e.g., Avanzi et al., 2016; Juras et al., 2017; Pietzsch, 2009; Waldner et al., 2004; Webb et al., 2018; Williams et al., 2010). However, according to Webb et al. (2018), the upper layer needs to have a grain size below 0.6 mm for a capillary barrier to form, which my findings contradict. It is possible that differences in methods can explain the contradicting results. Grain sizes were identified visually using a gridded snow crystal card in both studies. This is a qualitative estimate based on relatively few snow crystals and can be performed more thoroughly. Having more photos from the field could have assisted in this comparison, but dark and wet conditions were an obstacle.

The upper wet layer in Figure 18 formed in, according to the snow pit investigation, a seemingly homogenous layer of fist hard DF. The presence of a capillary barrier within the DF suggests that it was not as homogenous as perceived. Small differences in snow hardness, being the main method of layer identification, are difficult to detect in soft snow. Wet layers that were not identified during snow pit investigation have been observed by Williams et al. (2010) and Pietzsch (2009) as well.

I suspect that the moist snow at 40 cm depth for V2 in Figure 15 was a capillary barrier in the FC layer, because all six measurements registered the presence of liquid water at that depth. It is not visible in Figure 18, which could mean that liquid water is not as visible in FC as in DF, or that the two visible layers in Figure 18 had higher LWC, making them more visible.

Liquid water could also be seen pooling at layer boundaries during experiment 4. They were found mainly in the upper 40 cm of the snowpack, where the snowpack got wetter. One such layer was found at a MFcr forming a permeability barrier at 40 cm depth, and another occurred in the boundary between RG (1 mm grain size) and MF (2 mm grain size) at around 30 cm depth, matching the findings from experiment 7. This indicates that heterogenous snow promotes the formation of capillary barriers, especially where a layer of fine-grained snow lies atop a layer of coarser grains, but seemingly homogenous snow can also have them, likely due to heterogeneity at an undetectable scale for a standard snow pit investigation.

5.2.2. Flow finger discussion

The most important results on flow fingers were the ones gathered in experiment 7.1. Depressions in the snow surface could be seen (Figure 16), marking the location of preferential flow paths. A very rough estimate of spacing between the flow finger dimples in Figure 16 is 40 – 60 cm. Flow fingers may also have been spaced differently under the snow surface, but this was not measured. Marsh and Woo (1984) found the mean distance between the flow fingers in their study to be 13 cm, while Williams et al. (2010) report values between 3 cm and 50 cm. The diameter of the preferential flow path in experiment 7.1 was not measured precisely, but a rough estimate puts it at 10 cm. The mean flow finger width from Marsh and Woo (1984) was 3.6 cm, and according to Williams et al. (2010), values between 1 cm and 40 cm can be expected, suggesting that preferential flow occurs on multiple scales.

The snow in the flow finger measured in experiment 7.1. was significantly wetter than the surrounding snow at nearly all depths (Figure 17), and likely occurred in the funicular regime, meaning liquid water was continuous through the snowpack. This matches the descriptions of saturated, vertical channels with dry surrounding snow found in the literature (e.g., Katsushima et al., 2020; Marsh & Woo, 1984, 1985; Schlumpf et al., 2024; Schneebeli, 1995; Waldner et al., 2004).

The flow finger in experiment 7.1 was close to vertical through the whole snowpack, remaining continuous through the capillary barriers shown in Figure 18. This contradicts the findings of McGurk and Marsh (1995) and Williams et al. (2010), who found that flow fingers were discontinuous above and below hydraulic barriers. One possibility is that, as Pietzsch (2009) explains, the high rate of infiltration overcame the capillary barrier. Another possibility is that this occurred due to chance, that the breakthrough points that occur in capillary barriers (Katsushima et al., 2020), happened to be quite close. This is difficult to determine, due to the sample size of only one flow finger.

5.2.3. Modes of flow

Experiment 2 had an evenly wet snowpack above the thick ice layer at 10 cm depth. This could be a combination of preferential flow paths wetting parts, and matrix flow wetting the rest. Had more measurements series been taken, this distinction could have been made better. The thick ice layer was an effective permeability barrier, rerouting water laterally, potentially causing preferential flow outside of the snow pit.

Experiments 6 and 7 were similar to each other, with rain as the source of water, a uniform increase in

LWC at the surface and base, and dry snow in between. Preferential flow was the predominant mode of flow, leading water efficiently to the snowpack base. The background wetting front of matrix flow had not gone deeper than 5–10 cm during both experiments. The snowpacks had few layers and were relatively homogenous. This indicates that PP and DF are snow types prone to the formation of preferential flow. It can also mean that water input rate, being a controlling factor for vertical percolation speed (Clerx et al., 2022), may matter more than how stratified the snowpacks were.

For the experiments conducted during melting conditions (4 and 5), it was more difficult to immediately ascertain the mode of flow due to the snowpack being wet already at the first measurement series. The lower portion of the snowpack in experiment 4, where the DH was, likely experienced little flow, due to being so close to the irreducible water content. The upper portion got wetter through the day, and liquid water could be seen pooling at hydraulic barriers. The top 10 cm got statistically significantly wetter in an even manner, indicating matrix flow. At 20 cm and 30 cm depth, the data spread was large, which I suspect means the wet values came from preferential flow paths, while the dry measurements were from the drier surrounding snow. The snowpack in experiment 5 was ripe and the most homogenous of all, consisting solely of wet MF. The increase in LWC was relatively even throughout the snowpack, indicating matrix flow. The ripe snow in experiment 5 was likely an efficient transmitter of water, due to the increase in hydraulic conductivity a snowpack experiences with degree of wet metamorphism (Gude & Scherer, 1998). The water level rose 5 cm between the series, which could have been partially due to lateral flow, as discussed in Section 5.1.2.

It is difficult to isolate the effects of snow type, and other distinctions, e.g., degree of stratification or homogeneity, degree of ripeness, and presence of hydraulic conductivity contrasts, may be equally relevant. In this regard, the findings of this study match the literature well. Ice layers (experiment 2) can impede and reroute liquid water (Clerx et al., 2022; Eiriksson et al., 2013; Marsh & Woo, 1985). Non-ripe, stratified snow with hydraulic barriers (experiments 4) promotes preferential flow (Avanzi et al., 2016; Juras et al., 2017; Katsushima et al., 2020; Marsh & Woo, 1984; Schlumpf et al., 2024; Schneebeli, 1995; Waldner et al., 2004). Ripe, homogenous snow (experiment 5) promotes matrix flow (Armstrong & Brun, 2008; Brandt et al., 2022; DeWalle & Rango, 2008; Donahue & Hammonds, 2022; Williams et al., 2010). However, the non-ripe, relatively homogenous snowpacks of experiments 6 and 7 were the ones that showed clearest signs of preferential flow, making it difficult to separate the effect of snow characteristics from the effect of intensity of water input. This could be the basis of a future study.

5.3. Implications for slushflows

The main focus of this study has been on factors that promote or impede vertical infiltration of water into the snowpack. Better understanding of how different snow types and structural characteristics impact the rate at which water travels through the snowpack can improve predictions on the timing of slushflows. In this context, the mode of flow plays a pivotal role, as preferential flow (experiments 6 and 7) can efficiently transport large amounts of water to the base of the snowpack without having to wet the entire snowpack. Since water effectively bypasses most of the snowpack, this could cause slushflows to release earlier than expected, particularly if the base of the snowpack consisted of a vulnerable snow type like depth hoar (Hestnes et al., 1994; Sund et al., 2024). The formation of preferential flow paths might be controlled more by water supply volume and rate than the snow type present, similar to what Sund et al. (2020, 2024) suggest about slushflow release.

When assessing snowpack LWC, using a measure of central tendency is appropriate when matrix flow predominates. However, this approach may oversimplify conditions under preferential flow, potentially obscuring critical details of the behavior of the snowpack. For regional predictions, generalization and simplification may be necessary (Sund et al., 2024), though it may lead to loss of detail. Madore et al. (2022) echo this sentiment, noting that spatial variability in snow complicates regional assessments.

Experiments 5, 6, and 7 demonstrated water pooling at the base of the snowpack, forming or elevating a water table. This would not have been possible without impermeable ground conditions, such as saturated ground (experiment 5), frozen ground (experiments 6 and 7), and solid basal ice (experiment 7). This is reflected in the literature, with impermeable ground conditions being seen as a necessary ingredient for slushflow release (Gude & Scherer, 1998; Hestnes, 1998; Hestnes et al., 1994; Onesti & Hestnes, 1989; Sund et al., 2020, 2024).

Despite these conditions, none of the experiments resulted in a rise in the water table beyond approximately 5 cm, and no slushflows were triggered at the field sites. While the release of slushflows was not a direct objective of this study and was avoided for safety reasons, these observations suggest that impermeable ground conditions alone are insufficient for slushflow initiation. This highlights the significance of lateral flow, particularly at scales larger than the individual snow pits investigated in this study (Eiriksson et al., 2013). Funneling and focusing water from a larger catchment is much more likely to form slushflows than only the water from rain or a melting snowpack in a particular spot. Terrain features and topography that cause funneling and accumulation are important. Valleys are a good example of this, with water from the sides flowing to the valley floor (Gude & Scherer, 1998).

The importance of snow type altogether may be questioned, because all snow transitions to MF when in contact with liquid water, so why should the original grain form matter for slushflows? However, as indicated by the persistent moist DH observed in experiment 4, the relevance of snow type should not be dismissed. Perhaps original grain form is of less importance when the accumulation of water goes over several days, leaving the crystals time to transition to MF. For the rapid and intense water supply rates typical in this study, there may not be enough time for complete transformation to MF before slushflow release. This observation aligns with the literature (e.g., Hestnes et al., 1994; Skuset, 2018; Skuset & Sund, 2019; Sund et al., 2024) which collectively suggest that snow type does indeed influence slushflow susceptibility.

5.4. Evaluation of the SLF sensor

The secondary objective of this study was to evaluate the SLF sensor as a tool for measuring LWC. By this, I mean recalling how practical the sensor worked in the field and issues I came across during its use. In addition, values from the SLF sensor are compared with the traditional hand wetness test. Assessing the accuracy of the sensor is beyond the scope of this study, but the empirical calibration equations hold up well (Schlumpf et al., 2024), and the SLF sensor has served well for comparisons with other instruments (Donahue et al., 2022).

5.4.1. Field experience with the SLF sensor

Overall, the SLF sensor was a practical tool to use. Though I did not compare it to other instruments or methods than the hand wetness test, the SLF sensor is small, portable, easy to use, and gives precise values in the field. Many other instruments are larger and more cumbersome, e.g., the Finnish Snow Fork (Techel & Pielmeier, 2011), or are described as labor intensive and impractical (Kinar & Pomeroy, 2015a). There are, however, some downsides to the SLF sensor.

The requirement for a separate density measurement in order to calculate LWC is both time-consuming and a potential source of error. The instruction manual suggested performing density measurements before the snow got wet, e.g., in the morning before temperatures rise (FPGA Company, 2018). This includes some inherent error, though, because it does not account for structural changes and settling in the snowpack due to exposure to liquid water. While it may be appropriate for old layers of RG or MF, which have little room to settle further, a porous layer of PP will change considerably in contact with water.

Using the density of the unwetted PP would not be the same as a dry sample of the wetted PP. Waldner et al. (2004) observed significant densification in their snow samples as they got wet.

In this study, the snow was already wet during the first measurement series in some experiments. Therefore, I opted for the second option listed in the manual (FPGA Company, 2018), the iterative correction described in Section 3.2.1. The change in LWC was small, ranging between 0.001% to 0.99% for snow drier than 15 % LWC. The absolute change was largest between 8% and 9%, but as a percentage was largest for small values and decreased with increasing LWC. This fits quite well with what Donahue et al. (2022) calculated, with changes ranging from 0.4% to 1.2% and following the same patterns.

Experiment 7.2 was conducted to compare the two options for use of density. While the LWC profiles showed significant differences at many depths (Figure 19), the magnitude of the difference cannot be explained by difference in density alone. They were therefore more likely due to horizontal variations in the snowpack and mismatched measurement depths. In Figure 19, At 10 cm depth, percolating rainwater could have reached slightly deeper than in the adjacent V2 measurements, and the same could occur at the 60 cm mark, just in the opposite direction. As mentioned in Section 5.2.1, the measurement at 20 cm depth for VDSD may have been the upper wet layer shown in Figure 18, which was not registered in V2. At 40 cm depth, the opposite may have occurred, with V2 picking up a wet layer and VDSD missing it. This exemplifies a limitation of mismatched measurements between series, further discussed in Section 5.5.

5.4.2. Comparison with the hand wetness test

Data from all experiments was used in the comparison between wetness estimated using the hand wetness test and LWC measured with the SLF sensor (Figure 20). The median values from Techel and Pielmeier (2011) are lower than the ones from this study for each hand wetness class except “dry”, which is defined as $\theta_m = 0\%$ by everyone. Their LWC values increase more linearly with each hand wetness class. The difference is particularly clear for the wetter categories. For very wet snow, when moderately squeezing the snow releases water, the lowest value measured in this study is higher than their median. A possible reason for this is differences in the use of the hand wetness test, as it is a subjective test. Fierz et al. (2009) recommend avalanche workers to compare and calibrate against each other. The guidelines were standardized by Fierz et al. (2009), so Techel and Pielmeier (2011) used the same method. Techel and Pielmeier (2011) had four observers, meaning there was more room for inconsistency between operators compared to the single observer in this study. However, their data spread was similar or lower than mine, meaning their observers were likely consistent and well calibrated to each other. A second explanation is

that Techel and Pielmeier (2011) used a Snow Fork to measure LWC, not an SLF sensor. Differences between how the instruments work may give different results. They did, however, compare the Snow Fork measurements with a Denoth meter and got similar values. This discrepancy requires further investigation and is beyond the scope of this study.

However, the median values from this study fit quite well with the values from Fierz et al. (2009) for all classes, increasing exponentially with hand wetness class. The approximate range shown in Table 1, from Fierz et al. (2009), matches relatively well with the interquartile range of the measurements in this study, with the biggest difference in the "very wet" class. The LWC range for very wet snow from Fierz et al. (2009) is 8%–15%, while the interquartile range from this study is approximately 10%–13%. The close alignment in median values between this study and the established standard from Fierz et al. (2009) indicates that, despite the differences from Techel and Pielmeier (2011), the hand wetness test is an effective way to get an approximate value for LWC. A clear advantage over the SLF sensor is the speed in which it can be done. It is best suited for internal comparison with snow measured by the same operator, but can also be used for external comparison, if one is aware of the qualitative nature of the test. When looking for absolute values for LWC, the hand wetness test is not nearly accurate enough, making the SLF sensor a more suitable choice.

5.5. Limitations

In retrospect, higher temporal resolution and higher number of measurement series would have been beneficial. This would have provided a clearer picture of LWC change with time through the snowpack. More rapid measurements in the beginning of the wetting phase could catch the formation of flow fingers better. Measurements over a longer timespan would allow for better analysis of the transition between preferential flow and matrix flow, and the speed of the wetting front. Having more manpower could be a solution to this, though that includes a risk of increased error due to differences between operators.

With the resources and time available, however, a few improvements to the fieldwork include taking a second snow profile at the second timestamp in each experiment, in order to see how other snowpack parameters, such as grain form, change when wetted. The use of a waterproof camera or mobile phone would have allowed for the gathering of more photographic data. Photos were quite useful in post-fieldwork analysis, and wet conditions made it difficult to take as many as desired.

A clear limitation to this study is the destructive nature of the measurement process. Measuring the same

sample of snow during the second series of measurements was not possible, which introduces the significant effect of lateral variability in snow. It also made lining up the measurements between series slightly flawed. In this study, the snow surface was used as the reference point, which means that melting and settling snow also misaligns the follow-up measurements. Using the ground as the reference point may have improved this slightly, since most of the melting and settling occurred near the surface. Ideally, aligning measurements according to layer boundaries might have provided more accuracy.

Employing the median as a measure of central tendency may have oversimplified the data obtained from the SLF sensor. Median LWC values might not accurately represent the actual conditions within the snowpack, where significant variability in LWC can exist. It is, nevertheless, an efficient way to get an understanding of the general patterns that occur.

Proximity to weather stations is another limitation. Exact weather conditions can vary over quite short distances (Decaulne & Sæmundsson, 2006; Hestnes et al., 2012), making meteorological data from multiple kilometers away unreliable. The discrepancy between modeled and measured precipitation during experiment 6 exemplifies this. All values of estimated rain or melt are uncertain and need to be considered critically.

Although the field experiments performed in this study were done under realistic weather conditions for slushflows, controlled conditions may be better in some regards. A recommended approach for a future study would be conducting sprinkling experiments with close access to a weather station, removing the dependency on specific and rare weather events. This would also make the fieldwork itself much easier, as it could be performed in dry conditions and every single piece of equipment would not need to get wet.

6. Conclusion

This study has investigated the development of liquid water content in different snow types. This has been done by measuring liquid water content (LWC) profiles in snow, using an SLF Snow Sensor, before and during meteorological conditions that are favorable for slushflow release. This includes measurements in intense rain and during strong melting. The central findings of this study can be summed up restating the research objectives from Section 1.2.

Research objective 1: Investigate how liquid water develops in different snow types during weather situations where slushflows can occur.

- Thick ice layers can prevent vertical movement of water, at least locally, while thinner ice layers and melt-freeze crusts are not impermeable enough to completely halt the vertical flow.
- The differences between preferential flow and matrix flow are important for how water travels through snow. Water supply rate and volume may influence this.
- Ripe melt forms promote matrix flow.
- Precipitation particles and decomposing and fragmented particles may promote preferential flow in snow.
- Capillary barriers form in layer boundaries consisting of fine grains over coarse grains. They can be found in layer boundaries undetected in snow pit investigations.
- Moist depth hoar can persist for multiple hours, if not days, without fully melting or turning into melt forms.

Research objective 2: Evaluate the SLF Snow Sensor as a tool for measuring LWC in the field.

- The SLF sensor is practical, easy to use and gives good point-measurements of LWC in the field. However, the need for an additional density measurement increases the workload substantially.
- The hand wetness test is effective for approximate values of LWC, but when more precise values are needed, the SLF sensor is a more suitable tool

Recommendations for future work:

- Perform sprinkling experiments with varying water input rates in the same snowpack to investigate the effect of water supply rate and volume. Perform the experiments near a weather station
- Investigate the rate at which various grain forms transition to melt forms when subjected to various levels of LWC.

- Look into the maximum grain size for the upper layer in capillary barriers.
- Investigate the discrepancy in LWC measurements from Techel and Pielmeier (2011) compared to the values from Fierz et al. (2009) and this study.

7. References

Ahrens, C. D., & Henson, R. (2023). *Essentials of meteorology: An invitation to the atmosphere* (9th ed.). Brooks Cole.

American Avalanche Association. (2022). *Snow, Weather, and Avalanches: Observation Guidelines for Avalanche Programs in the United States* (4th ed.). American Avalanche Association.

Armstrong, R. L., & Brun, E. (Eds.). (2008). *Snow and climate: Physical processes, surface energy exchange and modeling*. Cambridge University Press.

Avanzi, F., Hirashima, H., Yamaguchi, S., Katsushima, T., & De Michele, C. (2016). Observations of capillary barriers and preferential flow in layered snow during cold laboratory experiments. *The Cryosphere*, *10*(5), 2013–2026. https://doi.org/10.5194/tc-10-2013-2016

Barry, R. G., & Gan, T. Y. (2022). *The Global Cryosphere: Past, Present, and Future* (2nd ed.). Cambridge University Press. https://doi.org/10.1017/9781108767262

Birkeland, K. W. (1998). Terminology and Predominant Processes Associated with the Formation of Weak Layers of Near-Surface Faceted Crystals in the Mountain Snowpack. *Arctic and Alpine Research*, *30*(2), 193. https://doi.org/10.2307/1552134

Brandt, W. T., Haleakala, K., Hatchett, B. J., & Pan, M. (2022). A Review of the Hydrologic Response Mechanisms During Mountain Rain-on-Snow. *Frontiers in Earth Science*, *10*, 791760. https://doi.org/10.3389/feart.2022.791760

Brun, E. (1989). Investigation on Wet-Snow Metamorphism in Respect of Liquid-Water Content. *Annals of Glaciology*, *13*, 22–26. https://doi.org/10.3189/S0260305500007576

Clerx, N., Machguth, H., Tedstone, A., Jullien, N., Wever, N., Weingartner, R., & Roessler, O. (2022). In situ measurements of meltwater flow through snow and firn in the accumulation zone of the SW Greenland Ice Sheet. *The Cryosphere*, *16*(10), 4379–4401. https://doi.org/10.5194/tc-16-4379-2022

Colbeck, S. C. (1978). The Difficulties of Measuring the Water Saturation and Porosity of Snow. *Journal of Glaciology*, *20*(82), 189–201. https://doi.org/10.3189/S0022143000198089

Colbeck, S. C. (1979a). Grain clusters in wet snow. *Journal of Colloid and Interface Science*, *72*(3), 371–384. https://doi.org/10.1016/0021-9797(79)90340-0

Colbeck, S. C. (1979b). Water flow through heterogeneous snow. *Cold Regions Science and Technology*, *1*(1), 37–45. https://doi.org/10.1016/0165-232X(79)90017-X

Colbeck, S. C. (1986). Of Wet Snow, Slush & Snowballs. *Weatherwise*, *39*(6), 314–318. https://doi.org/10.1080/00431672.1986.9929311

D'Amboise, C. J. L., Müller, K., Oxarango, L., Morin, S., & Schuler, T. V. (2017). Implementation of a physically based water percolation routine in the Crocus/SURFEX (V7.3) snowpack model. *Geoscientific Model Development*, *10*(9), 3547–3566. https://doi.org/10.5194/gmd-10-3547-2017

Decaulne, A., & Sæmundsson, Þ. (2006). Meteorological conditions during slush-flow release and their geomorphological impact in northwestern Iceland: A case study from the Bíldudalur valley. *Geografiska Annaler: Series A, Physical Geography*, *88*(3), 187–197. https://doi.org/10.1111/j.1468-0459.2006.00294.x

Denoth, A. (1980). The Pendular-Funicular Liquid Transition in Snow. *Journal of Glaciology*, *25*(91), 93–98. https://doi.org/10.3189/S0022143000010315

Denoth, A. (1994). An electronic device for long-term snow wetness recording. *Annals of Glaciology*, *19*, 104–106. https://doi.org/10.3189/S0260305500011058

DeWalle, D. R., & Rango, A. (2008). *Principles of Snow Hydrology* (1st ed.). Cambridge University Press. https://doi.org/10.1017/CBO9780511535673

Donahue, C., & Hammonds, K. (2022). Laboratory Observations of Preferential Flow Paths in Snow Using Upward-Looking Polarimetric Radar and Hyperspectral Imaging. *Remote Sensing*, *14*(10), 2297. https://doi.org/10.3390/rs14102297

Donahue, C., Skiles, S. M., & Hammonds, K. (2022). Mapping liquid water content in snow at the millimeter scale: An intercomparison of mixed-phase optical property models using hyperspectral imaging and in situ measurements. *The Cryosphere*, *16*(1), 43–59. https://doi.org/10.5194/tc-16-43-2022

Dunlop, S. (2008). Kelvin effect. In *A Dictionary of Weather*. Oxford University Press.

Eiriksson, D., Whitson, M., Luce, C. H., Marshall, H. P., Bradford, J., Benner, S. G., Black, T., Hetrick, H., & McNamara, J. P. (2013). An evaluation of the hydrologic relevance of lateral flow in snow at hillslope and catchment scales. *Hydrological Processes*, *27*(5), 640–654. https://doi.org/10.1002/hyp.9666

Fierz, C., Armstrong, R. L., Durand, Y., Etchevers, P., Greene, E., McClung, D. M., Nishimura, K., Satyawali, P. K., & Sokratov, S. A. (2009). *The International Classification for Seasonal Snow on the Ground* (IHP-VII Technical Documents in Hydrology No. 83 | IACS Contribution No. 1). UNESCO-IHP.

FPGA Company. (2018, October 24). *SLF SNOW SENSOR – USER MANUAL*. https://fpga-company.com/wp-content/uploads/2018/10/SLFSnowSensor-User-Manual-Version-1.3.pdf

Furbish, D. J. (1988). The Influence of Ice Layers on The Travel Time of Meltwater Flow Through A Snowpack. *Arctic and Alpine Research*, *20*(3), 265–272. https://doi.org/10.1080/00040851.1988.12002674

Gude, M., & Scherer, D. (1995). Snowmelt and Slush Torrents—Preliminary Report from a Field Campaign in Kärkevagge, Swedish Lappland. *Geografiska Annaler: Series A, Physical Geography*, *77*(4), 199–206. https://doi.org/10.1080/04353676.1995.11880440

Gude, M., & Scherer, D. (1998). Snowmelt and slushflows: Hydrological and hazard implications. *Annals of Glaciology*, *26*, 381–384. https://doi.org/10.3189/1998AoG26-1-381-384

Hao, J., Mind'je, R., Feng, T., & Li, L. (2021). Performance of snow density measurement systems in snow stratigraphies. *Hydrology Research*, *52*(4), 834–846. https://doi.org/10.2166/nh.2021.133

Harvey, A. H. (2023). Properties of Ice and Supercooled Water. In J. R. Rumble, T. J. Brunno, & M. J. Doa (Eds.), *CRC Handbook of Chemistry and Physics* (104th ed.). CRC Press.

Hestnes, E. (1985). A Contribution to the Prediction of Slush Avalanches. *Annals of Glaciology*, *6*, 1–4. https://doi.org/10.3189/1985AoG6-1-1-4

Hestnes, E. (1998). Slushflow hazard — where, why and when? 25 years of experience with slushflow consulting and research. *Annals of Glaciology*, *26*, 370–376. https://doi.org/10.3189/1998AoG26-1-370-376

Hestnes, E., & Bakkehøi, S. (2004). Slushflow hazard prediction and warning. *Annals of Glaciology*, *38*, 45–51. https://doi.org/10.3189/172756404781814889

Hestnes, E., Bakkehøi, S., & Kristensen, K. (2012). Slushflow formation, flow regimes and consequences (Short version). *Proceedings of the International Snow Science Workshop*, 414–419. https://ngi.brage.unit.no/ngi-xmlui/bitstream/handle/11250/3083809/Hestnes_Bakkeh%C3%B8i_Kristensen%282012%29.pdf?sequence=1&isAllowed=y

Hestnes, E., Bakkehøi, S., Sandersen, F., & Andresen, L. (1994). Weather and snowpack conditions essential to slushflow release and downslope propagation. *Proceedings of the International Snow Science Workshop*, 40–57. https://ngi.brage.unit.no/ngi-xmlui/bitstream/handle/11250/3083732/Hestnes_Bakkeh%C3%B8i_Sandersen_Andresen(1994).pdf?sequence=1

Hirashima, H., Avanzi, F., & Wever, N. (2019). Wet-Snow Metamorphism Drives the Transition From Preferential to Matrix Flow in Snow. *Geophysical Research Letters*, *46*(24), 14548–14557. https://doi.org/10.1029/2019GL084152

Juras, R., Würzer, S., Pavlásek, J., Vitvar, T., & Jonas, T. (2017). Rainwater propagation through snowpack during rain-on-snow sprinkling experiments under different snow conditions. *Hydrology and Earth System Sciences*, *21*(9), 4973–4987. https://doi.org/10.5194/hess-21-4973-2017

Kalland, H. D. (2022). *Snow forces, avalanches, and avalanche mitigation methods* [Master's thesis, NTNU]. https://ntnuopen.ntnu.no/ntnu-xmlui/handle/11250/3025989

Katsushima, T., Adachi, S., Yamaguchi, S., Ozeki, T., & Kumakura, T. (2020). Nondestructive three-dimensional observations of flow finger and lateral flow development in dry snow using magnetic

resonance imaging. *Cold Regions Science and Technology*, *170*, 102956. https://doi.org/10.1016/j.coldregions.2019.102956

Katsushima, T., Yamaguchi, S., Kumakura, T., & Sato, A. (2013). Experimental analysis of preferential flow in dry snowpack. *Cold Regions Science and Technology*, *85*, 206–216. https://doi.org/10.1016/j.coldregions.2012.09.012

Kinar, N. J., & Pomeroy, J. W. (2015a). Measurement of the physical properties of the snowpack. *Reviews of Geophysics*, *53*(2), 481–544. https://doi.org/10.1002/2015RG000481

Kinar, N. J., & Pomeroy, J. W. (2015b). SAS2: The system for acoustic sensing of snow. *Hydrological Processes*, *29*(18), 4032–4050. https://doi.org/10.1002/hyp.10535

Kobayashi, S., Izumi, K., & Kamiishi, I. (1994). Slushflow disasters in Japan and its characteristics. *Proceedings of the International Snow Science Workshop*, 657–665. https://arc.lib.montana.edu/snow-science/objects/issw-1994-657-665.pdf

Koch, F., Henkel, P., Appel, F., Schmid, L., Bach, H., Lamm, M., Prasch, M., Schweizer, J., & Mauser, W. (2019). Retrieval of Snow Water Equivalent, Liquid Water Content, and Snow Height of Dry and Wet Snow by Combining GPS Signal Attenuation and Time Delay. *Water Resources Research*, *55*(5), 4465–4487. https://doi.org/10.1029/2018WR024431

Koch, F., Prasch, M., Schmid, L., Schweizer, J., & Mauser, W. (2014). Measuring Snow Liquid Water Content with Low-Cost GPS Receivers. *Sensors*, *14*(11), 20975–20999. https://doi.org/10.3390/s141120975

LaChapelle, E. R., & Armstrong, R. L. (1977). *Temperature Patterns in an Alpine Snow Cover and Their Influence on Snow Metamorphism.* Institute of Arctic and Alpine Research, University of Colorado. https://apps.dtic.mil/sti/pdfs/ADA040169.pdf

Louchet, F. (2021). *Snow avalanches: Beliefs, facts, and science*. Oxford University Press.

Madore, J.-B., Fierz, C., & Langlois, A. (2022). Investigation into percolation and liquid water content in a multi-layered snow model for wet snow instabilities in Glacier National Park, Canada. *Frontiers in Earth Science*, *10*, 898980. https://doi.org/10.3389/feart.2022.898980

Marsh, P., & Woo, M. (1984). Wetting front advance and freezing of meltwater within a snow cover: 1. Observations in the Canadian Arctic. *Water Resources Research*, *20*(12), 1853–1864. https://doi.org/10.1029/WR020i012p01853

Marsh, P., & Woo, M. (1985). Meltwater Movement in Natural Heterogeneous Snow Covers. *Water Resources Research*, *21*(11), 1710–1716. https://doi.org/10.1029/WR021i011p01710

Marshall, H.-P., & CryoGARS. (2014). Water in Snow Likes to Go with the Flow: Dynamics of Liquid Water in Snow and Its Impact on Stability. *Proceedings of the International Snow Science Workshop*, 43–48. https://arc.lib.montana.edu/snow-science/objects/ISSW14_paper_O2.03.pdf

Martin, J., & Schneebeli, M. (2023). Impact of the sampling procedure on the specific surface area of snow measurements with the IceCube. *The Cryosphere*, *17*(4), 1723–1734. https://doi.org/10.5194/tc-17-1723-2023

Mavrovic, A., Madore, J.-B., Langlois, A., Royer, A., & Roy, A. (2020). Snow liquid water content measurement using an open-ended coaxial probe (OECP). *Cold Regions Science and Technology*, *171*, 102958. https://doi.org/10.1016/j.coldregions.2019.102958

McClung, D., & Schaerer, P. A. (2022). *The avalanche handbook* (4th edition). Mountaineers Books.

McGurk, B. J., & Marsh, P. (1995). Flow-finger continuity in serial thick-sections in a melting Sierran snowpack. In K. A. Tonnessen, M. A. Williams, & M. Tranter (Eds.), *Biogeochemistry of seasonally snow-covered catchments* (pp. 81–88). International Association of Hydrological Sciences.

NVE. (2020). *Snøomvandling* (Faktaark 01/2020). Norwegian Water Resources and Energy Directorate. https://publikasjoner.nve.no/faktaark/2020/faktaark2020_01.pdf

NVE. (2022). *Felthåndbok for snø- og skredobservasjoner*. Norwegian Water Resources and Energy Directorate.

Onesti, L. J., & Hestnes, E. (1989). Slush-Flow Questionnaire. *Annals of Glaciology*, *13*, 226–230. https://doi.org/10.3189/S0260305500007941

Pietzsch, E. H. (2009). *Water movement in a stratified and inclined snowpack: Implications for wet slab avalanches* [Master's thesis]. Montana State University.

Pinzer, B. R., Schneebeli, M., & Kaempfer, T. U. (2012). Vapor flux and recrystallization during dry snow metamorphism under a steady temperature gradient as observed by time-lapse micro-tomography. *The Cryosphere*, *6*(5), 1141–1155. https://doi.org/10.5194/tc-6-1141-2012

Pirazzini, R., Leppänen, L., Picard, G., Lopez-Moreno, J. I., Marty, C., Macelloni, G., Kontu, A., Von Lerber, A., Tanis, C. M., Schneebeli, M., De Rosnay, P., & Arslan, A. N. (2018). European In-Situ Snow Measurements: Practices and Purposes. *Sensors*, *18*(7), 2016. https://doi.org/10.3390/s18072016

Relf, G., Kendra, J. M., Schwartz, R. M., Leathers, D. J., & Levia, D. F. (2015). Slushflows: Science and planning considerations for an expanding hazard. *Natural Hazards*, *78*(1), 333–354. https://doi.org/10.1007/s11069-015-1716-8

Scherer, D., Gude, M., Gempeler, M., & Parlow, E. (1998). Atmospheric and hydrological boundary conditions for slushflow initiation due to snowmelt. *Annals of Glaciology*, *26*, 377–380. https://doi.org/10.3189/1998AoG26-1-377-380

Schlumpf, M., Hendrikx, J., Stormont, J., & Webb, R. (2024). Quantifying short-term changes in snow strength due to increasing liquid water content above hydraulic barriers. *Cold Regions Science and Technology*, *218*, 104056. https://doi.org/10.1016/j.coldregions.2023.104056

Schneebeli, M. (1995). Development and stability of preferential flow paths in a layered snowpack. *Biogeochemistry of Seasonally Snow Covered Basins*, *228*.

Shea, C., & Jamieson, B. (2011). Some fundamentals of handheld snow surface thermography. *The Cryosphere*, *5*(1), 55–66. https://doi.org/10.5194/tc-5-55-2011

Sidorova, T., Belaya, N., & Perov, V. (2001). Distribution of slushflows in northern Europe and their potential change due to global warming. *Annals of Glaciology*, *32*, 237–240. https://doi.org/10.3189/172756401781819742

Skaugen, T., & Saloranta, T. (2015). *Simplified energy-balance snowmelt modelling* (31/2015). Norwegian Water Resources and Energy Directorate. https://publikasjoner.nve.no/rapport/2015/rapport2015_31.pdf

Skuset, S. (2018). *Utløysing av sørpeskred i ulike snøtypar—Utvikling av forsøksdesign, metode og utstyr for feltforsøk, med formål å undersøke utløysing av sørpeskred i ulike snøtypar* [NTNU]. http://hdl.handle.net/11250/2564441

Skuset, S., & Sund, M. (2019). *Studie av vasstilførsel for utløysing av sørpeskred i ulike snøtypar* (36/2019). Norwegian Water Resources and Energy Directorate. http://publikasjoner.nve.no/rapport/2019/rapport2019_36.pdf

Sund, M., Grønsten, H. A., & Seljesæter, S. Å. (2024). A regional early warning for slushflow hazard. *Natural Hazards and Earth System Sciences*, *24*(4), 1185–1201. https://doi.org/10.5194/nhess-24-1185-2024

Sund, M., Grønsten, H. A., & Skuset, S. (2020). *Varsling av regional sørpeskredfare* (42/2020). Norwegian Water Resources and Energy Directorate. https://doi.org/10.13140/RG.2.2.20507.69926

Techel, F., & Pielmeier, C. (2011). Point observations of liquid water content in wet snow – investigating methodical, spatial and temporal aspects. *The Cryosphere*, *5*(2), 405–418. https://doi.org/10.5194/tc-5-405-2011

Techel, F., Pielmeier, C., & Schneebeli, M. (2011). Microstructural resistance of snow following first wetting. *Cold Regions Science and Technology*, *65*(3), 382–391. https://doi.org/10.1016/j.coldregions.2010.12.006

Varsom. (n.d.). *Snøkart*. https://senorge.no/Snowmap

Varsom. (2023, April 19). *Sørpeskred går også på solskinsdagar*. Varsom. https://www.varsom.no/nyheter/nyheter-flom-og-jordskred/sorpeskred-gar-ogsa-pa-solskinsdagar/

Varsom. (2024a). *Varsom Regobs*. https://www.regobs.no/

Varsom. (2024b). *Varsom Xgeo*. https://www.xgeo.no/

Waldner, P. A., Schneebeli, M., Schultze-Zimmermann, U., & Flühler, H. (2004). Effect of snow structure on water flow and solute transport. *Hydrological Processes*, *18*(7), 1271–1290. https://doi.org/10.1002/hyp.1401

Webb, R. W., Fassnacht, S. R., Gooseff, M. N., & Webb, S. W. (2018). The Presence of Hydraulic Barriers in Layered Snowpacks: TOUGH2 Simulations and Estimated Diversion Lengths. *Transport in Porous Media*, *123*(3), 457–476. https://doi.org/10.1007/s11242-018-1079-1

Williams, M. W., Erickson, T. A., & Petrzelka, J. L. (2010). Visualizing meltwater flow through snow at the centimetre-to-metre scale using a snow guillotine. *Hydrological Processes*, *24*(15), 2098–2110. https://doi.org/10.1002/hyp.7630

Wolfspeger, F., Geisser, M., Ziegler, S., & Löwe, H. (2023). A new handheld capacitive sensor to measure snow density and liquid water content. *Proceedings of the International Snow Science Workshop*, 1532–1536. https://arc.lib.montana.edu/snow-science/objects/ISSW2023_P3.52.pdf

Yamaguchi, S., Katsushima, T., Sato, A., & Kumakura, T. (2010). Water retention curve of snow with different grain sizes. *Cold Regions Science and Technology*, *64*(2), 87–93. https://doi.org/10.1016/j.coldregions.2010.05.008

Yamaguchi, S., Watanabe, K., Katsushima, T., Sato, A., & Kumakura, T. (2012). Dependence of the water retention curve of snow on snow characteristics. *Annals of Glaciology*, *53*(61), 6–12. https://doi.org/10.3189/2012AoG61A001

8. Appendices

Appendix A: Snow profiles

Appendix A.1.

Bontveit
Hordalandskysten
Norway
Elevation: 292 m
Aspect: E
Specifics:

Thor Parmentier
24/01/2023 - 16:00
Co-ord: 32V 306107E 6693547N
Slope Angle: 11°
Wind Loading:

Stability:
Air Temperature: 2.7°C
Sky Cover: OVC
Precipitation: RM
Wind:

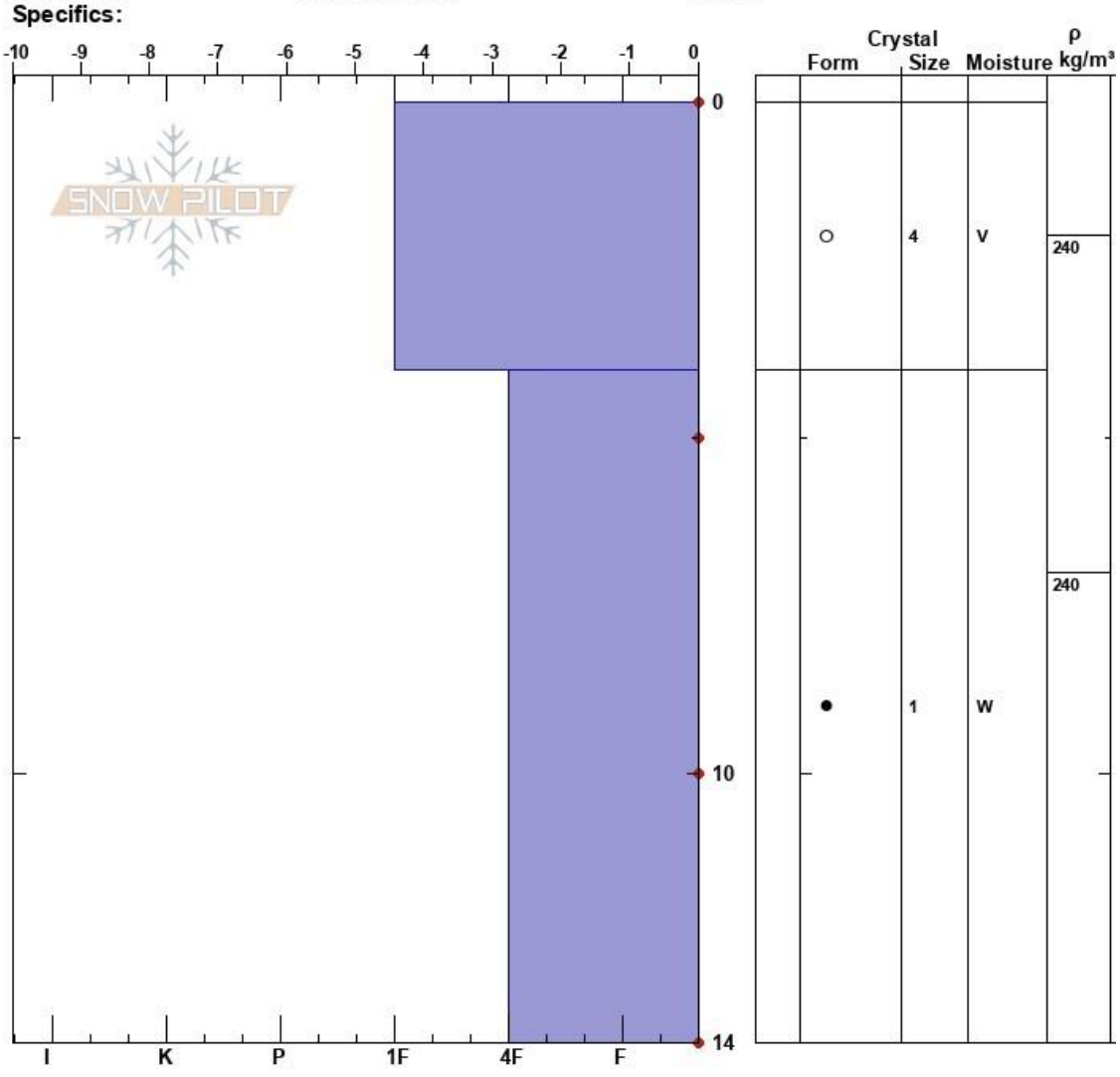

Appendix A.2.

Træn
Voss
Norway
Elevation: 453 m
Aspect: E
Specifics:

Thor Parmentier
28/01/2023 - 20:00
Co-ord: 32V 345411E 6722241N
Slope Angle: 2°
Wind Loading:

Stability:
Air Temperature: 1.3°C
Sky Cover: OVC
Precipitation:
Wind:

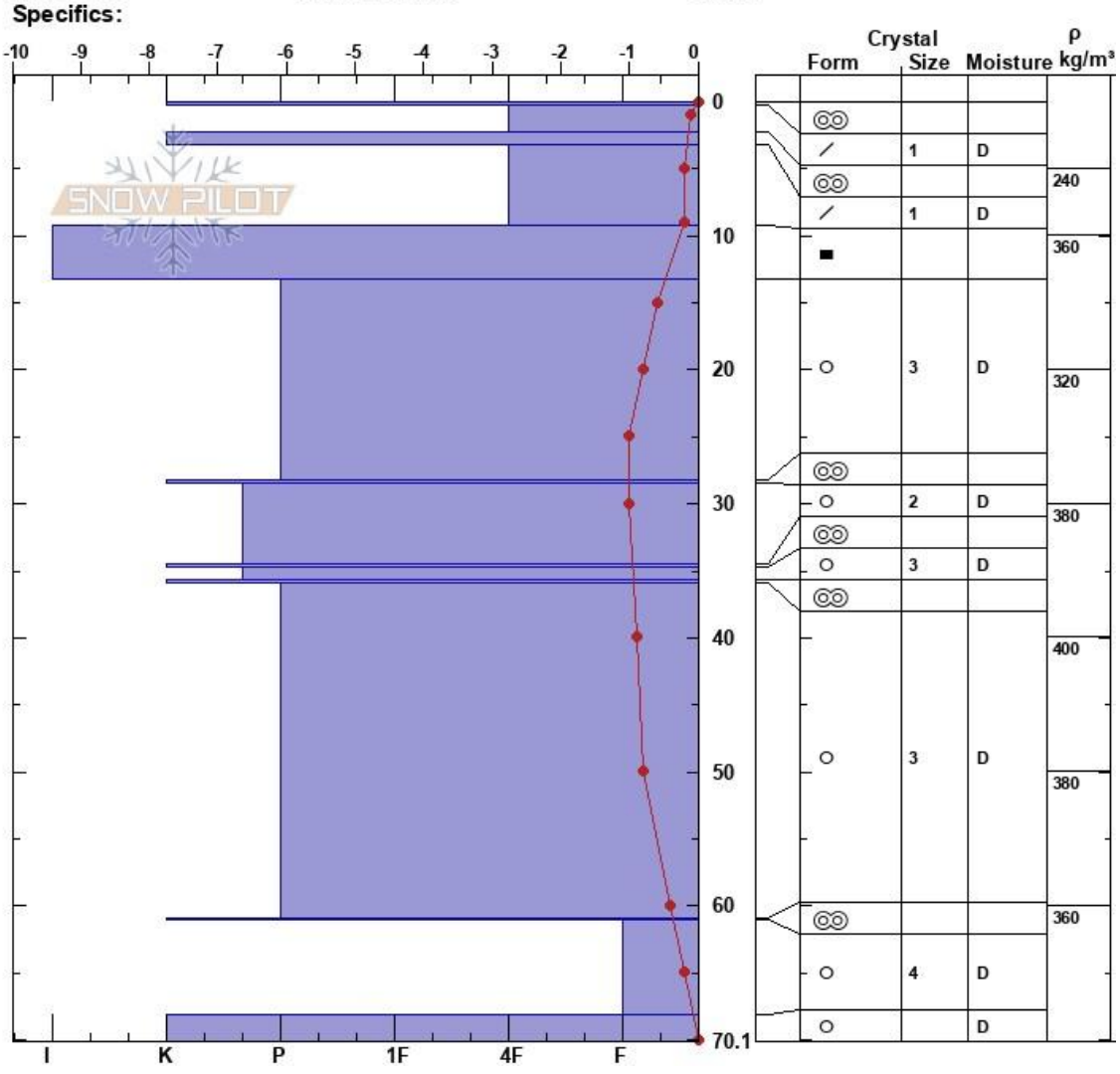

Appendix A.3.

Dalsdalen
Indre Sogn
Norway
Elevation: 201 m
Aspect: S
Specifics:

Thor Parmentier
20/02/2023 - 02:00
Co-ord: 32V 414481E 6819635N
Slope Angle: 5°
Wind Loading:

Stability:
Air Temperature: -2.9°C
Sky Cover: OVC
Precipitation: S5
Wind:

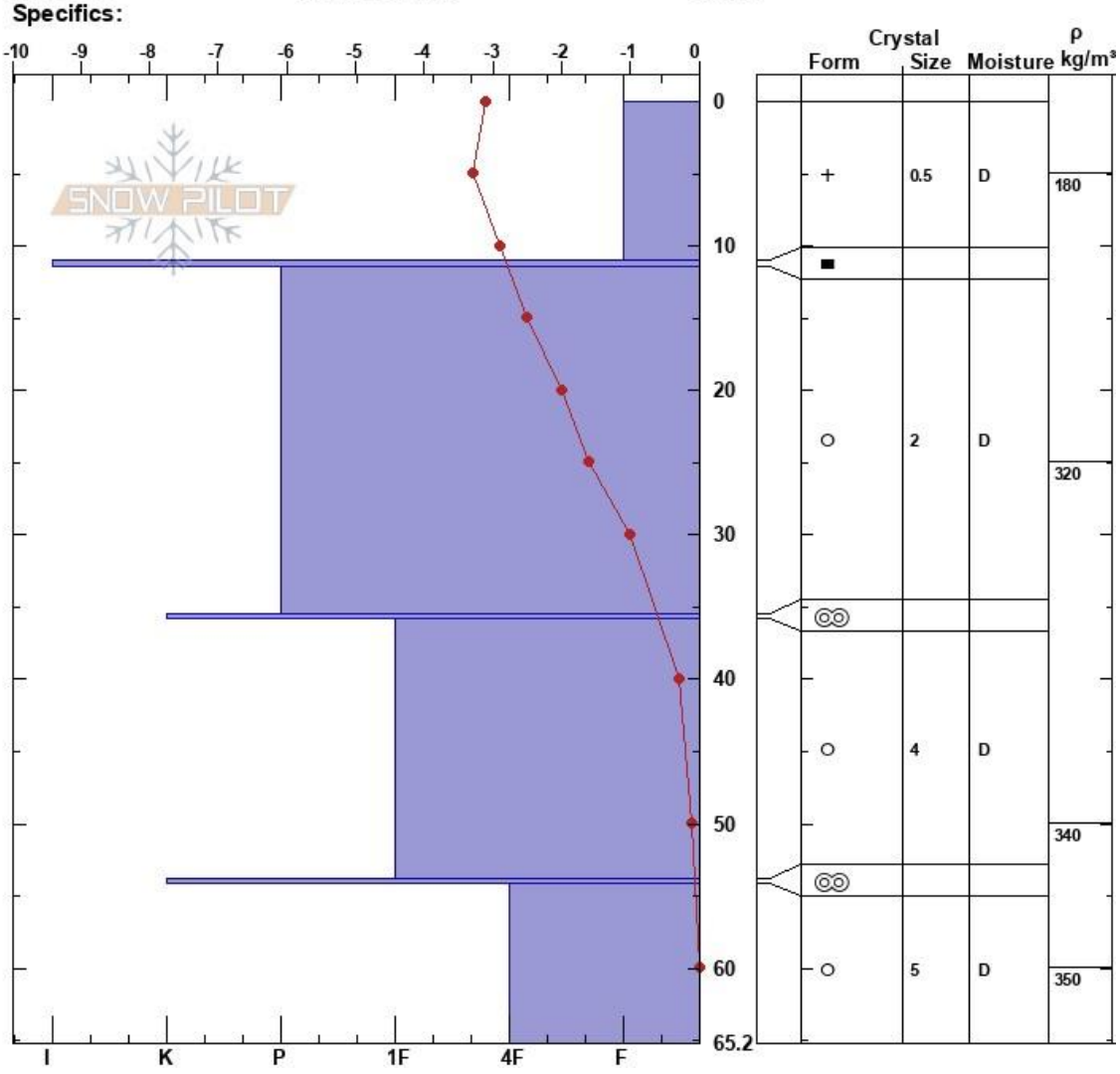

Appendix A.4.

Filefjell
Fv. 53 Tyin Årdal
Norway
Elevation: 974 m
Aspect:
Specifics:

Thor Parmentier
21/04/2023 - 09:40
Co-ord: 32V 457425E 6783684N
Slope Angle: 0°
Wind Loading:

Stability:
Air Temperature: -1.9°C
Sky Cover: CLR
Precipitation: NO
Wind: Calm

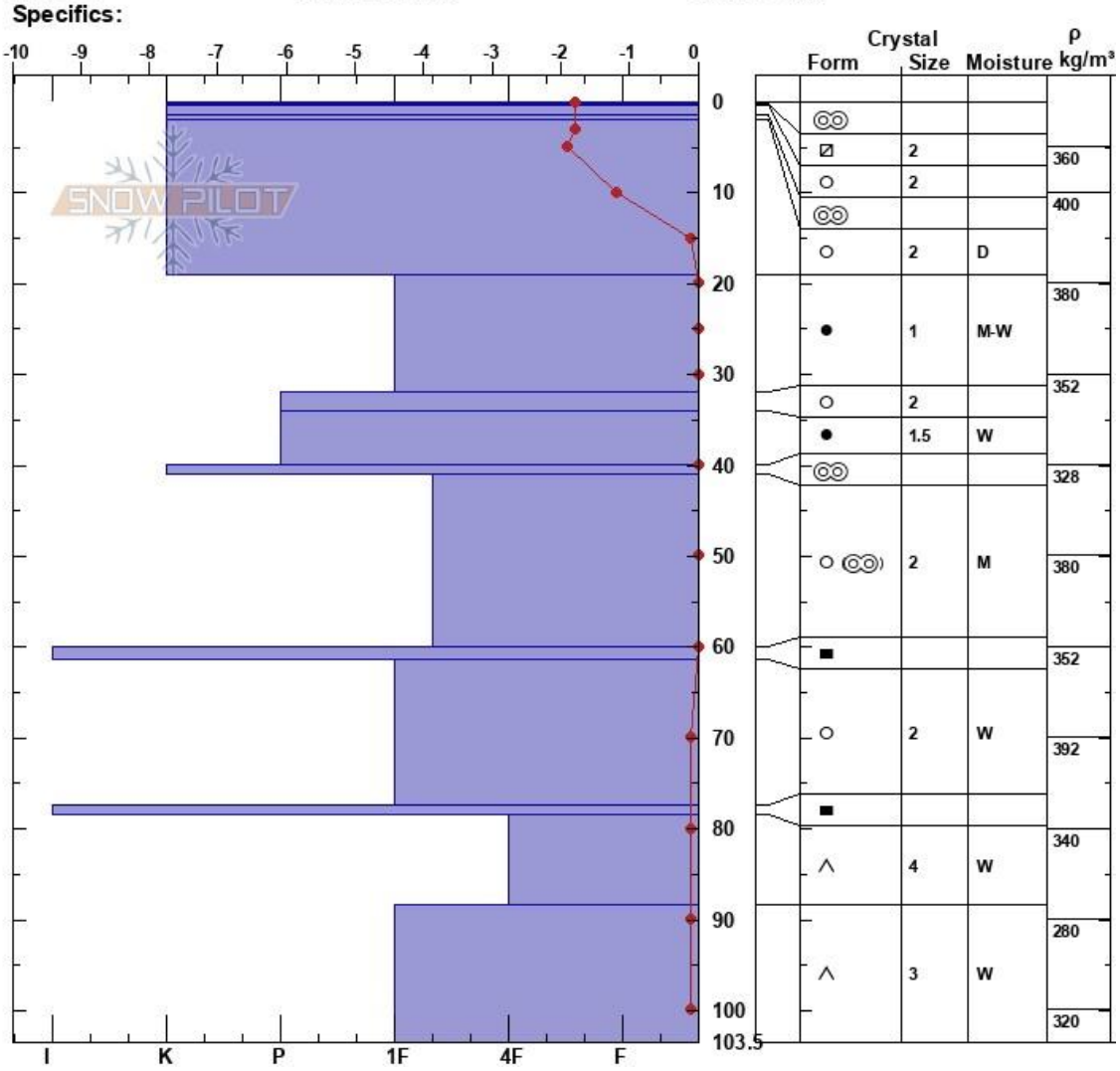

Appendix A.5.

Bingen hans Sjur
Indre Sogn
Norway
Elevation: 1056 m
Aspect:
Specifics:

Thor Parmentier
14/05/2023 - 10:00
Co-ord: 32V 436564E 6820218N
Slope Angle: 0°
Wind Loading:

Stability:
Air Temperature: 7.5°C
Sky Cover: FEW
Precipitation: NO
Wind: E Light Breeze

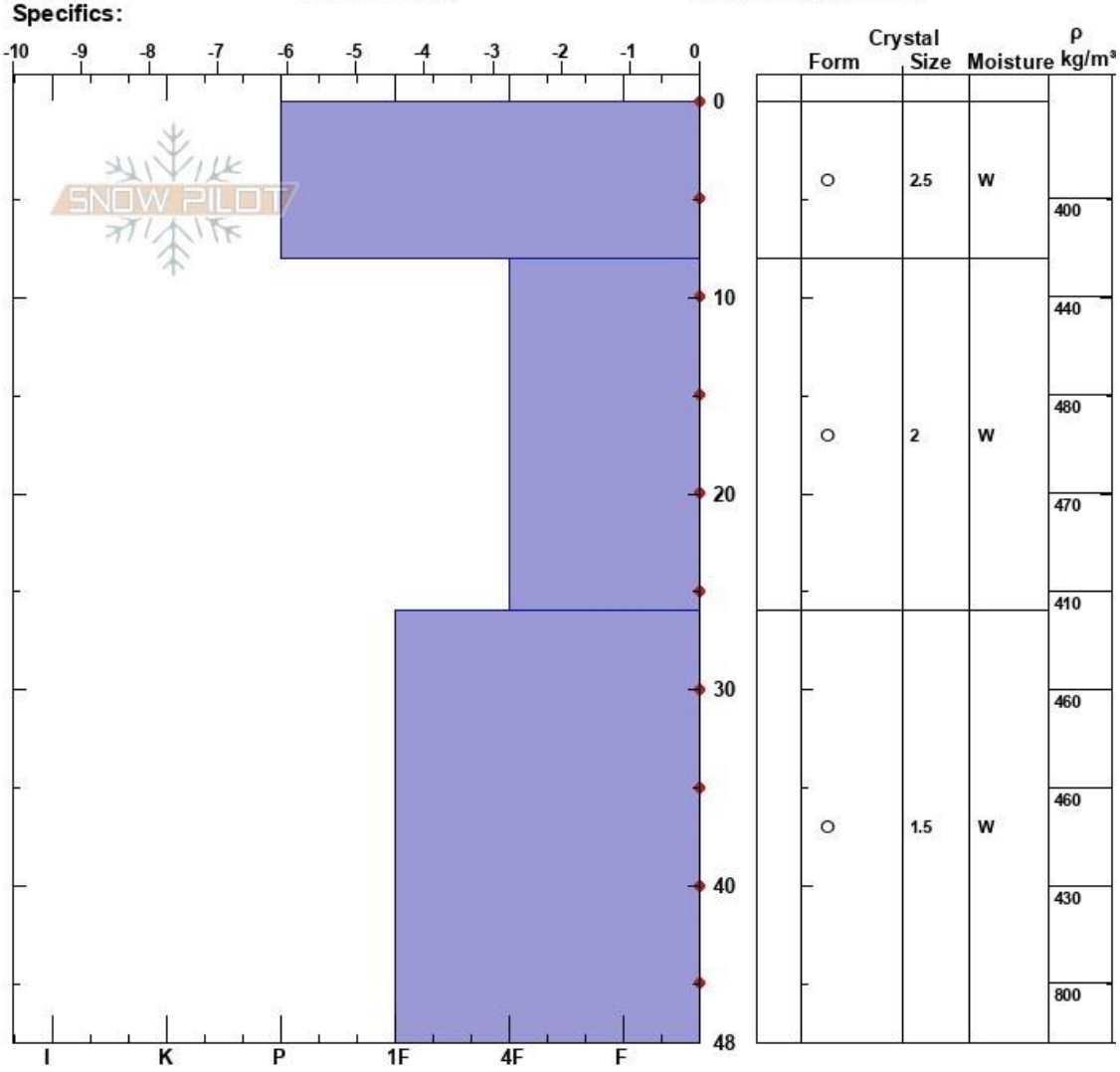

Appendix A.6.

Røssesete
Indre Sogn
Norway
Elevation: 752 m
Aspect:
Specifics:

Thor Parmentier
15/12/2023 - 17:30
Co-ord: 32V 415669E 6813507N
Slope Angle: 0°
Wind Loading:

Stability:
Air Temperature: 0.3°C
Sky Cover: OVC
Precipitation: NO
Wind:

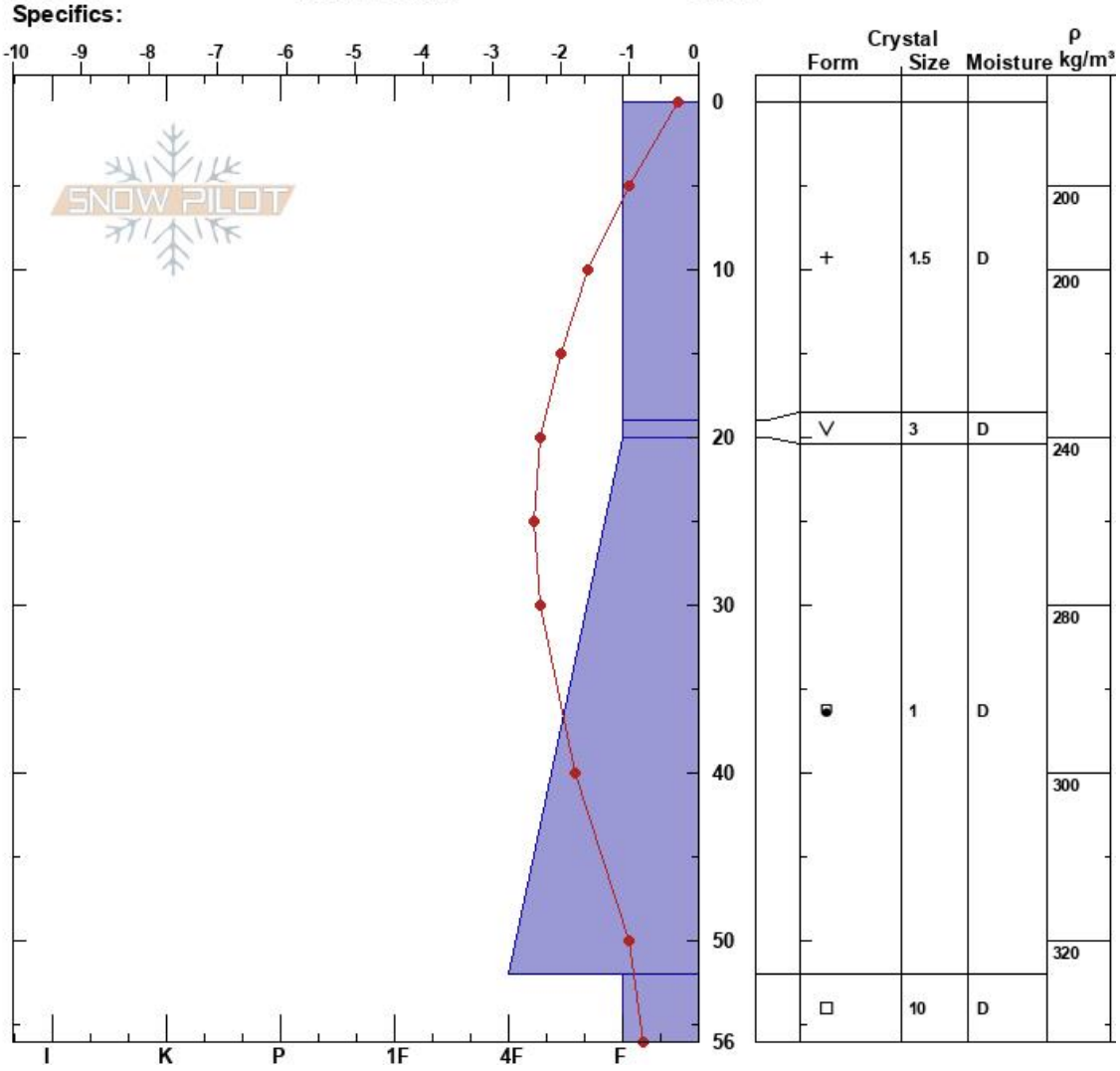

Appendix A.7.

Vinje
Voss
Norway
Elevation: 225 m
Aspect:
Specifics:

Thor Parmentier
21/01/2024 - 23:00
Co-ord: 32V 364217E 6741552N
Slope Angle: 0°
Wind Loading:

Stability:
Air Temperature: 0.1°C
Sky Cover: OVC
Precipitation: RL
Wind:

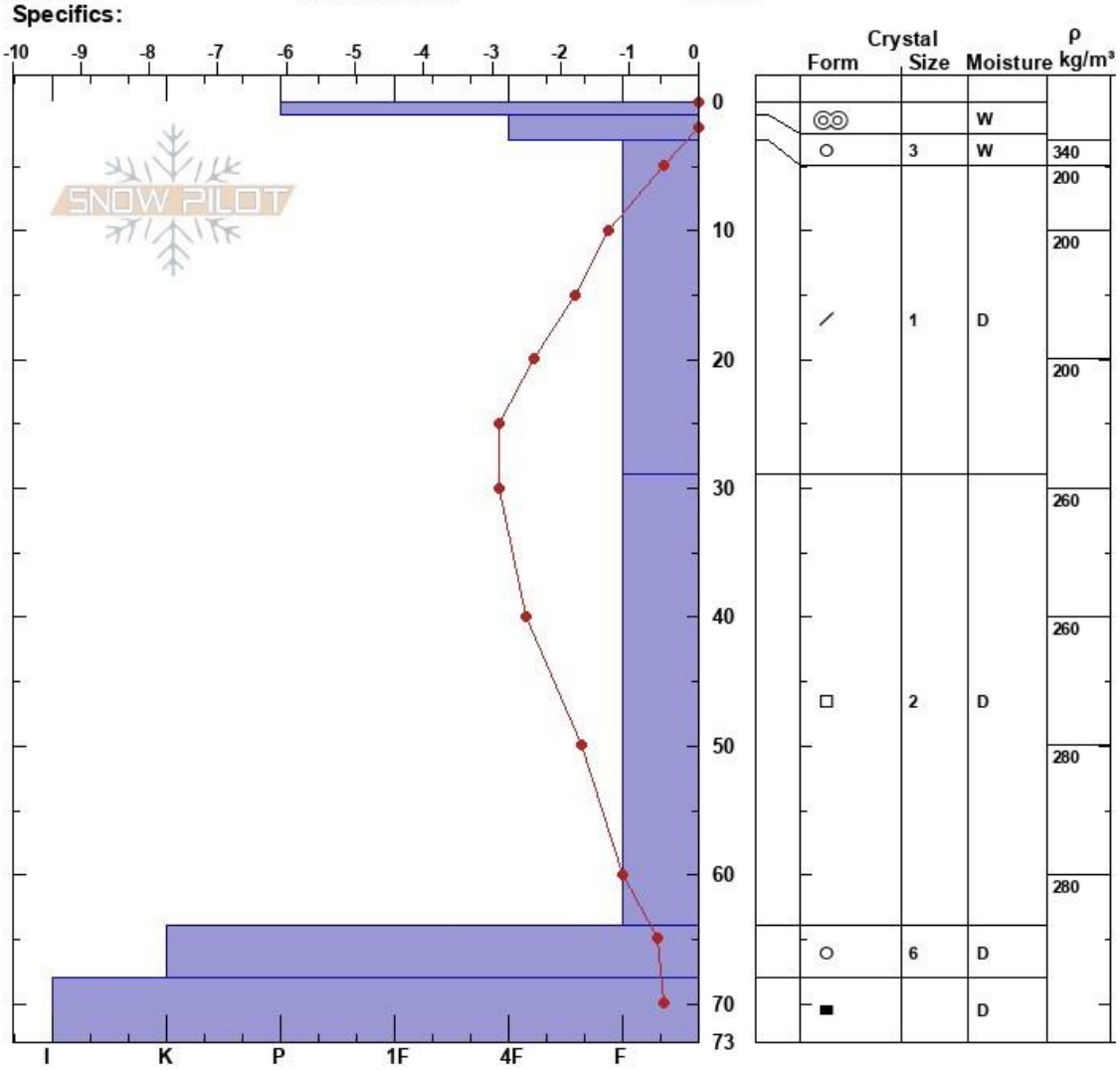

Appendix A.8.

Filefjell hand test
Jotunheimen
Norway
Elevation: 973 m
Aspect:
Specifics:

Thor Parmentier
24/02/2024 - 13:30
Co-ord: 32V 457439E 6783699N
Slope Angle: 0°
Wind Loading:

Stability:
Air Temperature: 1°C
Sky Cover: BKN
Precipitation:
Wind: SW Calm

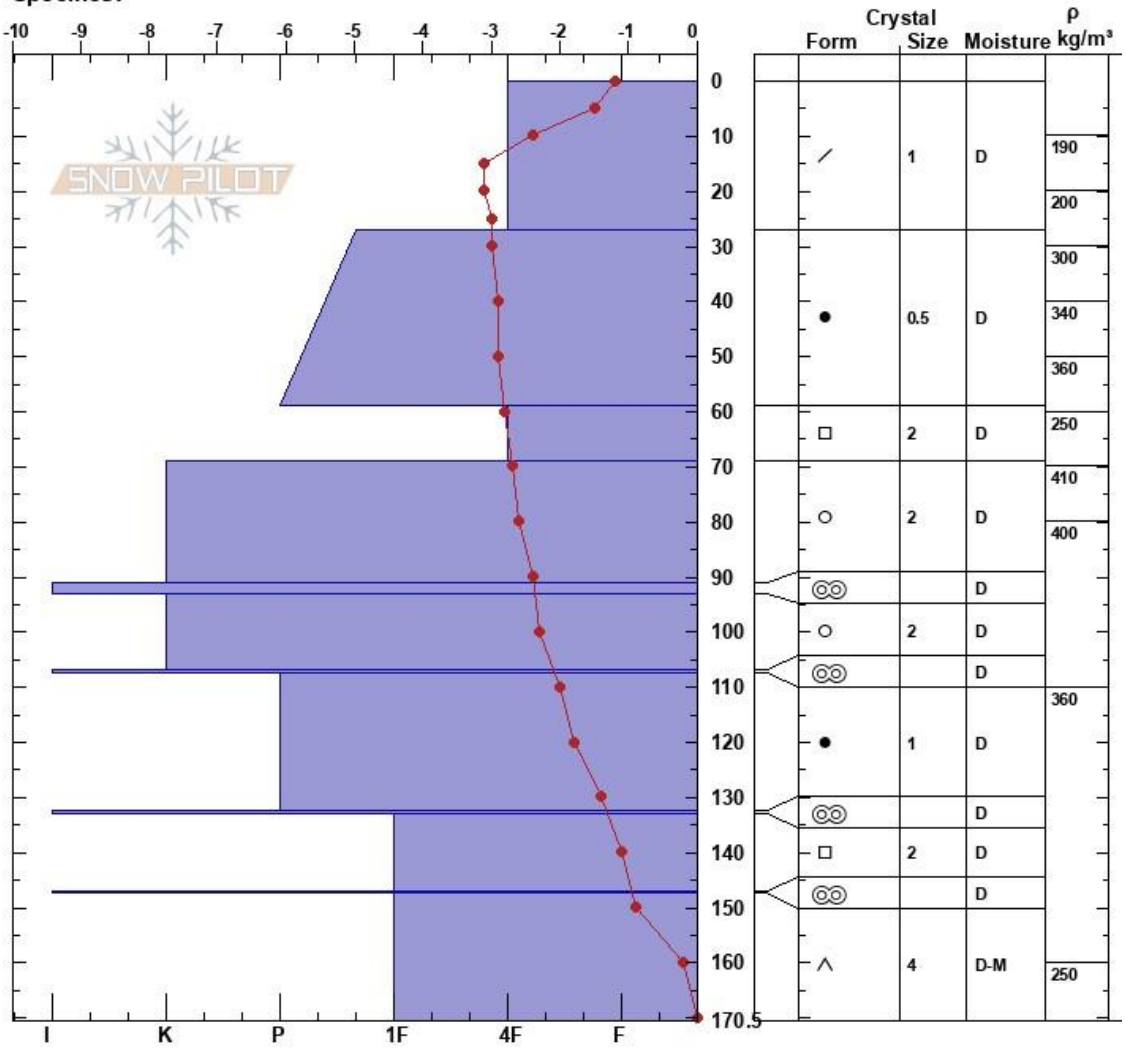

Appendix B: Declaration of the use of generative artificial intelligence

In this scientific work, generative artificial intelligence (AI) has been used. All data and has been processed in accordance with the University of Bergen's regulations, and I, as the author of the document, take full responsibility for its content, claims, and references. An overview of the use of generative AI is provided below.

The service UiBchat, powered by ChatGPT-4 was used in both the coding and writing processes. During coding, UiBchat was used for troubleshooting and for providing specific details, e.g., RGBA codes in the right format for graph colors. In the writing phase, UiBchat was used for brainstorming on thesis structure, inspiration for phrasing, and as a thesaurus. Note that while UiBchat contributed ideas and suggestions, no code or text was directly used without substantial alterations.